HYDRODYNAMIC LOADING AND RESPONSES OF SEMISUBMERSIBLES

by

Amany Mohamed Ahmed Hassan Mohamed, B.Sc.

Submitted as a Thesis for the Degree of

Doctor of Philosophy

School of Marine Science and Technology
Newcastle University
Newcastle upon Tyne
2011

(Submitted September, 2011)

Abstract

In moderate sea states, the predictions of the wave drift forces based on the potential theory correlate well with measurements. However, in severe wave conditions model tests have shown that there is an increase in wave drift forces as the sea states increases. Such difference is explained by the viscous drift forces acting in the waterline zone of a structure.

This thesis presents an experimental study of the low-frequency surge motion loading on and response of a semisubmersible model in different sea states ranging between moderate and extreme. In addition to the experimental study, the thesis includes numerical simulations.

The experimental tests were conducted in MARINTEK ocean basin with a 1/50 scale model which was moored using horizontal springs and catenary mooring lines. The environmental conditions included waves, current and combined wave and current fields. The waves used included both regular and irregular waves. In addition, decay tests were conducted in still water and in current.

For irregular waves, statistical analysis of the values of mean value and standard deviation of the motion responses was carried out to investigate the effect of wave-current interaction and different sea states on these values.

As for the numerical simulations, a mathematical model that is based on Morison's approach was used to predict the dynamic surge motion loading on and responses of a semisubmersible platform. In addition, the steady and slowly varying wave forces are predicted using Pinkster's procedure.

The second numerical simulation was carried out using three-dimensional diffraction program that estimates the six degrees of freedom loading and responses in regular waves with and without the viscous damping effects.

The damping of the system stems from both the hull and the mooring system. The mooring system damping was studied using the energy dissipation method to estimate the damping of the mooring line using the amplitude of the surge motion of the vessel.

Acknowledgments

I would like to acknowledge that it would not have been possible to conduct this research without the advice, help and guidance of my supervisors; Professor Atilla Incecik and Professor Martin J. Downie throughout my PhD.

In addition, I would like to thank Dr Hoi-Sang Chan for his supervision and for allowing me to use his software to produce some of the numerical results presented in this thesis.

The experiments presented in this thesis were conducted in MARINTEK ocean basin, Trondheim, Norway and were funded through the sixth EC Framework Programme-integrated infrastructure initiative Hydra lab III and I am grateful to Statoil Hydro for the permission to use the platform model in the experiments. I would like to thank the MARINTEK team (R. Baarholm, P.A. Berthelsen, C. Pakozdi and C.T. Stansberg) for their much appreciated help and advice during and after the experimental tests.

I would like to thank the Egyptian Ministry of Higher Education and Scientific Research for the financial support during my PhD studentship in UK.

Finally, I want to thank my family and my husband for their love and support.

Contents

List of Tables

List of Figures

Nomenclature

A	Area of waterplane
A_Y	First moment of water-plane area about y-axis
A_{yy}	Second moment of water-plane area about y-axis
A_{jk}	Hydrodynamic added mass in the j^{th} direction due to the k^{th} mode of motion
B_r	Characteristic breadth of the body
B	Linearized mooring line damping coefficient
B_{jk}	Hydrodynamic damping coefficient in the j^{th} direction due to the k^{th} mode of motion
C_{jk}	Hydrostatic restoring coefficient in the j^{th} direction due to the k^{th} mode of motion
C	Damping coefficient
C_{cr}	Critical damping
C_D	Drag coefficient
C_m	Inertia coefficient
D	Height of pontoon
D_L	Mooring line diameter
D_C	Column Diameter
D_H	Diameter of circular hull pontoon / Width of rectangular hull pontoon
D_R	Draught
E	Energy dissipated during on one surge motion cycle
E_m	Energy dissipated due to damping of the high- frequency motion
E_O	Energy dissipated in the mooring line in the case of no superposed high-frequency motion
$\vec{F}$	Force vector
F_D	Drag force on a mooring line

F_j^{δ}	Hydrostatic restoring force in the jth direction
F_j^{R}	Hydrodynamic reactive force in the jth direction
F_J^{V}	Viscous excitation force in the jth direction
F_j^{W}	Wave exciting force in the jth direction
$\bar{F}_j^{(2)}$	Mean second-order force in the jth direction
GM_T	Transverse metacentric height.
Hw	Wave height
H_C	Height of column
H_D	Height of deck
H_W	Wave height of regular wave
Im	Imaginary part of a complex quantity
$J_o(x)$	Bessel function of the first kind of zero order
$J_1(x)$	Bessel function of the first kind of first-order
KG	Centre of gravity height
Kx	Surge stiffness
L_p	Pontoon length
L_o	Intersection line of the body surface So and the undisturbed free surface S_F
L	The mooring line length
L_s	Suspended length of the mooring line
M	Mass of the structure
M_X	Surge added-mass
M_{XX}	Roll moment of inertia
M_Y	Sway added mass
M_{YY}	Pitch moment of inertia
M_Z	Heave added-mass

M_{ZZ}	Yaw moment of inertia
M_{ij}	Element of mass matrix
$\vec{M}$	Moment vector
Re	Real part of a complex quantity
S	Fluid boundary surface exterior of the body
S_F	Undisturbed free surface exterior of the body
S_o	Mean wetted body surface
S_W	Wetted body surface in unsteady flow
Ts	Wave period
T	Mooring line pre-tension
T_H	Horizontal tension in the mooring line
T_O	Horizontal tension in the mooring line in reference position
T_t	Total tension in the mooring line
T_V	Vertical tension in the mooring line
U	Mean forward speed of the body or mean current speed
V	Displaced volume of the structure
$W(\vec{x};\ \vec{\zeta})$	Far-field function
$\vec{W}$	Velocity field of steady flow
b_{jk}	Potential damping term in the j^{th} force equation due to motion in the k^{th} mode
$\hat{b}_{jk}$	Viscous damping term in the j^{th} force equation due to motion in the k^{th} mode
d	Damping ratio
$\vec{e}_j$	Vectors are the normal unit vectors
g	Gravitational constant
h	Water depth

i	$\sqrt{(-1)}$
$\vec{\imath}, \vec{j}, \vec{k}$	Unit vectors in x, y and z directions respectively
$\vec{n}$	Normal vector outward the boundary surface
$o\text{-}x_O y_O z_O$	Space-fixed coordinate system
$o\text{-}xyz$	Steady translating coordinate system
p	Fluid pressure on the instantaneous wetted body surface
r	Magnitude of $\vec{x} - \vec{\zeta}$
s_L	Distance along the mooring line
s_{LO}	Distance along the mooring line at lift-off point
Δs_L	Length of the mooring line element
s_p	Pontoon Spacing
$\vec{x}$	Co-ordinations of a field point
w	Weight per unit length of submerged mooring line
zb	Vertical coordinates of the centre of buoyancy
z_G	Vertical coordinates of the centre of gravity of the body
α	Mooring line direction with respect to positive x-axis
$\vec{\alpha}$	Local oscillatory displacement vector
β	Wave angle of incidence with x-axis
γ	Angle of Current propagation with x-axis
δ_{ij}	Kronecker delta symbol
ε	Perturbation parameter
ζ	Free surface elevation
ξ	Horizontal motion of the fairlead point in the plane of the line
$\bar{\zeta}$	Steady wave free surface elevation
$\dot{\zeta}$	Fluid particle velocity

$\ddot{\zeta}$	Fluid particle acceleration
η	Motion of the line element Δs in the direction normal to the line tangent
η_O, η_m	Low- and high-frequency motion amplitude respectively
λ	Wave length
v	Wave number $= 2\pi/\lambda$
ρ	Density of fluid
ρ_A	Density of air
ρ_W	Density of water
ρ_B	Density of body material
θ	Tangent angle of the mooring line with x-axis
φ	Total velocity potential of fluid flow
φ_7	Diffraction wave potential per unit amplitude
φ_B	Body potential
φ_j	Radiation wave potential per unit amplitude
φ_o	Incident wave potential per unit amplitude
$\bar{\varphi}_j$	Reverse flow radiation potential
$\bar{\Phi}$	Velocity potential of steady flow
$\tilde{\Phi}$	Velocity potential of unsteady flow
$\vec{\Omega}$	Unsteady rotational displacement vector
ω	Frequency of oscillation
ω_o	Incident wave frequency
ω_O, ω_m	Frequency of low- and high-frequency components, respectively
∇	Grad operator
∇^2	Laplace's operator

Chapter 1. Introduction

1.1 Background

The growing demand for oil-production has necessitated the exploration of new areas for oil-production, such as in deep-water. The continued expansion of oil-production in deep-water sea areas requires the improvement of offshore technology and the study of different environmental factors affecting the marine structures in various sea states. Consequently, oil-production in deeper water requires the improvement of available design and analysis methods in order to reduce the cost of production and to keep the production facilities as safe and as stable as possible.

One of the major challenges faced by the designers is in the study of severe sea conditions where the wave pattern is irregular. Traditional fixed structures (bottom-mounted structures) such as jacket structures are found to be suitable to be used in water depths of up to 450 m. However, in greater water depths, the installation of fixed structures is not a viable option and other solutions are needed.

Other solutions include Floating Production Systems (FPSs) and Floating Production Storage and Offloading vessel (FPSOs) which are considered suitable options for working in water depth ranging between 150 and 1500 m. Most FPSOs tend to be ship shaped hulls, particularly owing to their crude oil storage capacity. Ship shaped FPSOs usually have turret mooring systems about which they rotate in order to maintain their headings into the seas.

Another solution is the semisubmersibles which are commonly used for several roles in marine industry such as offshore oil drilling, oil production, and heavy lift cranes and are useful as exploration platform. Semisubmersibles are considered to have better motion characteristics than ship-shaped hulls due to their small waterplane area. In addition, semisubmersibles do not require their heading to be changed as the predominant direction of the weather changes.

A semisubmersible structure consists of large deck area connected to underwater pontoons via number of columns which are usually of circular or rectangular cross section. The number of columns and the shape of the pontoons depend on the selected structural configuration. A semisubmersible is held in place using either mooring or dynamic positioning systems. Mooring systems are the more common due to their relatively lower cost than the dynamic positioning system.

Forces due to waves are classified as being first and second-order forces. The first-order force oscillates at the wave frequency and induces motions known as high frequency, or

wave frequency motion. The second-order force, also known as drift force, consists of a steady component (also known as the mean wave drift force), and components whose oscillations will be with a frequency below the wave frequency and induce low frequency motions. These are of second-order with respect to the wave amplitude. The second-order forces are smaller in magnitude than the first-order forces, but due to low damping at low frequencies they may induce large overall rigid body motions around the resonance frequency. Hence, the study of the low-frequency forces is essential for the determination of the expected loads acting on both the structure and the mooring system.

1.2 Review of Literature

The research described in the following chapters concerns the hydrodynamic loading on, and responses of, semisubmersible structures in extreme environments. In this section a review of the published literature on selected related work carried out by other researchers is presented with a view to introducing the areas of interest, and the knowledge gaps, in this topic.

The range of marine offshore structures can be classified as fixed and floating types including moored structures. Floating structures, including semisubmersibles, Tension Leg Platform (TLPs), Floating Production Storage and Offloading (FPSO), and spar structures, are considered to be suitable solutions for oil drilling in water that is deeper than 450 metres. In addition, semisubmersibles may be used as re-locatable structures for resource exploration work. The concept of semisubmersibles for drilling operations was discussed in (McClure, 1965) and it was concluded that the best design is achieved by a large ship-type or a column stabilized platform and that the greatest loads are those caused by waves acting on submerged hulls and columns.

Subsequently, many studies were made to investigate the loading on and responses of the different configurations of semisubmersibles in both regular and irregular seas, and in both shallow and deep waters. The water depth combined with the wave length determines if the water depth is to be considered as deep, intermediate or shallow water from a hydrodynamic point of view. The water depth is considered to be deep if it is larger than half the maximum potential wavelength and considered shallow if smaller than 0.05 of the wavelength (Sarpkaya and Isaacson, 1981).

Research in this field would typically make use of full scale trials, scale modelling, and numerical simulations. Full scale trials, however, are too expensive and time consuming

to undertake with any frequency and they would not provide as much data as that which can be obtained from scale modelling and/or numerical simulations. In addition, the environmental conditions could not be controlled in the full trial tests. Froude-scaled model tests at the largest practical scale compatible with the available test facilities are likely to offer the most reliable and accurate means of investigating the loading and responses of a marine structure in different sea states including wave headings particularly for a proposed new design. Hence, model tests are considered one of the most reliable methods in studying the hydrodynamics of structures. However, this approach has its own issues. For example, when the mechanically created waves meet the tank boundary thus generating additional waves and this may increase or decrease the low frequency forces (Standing, 1988).

Another problem of the experimental tests approach is in the modelling of mooring systems in deep and ultra deep water with reasonable modelling scale due to equivalent water depth limitations in available facilities. (Baarholm et al., 2006) presented a new technique that is intended to improve the efficiency of the modelling of such mooring systems using a truncated mooring system, which will have the same wave drift force coefficient, and resulting model motions as the actual configuration. The new truncated mooring systems are designed with elements with low axial stiffness inserted in the line or, alternatively, the geometrical stiffness is reduced (by adding weight and/or buoyancy components) in order to maintain same motion characteristics at the test tank controlled reduced water depth.

In addition, the experimental tests cannot cover wide range of wave headings and sea states without the associated cost and time needed to reorient the model for each heading change. Hence, the usage of the numerical simulations is well established in the hydrodynamics field in order to substitute for the limitations and shortages imposed by the experimental data. On the other hand, experimental data are still needed to validate any new numerical simulation method and to assess its accuracy.

The numerical simulations are to be based on the best available analytical theories. There are several theories that can be used to study the motions and responses of marine structures. Each theory has its advantages and disadvantages depending on the physical /geometrical nature of the structure and the environmental conditions. The appropriate choice of the applicability of each method depends on the criteria of both the structure (such as shape and dimensions) and the environment (such as water depth and wave length, and the nature of the sea state such as regular or irregular waves).

For the study of the wave forces in regular waves, (Hogben, 1976) suggested that the hydrodynamic problems of cylinders could be classified into three regions according to cylinder diameter, wave length and wave height. The first region is where $H/D > 1$ and where Morison's equation is more suitable than the diffraction method. The second region is where $D/\lambda > 0.2$ and where the diffraction method is the more suitable. The third region is where $D/\lambda < 0.2$ and $H/D < 1$ and both methods can be equally suitable and applied where H, λ and D are the wave height, wave length and cylinder diameter, respectively.

(Chakrabarti, 1985) gave a simpler suggestion which is that the Morison's equation is to be applied to structures those dimensions are small compared to the wave length. On the other hand, if the structure is large compared to the wave length, the structure will alter the wave field and hence the diffraction theory is the more accurate.

The wave forces acting on marine structures in irregular waves are by convention classified as first-order oscillatory forces and second-order forces. The first-order forces are proportional of the wave height and with a frequency that is the same frequency as the waves. On the other hand, second-order slowly varying forces oscillate at a frequency lower than the wave frequency. The steady component of the second-order forces is proportional of the square of the wave height. Although the second-order forces are small in magnitude however they can nevertheless cause low frequency large amplitude horizontal motions (Remery and Hermans, 1971).

In addition, (Standing, 1988) agreed on the importance of the low frequency second-order wave loads for the design of moorings when the level of damping is low and the vessel presents a large area to the waves, thus causing considerable diffraction. However, the semisubmersible configuration presents a small area at the wave surface, which causes only a little wave diffraction and the resulting second-order wave drift forces are small. Although the low frequency forces are relatively small in magnitude, they excite large amplitude horizontal motions in moored vessels due to the very low damping. This makes the study of the second-order forces acting on semisubmersibles to be important since they affect the design of risers and mooring systems (Pinkster, 1980; Pinkster, 1979). In addition, Standing presented a discussion of the validity of the quasi-static approach for a large moored structure.

Helvacioglu in (Helvacioglu, 1990) gave a description of the main methods of evaluating the second-order forces which are the near field and the far field methods.

The far field method was presented by (Newman, 1967) and (Maruo, 1960) in which the hydrodynamic properties of the body were evaluated on a control surface far away from the body in order to be estimating the forces acting on the structure.

On the other hand, the near field method was presented by (Pinkster, 1975) where the hydrodynamic properties were evaluated on the wetted surface of the body. In this method, it was assumed that the irregular waves were a group of regular waves with only a small difference in their frequencies, and a method to calculate mean and low frequency wave drifting forces in all the six degrees of freedom was presented. Pinkster's approach is based on direct integration of all contributions to second-order forces over the instantaneous wetted surface. In the case of a regular wave group, the total second-order force contains a component that corresponds to the sum of the mean or constant forces exerted by each of the regular waves, making up the regular wave group. An advantage of this method is that the components of second-order forces can be examined separately.

Potential theory is widely used for the study of the hydrodynamics of offshore structures. There are several different methods that can be used to apply the potential theory approach to determine the drift forces. These methods were classified by Pinkster in (Pinkster, 1980) into: potential theories, which calculate mean second-forces based on momentum and energy considerations: potential theories, which deduce mean/low frequency second-order forces and moments through direct integration of the fluid pressures acting on the wetted surface; and potential theories which deduce second-order forces damping by equating the energy radiated by an oscillating vessel to work done by incoming waves. Other theories include descriptions such as: diffraction theory, strip theory, 3D potential theory, and the integration of pressure and also approximate theories based on Morison's equation and relative motion concepts.

Pinkster in (Pinkster, 1979) stated that the procedure for the solution of the second-order problem within the potential theory starts with obtaining the first-order solution. Afterwards, the second-order forces, in the absence of motions by these forces and corresponding hydrodynamic reaction forces (added mass and damping) are determined. In other words, the second-order problem within the potential theory can be solved only by first obtaining the first-order solution.

(Wichers, 1988) employed a 3D diffraction potential theory based method in order to estimate the wave drift forces for small values of forward speed. This method was

applied to a moored tanker and good agreement was found with the results obtained from experiments.

(Hermans, 1999) using potential theory found that the main result was that for moderate sea states the damping is dominated by viscous effects; however in survival sea states the wave-drift damping due to the velocity dependency of the wave-drift force becomes dominant. The existence of viscous forces was not included in the analyses.

In (Drake et al., 1984), the potential theory was applied to investigate the wave induced harmonic responses and the mean drift of an articulated column in regular waves. The mean drift horizontal force was evaluated using the Stokes expansion to second-order in wave steepness. It was found that the second-order drift forces on a column could excite pitch responses of first-order: this was explained by the fact that the articulated columns are designed to have a low natural frequency in the tilt mode, relative to wave frequencies.

In moderate sea states the predictions that are made based on potential theory give good results compared with the results obtained from the experimental measurements. However, in severe wave conditions, model tests have shown that there is an increase in wave drift forces as the sea states increase (Dev and Pinkster, 1994). This effect was explained by viscous drift forces acting in the waterline zone of a structure (Dev and Pinkster, 1997; Stansberg, 1994).

(Stansberg et al., 1998) agreed with (Dev and Pinkster, 1994), that there is a difference between the measurements and the results obtained from potential theory and presented a study of the surge and pitch motions of a semisubmersible model in irregular waves. In (Dev and Pinkster, 1997), it is showed that the explanation is partially due to viscous drift forces in the splash zone (the oscillating free surface zone). In addition, this study showed that the total damping for surge motion increases strongly with the increase in sea state, and empirical compensation for drift force coefficients should be applied when using the cross-bi-spectral analysis method.

Discrepancies between the measured and theoretical mean drift forces acting on moored structures, such as semisubmersibles, in regular and irregular waves were also noted by (Dev and Pinkster, 1994). Such discrepancies were to be dominant in the low frequency range where diffraction effects are small and are thus considered to be caused by viscous effects. Hence, a study of regular waves and waves plus current was carried out for a single vertical cylinder. The study used a theory based on a relative horizontal

velocity and a relative surface elevation. It was found that the splash zone of the vertical columns was the major source of the viscous contributions in waves. Thus, the viscous mean drift forces in irregular waves should not be treated as a quadratic transfer function (the viscous mean drift force is a cubic transfer function) by subtracting the steady forces due currents from those that are due to combined waves and currents. The viscous mean drift force in a wave-current co-existing flow field was recommended to be dealt with as being associated with two separate hydrodynamic zones (that is the splash zone and the submerged zone, respectively).

(Dev and Pinkster, 1997) showed in their study of the effects of viscous contributions to low frequency drift forces on semisubmersibles, that the slowly varying component of the drift force is important for compliant structures, such as semisubmersibles, which possess low restoring forces in horizontal motion modes. Computational techniques with 3D potential theory were found to underestimate the mean drift forces. This was explained by the observation that the viscous effects originate from the surface piercing structures, which is important for structures with a small cross-sectional waterplane areas such as semisubmersibles have. A theory based on a relative horizontal velocity and a relative surface elevation concept was applied in order to improve the theoretical predictions for the mean drift forces.

Other methods were used in the literature in order to estimate the slowly varying forces and motions. (Graham and Neish, 1997) presented a combined computational method (based on a wave panel and viscous code) to predict slow drift sway motion damping and responses in both regular and random waves for a tanker hull.

(Sarkar and Taylor, 2001) developed a method that is used to estimate the low frequency forces on moored structures. It was found that there is an increase in the first-order low frequency forces which is due to nonlinear mooring stiffness interaction with waves. This method was applied on a single floating column example.

(Drake, 2011) presented an analytical solution for the horizontal drift forces acting on a uniform circular cylinder undergoing surge and pitch motions in regular waves. The method is intended as an analytical approximation for the study of the horizontal drift forces on a deep draft spar.

The estimation of the motion responses of a floating structure, such as a semisubmersible, requires knowledge of the characteristics of the structure and those

factors which control the responses, such as the system stiffness and damping (Clough and Penzien, 1993).

The slowly varying oscillation amplitudes are affected by the amount of the system slow drift damping. The main physical contributions to the slow drift damping are the wave drift damping, the viscous hull damping, the wave radiation damping, the mooring and riser line damping and the aerodynamic damping. (Stansberg, 1994) investigated surge motion records from model tests that had been carried out with a moored semisubmersible in irregular waves in order to give quantitative information on the slow-drift hydrodynamic excitation forces and on the associated damping coefficients. The motion responses were obtained by using the second-order wave force model and assuming linearized slow-drift dynamics. An over-prediction of the extreme event in one of the cases may be explained by the fact that the wave drift damping tends to reduce the extreme responses that are predicted by the model. The estimated surge drift force coefficients, as well as the relative damping, appear to increase with increase in the sea states. The current effect was studied and it was concluded that a small amount of current could cause large mean drift forces due to the non-linear wave-current interaction effects, which depends on the values of current velocities and wave heights.

(Kinoshita and Takaiwa, 1990) presented a study of damping which showed an increase in damping due to an increase in wave height. It was stated that for a semisubmersible model, forced oscillation tests in regular waves was the best way to obtain the slow motion damping values. An added mass change due to waves for the slow drift motion of a moored vessel was experimentally determined and its effects on a power spectrum of the simulated slow drift motions in irregular waves were given.

(Wichers and Huijsmans, 1984) explained the viscous damping to be due to the interaction of the vessel and the surrounding fluid (still water), and that it found to be linearly proportional to the low frequency velocity of the vessel.

A theoretical analysis was presented by (Bearman et al., 1985) to investigate the drag and inertia coefficients of a viscous oscillatory flow at low Keulegan–Carpenter numbers. Results were compared to experimental measurements and showed that the analysis is valid at Keulegan–Carpenter numbers that are less 2. It was found that for higher Keulegan–Carpenter numbers, the drag coefficient is directly proportional to the Keulegan-Carpenter number if the viscous contribution is first subtracted, whilst the inertia coefficient decreases rapidly with increasing Keulegan-Carpenter number.

(Standing et al., 1987) gave a method to estimate wave damping via differentiating the mean wave drift forces transfer function. The obtained results were found to be sensitive to the drift force interpolation curve points of the available data points.

In (Saito and Takagi, 1988) the viscous effect on the increased damping of a semisubmersible was investigated via an approximation based on a method that was used for ship-shaped hulls. This study showed that in short and high waves the damping due to waves has an effect on the motions and which may be due to hydrodynamic interaction between waves, but no definite conclusions were made.

(Söylemez and Incecik, 1997) investigated the nonlinear coupled modes of motions and it was found that the coupled motions provide higher responses than those obtained from linear uncoupled equations. The study focused on the heave and roll motions and it was found that coupled heave and roll responses are 33% and 36% higher than the uncoupled heave and roll responses, respectively.

Several methods have been used in the literature in order to evaluate non-linear second-order forces. Molin's method (Chen and Molin, 1990) evaluates non-linear second-order forces without explicitly solving for the second-order potential. In this paper, Trantafyllou's theory on the horizontal surge, sway and yaw motions were extended to the full six degrees low frequency motions. The damping is composed of a radiation part and a viscous part. At low frequencies, the radiation part is found to be negligible. The viscous part is presented by linear and quadratic models in the time simulation.

The linear diffraction/radiation theory provides an acceptably accurate estimation of the damping of most degrees of freedom except for roll. (Chakrabarti, 2001) presented an empirical study of the damping coefficients of ships and barges using the results from both full scale and model scale experiments. The roll damping was divided into several components and any interactions between them were neglected. These components are hull skin friction, eddy making damping, free surface waves (wave damping), lift effect damping, and bilge keel damping. The damping coefficients were estimated empirically and the ship forward speed effect was taken in consideration.

Nonlinear roll damping was studied by (Jang et al., 2010) via a method that estimates the nonlinear roll damping as an integral equation of the first kind of unknown function which is classified as Volterra- type integral equation (Jang et al., 2009) . The obtained solution was found to be unstable and the employed procedure was improved via a regularization technique. Good agreement was then found when compared to measured

data from experiments. This paper dealt with only a particular ship and thus needs to be generalised in order to be applicable for other ship structures.

(Chan, 1990) presented a three-dimensional model that studied the loadings and responses of a ship that is advancing in waves and using a translating pulsating source modelling method. This method was subsequently improved by the including and the effect of viscous forces via a cross-flow approach as shown in (Chan, 1992). This method of analysis was applied on different types of marine structures such as RO-RO ships and catamarans (Fang and Chan, 2007; Chan et al., 2002).

(Sunahara, 2004) investigated the forces acting on a 16-column platform model and measured the hydrodynamics forces on each column simultaneously. Sunahara verified if the measured large forces were viscous forces. It was confirmed that the significant viscous drift forces act on circular cylinders for long wave periods. In addition, an investigation of an applicable region of viscous and potential components of the wave drift forces acting on vertical circular cylinders was presented.

(Xiao et al., 2009) investigated the low frequency heave, roll and pitch motions of a semisubmersible both numerically and experimentally. They found that the viscous forces are significant for the roll and pitch motions and negligible for the heave motion. In addition, it was observed that the resonant roll and pitch induced due to the slowly varying wind drift force are much larger than ones induced by the wave drift force.

The mooring lines systems affect the body motions of a platform in two ways (Yilmaz and Incecik, 1996). The first effect is through line stiffness, which determines the platform resonant periods. The second effect is due to the motion damping of the mooring lines themselves. The effect of drag forces on mooring lines was studied. Yilmaz and Incecik found that the mooring line contribution an important part of the total surge and sway damping of semisubmersibles where the measured surge amplitudes were observed to be reduced by 20 to 25%.

(Sarkar and Taylor, 2002) studied the nonlinear fluid-drag force acting on mooring cables using the statistical linearization technique. Current velocity and sea bed effects were included. The linearized drag, which is an unknown function of position along the cable, was determined iteratively. In addition, the effect of the drag coefficient on the surge responses at different drag coefficients was presented.

Before (Huse, 1986), it was normal to neglect mooring line drag based on the inference that the drag area of a line is very small relative to the drag area of the vessel itself.

However, (Huse and Matsumoto, 1988; Huse, 1986) presented a method that estimates the energy dissipated due to the drag forces of the mooring lines motion. The method takes into account the high frequency motions of the mooring lines.

From the above review, it was concluded that certain areas of the topic required further investigation with a view to improving the prediction methodologies. The objectives given in the next section reflect these knowledge gaps.

1.3 Objectives of the Study

In the design process of a semisubmersible structure and its mooring system configuration, it is very important to evaluate the effect of different sea states induced forces acting on and responses of the platform realistically to be able to predict the mooring loads. The wave induced forces are to be convention classified as first and second –order forces. In addition, the second-order induced motions or the slowly varying motions of the structure are affected by the system damping. Thus, the correct estimation of both the hull and mooring system damping is a necessity in order to correctly evaluate the motion responses of the vessel. Therefore, the damping of the catenary mooring lines is given a special attention in this thesis.

In addition, the damping of the mooring system and its effect on the motion response of the semisubmersible may be investigated by conducting experiments with the Froude-scale model moored by catenary mooring lines, followed by experiments under the same environmental conditions but using horizontal mooring lines only. A horizontal mooring system that is attached above water level does not represent a practical method of mooring but is used to study the loading on and response of the semisubmersible in the absence of the catenary mooring lines. This leads to a better understanding of the effects of the catenary mooring lines on the damping and motion responses.

Thus, the main objectives of this research can be summarized as follows:

The first objective was to investigate the application of different hydrodynamic models to predict the first- and second-order forces and resulting motions with emphasis on improving the modelling of the viscous damping.

The second objective was to plan and conduct experimental tests to measure wave and low frequency motions of a semisubmersible moored in both regular and irregular waves.

The third objective was to correlate the results of the second-order forces obtained from the analytical predictions and the experimental measurements with a view to identifying the areas that require enhancement.

It addition , it was planned to investigate the role of the mooring lines on the slowly varying motions with reference to factors such as mooring stiffness and mooring line damping.

Final objective was to evaluate the effect of the catenary mooring lines on the slowly varying motion via experimental measurements of the semisubmersible model moored alternatively with both horizontal and catenary mooring systems.

1.4 Outline of the Thesis

The thesis is organized as follows:

In Chapter Two, two mathematical approaches are presented that can be employed in order to estimate the first and second-order forces acting on a semisubmersible structure. The first mathematical approach is based on the three-dimensional linearized potential theory. The second approach is based on Morison's equation for the estimation of the first-order forces and responses and using Pinkster's procedure for the calculation of steady and slowly varying motion responses due to waves.

Chapter Three deals with the experimental tests performed and describes the structural model used, the experimental set up, and the test programme which included decay tests, static-pull out tests, regular waves, and irregular waves, both with and without a current. In addition, calculations of the relative damping values estimated from the decay tests are presented.

In Chapter Four, the damping of mooring lines oscillations is calculated for several study cases using the energy dissipation method.

Chapter Five presents the numerical results obtained using the mathematical methods given in Chapter Two. Additionally, comparisons are made between the numerical simulation results and the experimental data that was obtained.

Finally; Chapter Six is a summary of the conclusions that have been drawn from this research and of recommendations for future work.

1.5 Summary

This chapter presented a review of the published literature on selected related work. In addition, the objectives of this study and the outline of the thesis chapters were given.

Chapter 2. Mathematical Models

2.1 Introduction

The motion displacements and responses of a moored offshore structure are due to the combined effects of the environmental forces, namely waves, winds and currents. These environmental loading forces can be classified as steady and low frequency motions due to waves, steady and low frequency motions due to wind, and steady motions due to current.

In this chapter, two mathematical models are presented that can be employed to estimate the first and second-order wave loading forces and responses on a semisubmersible model in waves both with and without currents. The first model transforms the three-dimensional problem of a floating structure in waves and currents into linearized diffraction and radiation problems. Second mathematical model is based on Morison's equation. Each of the two models will be presented in details in the following sections of this chapter. The results of the numerical calculations and correlations will be presented in Chapter Five.

2.2 The three-dimensional model

This three-dimensional model presented in (Chan, 1990) solves the hydrodynamic problem of a marine structure advancing in waves by transforming the problem into two problems known as diffraction and radiation problems using translating pulsating source modelling method.

The diffraction problem is where the object is prevented from any form of oscillating motion and is subjected to waves. The forces caused by the waves acting on the object in this case are known as the hydrodynamic exciting forces. On the other hand, the radiation problem is where the object is oscillating in still water. The oscillations are related to the effective hydrodynamic added mass and damping. The acting forces on the object in this case, are known as hydrodynamic reactive forces and can be expressed in terms of added mass and damping coefficients.

The mathematical solution of the oscillating object in waves is undertaken by transforming the potential problem into simultaneous linearized radiation and diffraction problems using the perturbation expansion technique. Both problems are defined as being first-order hydrodynamic problems. The interactions between those two first-order problems are of a second-order in terms of the oscillatory amplitude of the responses of the object and therefore are normally neglected in the first-order theory.

The solution is carried out by solving the three-dimensional Green function integral equations over the mean wetted body surface. Hence, the first-order forces and object responses are so estimated. Based on the first-order solution, the mean second-order forces and moments are then obtained by direct integration of the second-order pressures obtained from Bernoulli's equation over the mean wetted body surface. The double Fourier transformation technique is used to derive the current speed free surface Green function that represents a translating pulsating source potential. To solve the three-dimensional Green function integral equations, symmetry properties of the Green functions and of the body wetted surface are applied in the numerical simulation.

Chan (1990) presented the theoretical formulations for this method that are summarized in the following sections. The created software packages based on these formulations and provided by Chan were so developed in order to predict the first-and second-order hydrodynamic forces on marine vehicles advancing through waves. In this research, for the study of the behaviour of moored semisubmersibles, the advancing velocity is replaced by the current speed acting on a moored semisubmersible platform and the mooring forces are taken into consideration. This technique was applied in (Chan, 1990) on a series-60 ship and on a tanker where good agreement with experimental results was found.

In addition, in order to estimate the viscous effects (Chan, 1992) presented the formulation for a technique that uses the above three-dimensional technique in association with a cross-flow approach. After conducting the three-dimensional technique mentioned earlier using a three-dimensional oscillating source distribution method, the hydrodynamic coefficients and wave excitation forces and moments associated with the equations of motion are thus obtained. An empirical method based on the cross-flow approach is applied for the determination of linear cross-flow drag damping terms in the equations of motion. The linear coupled equations of motions are then solved. Subsequently, the integration of the hydrodynamic pressures and cross-flow drag forces are used to provide the wave loads applied, both forces and moments, over the wetted surface including the viscous effects.

2.2.1 Definition of the coordinate system

A fixed right-handed orthogonal co-ordination system is defined with its origin at the centre of the *o-xy* plane of the platform at the still water surface level. A sketch of the coordination system is given in Figure 2-1.

The definitions of the positive axes of the co-ordination system are as follows:

x-direction parallel to mean still water level with $x = 0$ at the water surface and at the middle of platform width. Generally, the wave may approach the semisubmersible from any heading angle. On the other hand, this study focused on the following sea states in which the wave-heading angle is same as x- axis positive direction.

y-direction in the horizontal plane perpendicular to the axis of the wave propagation with the origin $y = 0$ at the platform centre at water surface and positive direction is according to right hand rule.

z-direction directed vertically upward (positive) with $z = 0$ located at the still water surface. In the case of existence of current velocity, the above described coordination system translates with the structure at the same velocity.

In addition, $\vec{\imath}, \vec{\jmath}$ and $\vec{k}$ are the unit vectors in x, y and z directions, respectively. The rigid body six degrees of freedom in the directions of the axes are defined as ζ_j where j = 1, 2, 3, 4, 5, and 6 and correspond to surge, sway, heave, roll, pitch and yaw motions, respectively.

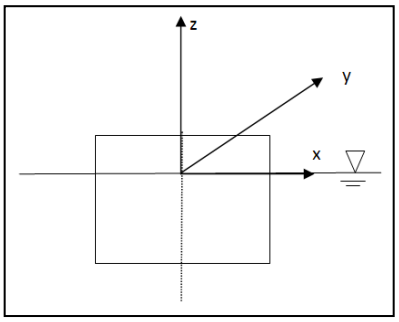

Figure 2-1 Coordination system

2.3 The mathematical model based on the three-dimensional technique

In this section, a brief description of the mathematical model of the three-dimensional technique that was introduced in (Chan, 1992; Chan, 1990) is presented. In this technique, the equations of motion of a free oscillating body in waves are derived by equating the external forces to the inertial forces that are associated with the accelerations of the body. The procedure for the estimation of the mean second-order forces is presented in Section 2.3.6. In the current section, the viscous effects are ignored. The study of the viscous effects is presented separately later in Section 2.3.7.

In the study, in order to simplify the evaluation of the structure in regular waves and current, the problem is divided into steady motion at constant forward speed U and rigid body harmonic oscillations.

Thus, the external forces acting on the structure are the unsteady hydrodynamic loads due to the regular waves, also known as the hydrostatic restoring forces, the hydrodynamic exciting forces, and the hydrodynamic reactive forces. A description of each of these forces is given in the following sections.

As mentioned earlier, the complex problem of the structure moving in waves is solved linearly by dividing the problem into diffraction and radiation components.

Firstly, the hydrostatic restoring forces are the fluid forces that act to restore the body to its original static equilibrium state when the body is displaced freely from the rest position.

Secondly, the hydrodynamic excitation forces refer to the forces that are experienced by the body in the diffraction condition due to the incident and scattered (diffracted) waves. These forces are dependent on the incident wavelength, wave frequency, wave heading angle, current speed, body geometry and are proportional to the wave amplitude.

Finally, the hydrodynamic reactive forces are the forces that are involved in the radiation problem, are due to the oscillatory motions of the body in still water, and are related to the hydrodynamic added mass and viscous damping coefficients. These coefficients are functions of the forward speed of the object, the body geometry and the frequency of motion, but not of the motion amplitude.

2.3.1 Hydrodynamic Forces

The fluid oscillatory motions surrounding the hull or the body are the cause of the hydrodynamic pressure forces that are the main contributing forces that result in the hull or body motions investigated in this study. These forces are calculated by integrating the hydrodynamic pressures in terms of the appropriate velocity potential and its derivatives over the mean wetted body surface.

The instantaneous fluid pressure p on the local wetted body surface area S_w is given by Bernoulli's equation in terms of the total velocity potential φ as

$$p(\vec{x};t) = -\rho\left\{\varphi_t + \frac{1}{2}\nabla\varphi \bullet \nabla\varphi - \frac{1}{2}U^2 + gz\right\} \tag{2-1}$$

where

g Gravitational constant,

P Fluid particle pressure,

U Current velocity,

$\vec{x}$ Co-ordinations of a field point,

ρ Water density,

φ Velocity potential, and

∇ Grad operator.

Since the exact wetted body surface S_w, is displaced and rotated with respect to the mean wetted surface S_o, then local fluid pressure p on S_o is obtained by means of a Taylor series expansion as follows

$$(p)_{S_w} = (p + \vec{\alpha} \bullet \nabla p + \ \ldots)_{S_o} \qquad \text{on } S_w, S_o \tag{2-2}$$

The vector $\vec{\alpha}$ is the local displacement of a point of the fluid on S_w due to translational and rotational motions with respect to S_o. Under the usual assumptions of linearization, the perturbation expansion of the total velocity potential φ is given by

$$\Phi(\vec{x};t) = \bar{\Phi}(\vec{x}) + \varepsilon\, \tilde{\Phi}^{(1)} + \ \varepsilon^2\, \tilde{\Phi}^{(2)} + \ \ldots \tag{2-3}$$

The velocity potential $\bar{\Phi}(\vec{x})$ and $\tilde{\Phi}\ (\vec{x};t)$ are the steady and unsteady parts respectively. Substituting equations (2-1) and (2-3) into (2-2) and retaining the expansion up to $O\ (\varepsilon)$ results in estimating the local pressure p as

$$p(\vec{x};t) = -\rho\left\{\frac{1}{2}\left(\overrightarrow{W} \bullet \overrightarrow{W} - U^2\right) + \ \left(gz + g\vec{\alpha}\ \bullet \vec{k}\right) + \ \varepsilon\left\{\varphi_t^{(1)} + \overrightarrow{W} \bullet \right.\right.$$
$$\left.\left.\nabla\tilde{\varphi}^{(1)} + \frac{1}{2}\ \vec{\alpha} \bullet \nabla\left(\overrightarrow{W} \bullet \overrightarrow{W}\right)\right)\right\} + \ O\ (\varepsilon^2\ ) \quad \text{on } S_w\ ,\ S_o \tag{2-4}$$

where W and $\overrightarrow{W}$ are the far-field function and the velocity field of the steady flow. The previous equation shows that the three components of the local combined pressure are the steady pressure due to the steady velocity field W, the hydrostatic pressure and its fluctuation, and the first-order hydrodynamic pressure. The forces and moments acting on the body can be then obtained by integrating the fluid pressure over the body surface S in the form

$$F_j = -\iint_{S_w} p\ n_j\ ds = -\iint_{S_o} p\ n_j\ ds - \iint_{\delta S_o} p\ n_j\ ds \quad ;\ j = 1, 2,.., 6 \tag{2-5}$$

where n_j is the generalized direction cosine. The integration is conducted over the wetted body surface area S_w that is divided into the mean wetted body surface and the oscillatory part δ_{So}. Afterwards, the time dependant terms and the first-order relative wave elevation over the steady flow field are both neglected. In addition, the buoyancy force for the oscillatory motions in a steady velocity field is small and can be neglected. The unsteady velocity potential is linearly decomposed into potentials due to incident waves, to diffraction waves and to radiation waves. Thus, the first-order dynamic forces can be written as

$$F_j = F_j^{\delta} + F_j^{W} + F_j^{R} \quad ; \text{j=1,2,..,6} \tag{2-6}$$

in which

The hydrostatic restoring forces $F_j^{\delta} = \rho\, g \iint_{S_o} (\vec{\alpha} \bullet \vec{k}) n_j \, ds$ (2-7)

The wave excitation forces

$$F_j^{W} = -\rho \iint_{S_o} (i\omega - \overrightarrow{W} \bullet \nabla)(\Phi_0 + \Phi_7) e^{-i\omega t} n_j ds \tag{2-8}$$

The hydrodynamic reactive forces

$$F_j^{R} = -\rho \sum_{k=1}^{6} \zeta_k \iint_{S_o} (i\omega - \overrightarrow{W} \bullet \nabla) \Phi_k \, e^{-i\omega t} n_j ds \tag{2-9}$$

where

n_j Normal vector outward the boundary surface in the j[th] direction,

φ_7 Diffraction wave potential per unit amplitude,

φ_o Incident wave potential per unit amplitude, and

ω Frequency of oscillations.

The surface integral is reduced to a more simple formula as

$$\iint_{S_o} (\overrightarrow{W} \bullet \nabla \Phi) n_j ds = -U \iint_{S_o} \Phi m_j ds \tag{2-10}$$

where m_j is current speed related coefficient in the j[th] direction.

The amplitude of the profile of a regular wave of a wavelength λ and frequency ω_o can be expressed as

$$\zeta_i = \zeta_o \, e^{i[\nu(x\cos(\beta) + y\sin(\beta)) - \omega t]} \tag{2-11}$$

where ζ_o , v, ω and β are the incident wave amplitude, wave number , wave encounter frequency and angle of incidence with the x-axis, respectively. For a constant water depth, and assuming regular waves, the dispersion relation relates the wave number to the wave frequency and the water depth by $\frac{\omega_o}{g} = v \tanh(vh)$. The wave encounter frequency ω_o is related to the wave frequency and current velocity by the relationship $\omega = |\omega_o - v\, U \cos(\beta)|$

2.3.2 Hydrostatic restoring forces

These forces are evaluated by integrating the hydrostatic pressure at a point due to the variation in vertical displacement of the body. By converting the surface integral into a volume integral, the final form of the restoring force can be written as

$$F_j^{\delta} = -\sum_{k=1}^{6} C_{jk}\, \zeta_k\, e^{-i\omega t} \quad ; \text{j= 1 ,2, …,6} \tag{2-12}$$

C_{jk} is called the hydrostatic restoring coefficient, which is a function of the body geometry only and is independent of the motion ζ_k. Since the hydrostatic restoring forces originate from the hydrostatic pressure variation due to vertical movement, they only act vertically. Therefore, regardless of the body shape, the coefficients in the directions related to the surge, sway and yaw motions are equal to zero.

Assuming that the structure has a longitudinal symmetry axis, the force coefficients will vanish in the direction that is perpendicular to it and hence the remaining non-zero coefficients are

$$\left.\begin{aligned} C_{33} &= \rho g\, A \\ C_{44} &= \rho g\, A_{xx} + M\, g\, (z_b - z_G) = \rho\, g\, V\, GM_T \\ C_{55} &= \rho g\, A_{yy} + M\, g\, (z_b - z_G) = \rho\, g\, V\, GM_L \\ C_{35} &= C_{53} = -\rho g\, A_y \end{aligned}\right\} \tag{2-13}$$

A, A_x, A_y, A_{xx} and A_{yy} are the waterplane area, the first moment and the second moments of the water-plane area at $z = 0$. M is the mass of the body. z_b and z_G are the vertical coordinates of the centre of buoyancy and the centre of gravity of the body respectively. GM_T and GM_L are the transverse and longitudinal meta-centric heights and V is the volume of displacement.

2.3.3 Hydrodynamic exciting forces

The hydrodynamic exciting forces F_j^W are the result of the pressure associated with the diffraction potential due to the incident waves per unit amplitude. It can be expressed from (2-8) and (2-10) in the form

$$F_j^W = -\rho \iint_{S_o} (i\omega n_j + U m_j)(\varphi_o + \varphi_7) ds\, e^{-i\omega t} \quad ; j = 1,2,..,6 \tag{2-14}$$

Equation (2-14) requires the solution of the diffraction potential φ_7. However, instead of solving the diffraction potential problem, the hydrodynamic exciting force can be derived by using the body boundary condition of the reverse flow radiation problem with negative forward speed. The reverse flow radiation potential is given by

$$\frac{\partial \bar{\varphi}_j}{\partial n} = -i\,\omega n_j - U\, m_j \quad ; j= 1, 2,\ldots, 6 \tag{2-15}$$

where $\bar{\varphi}_j$ is the reverse flow radiation potential and determined via equation (2-15). Substituting (2-15) into (2-14) yields

$$F_j^W = \rho \iint_{S_o} \frac{\partial \bar{\varphi}_j}{\partial n} (\varphi_o + \varphi_7) ds\, e^{i\omega t} \tag{2-16}$$

The exciting force given by equation (2-14) can be decomposed into two components as

$$F_j^W = K_j + D_j \quad ; j =1,2,..,6 \tag{2-17}$$

in which

$$K_j = -\rho \iint_{S_o} (i\omega n_j + U m_j)\, \varphi_o\, ds\, e^{i\omega t} \tag{2-18}$$

$$D_j = -\rho \iint_{S_o} (i\omega n_j + U m_j)\, \varphi_7\, ds\, e^{i\omega t} \tag{2-19}$$

K_j is called the incident wave force and D_j is called the diffraction force coefficient. Since the steady flow field interacts with the unsteady flow field, the incident wave force is thus no longer independent of the forward speed. By neglecting the interaction effect and making $\vec{W} = -U\,\vec{i}$, the only effect of the gradient operator ∇ in equation (2-8) is on the incident wave potential φ_0, with the result that $i\,\omega - \vec{W} \bullet \nabla = i\,\omega_o$ and the incident wave force becomes the Froude-Krylov force in the form

$$K_j = -\rho i \omega_o \iint_{S_o} \varphi_o n_j\, ds\, e^{i\omega t} \tag{2-20}$$

The Froude-Krylov force, given by equation (2-20) involves the incident wave potential only and so it corresponds to the force experienced by the body when the incident wave trains pass through it unaffected and un-reflected by the body. Therefore, the Froude-Krylov force is significant in the long wave regime or for a thin body in head waves where scattering wave effects are small. On the other hand, the diffraction force given

by equation (2-19) becomes important in the short wave regime or for a large body with a large frontal area that is exposed to the incident waves.

2.3.4 Hydrodynamic reactive forces

The hydrodynamic reactive forces in the j[th] direction resulting from the motion ζ_k are obtained by

$$F_{jk}^{R} = -\rho \iint_{S_o} (i\,\omega n_j + U\, m_j)\varphi_k\, ds\, \zeta_k\, e^{-i\omega t} \quad \text{j,k = 1,2,..,6} \tag{2-21}$$

The reactive forces take into account the phase difference between the fluid reaction force and the current velocity. This is considered by using one component that is proportional to the body velocity and another that is proportional to the body instantaneous acceleration as follows

$$F_{jk}^{R} = -\left(A_{jk}\ddot{\zeta}_k + B_{jk}\dot{\zeta}_k\right) = \left(\omega^2 A_{jk} + i\omega B_{jk}\right)\zeta_k e^{-i\omega t} \tag{2-22}$$

The coefficients A_{jk} and B_{jk} are called the added mass coefficient and the damping coefficient, respectively. Their values are estimated by using the real and imaginary parts in equation (2-21) and (2-22). Thus, their values are

$$A_{jk} = -\frac{\rho}{\omega^2}\, Re \iint_{S_o} (i\omega n_j + U\, m_j)\varphi_k ds \tag{2-23}$$

$$B_{jk} = -\frac{\rho}{\omega}\, Im \iint_{S_o} (i\omega n_j + U\, m_j)\varphi_k ds \tag{2-24}$$

2.3.5 Equations of motion

The six components of the inertia force that is due to the body's acceleration in six degrees of freedom rigid body motions are as follows

$$F_j = \sum_{k=1}^{6} M_{jk}\ddot{\zeta}_k \qquad ; \text{j} = 1, 2, \ldots, 6 \tag{2-25}$$

where $\zeta, \dot{\zeta}\ and\ \ddot{\zeta}$ are the amplitude, velocity and acceleration of the body responses and M_{jk} is the body-inertia coefficients in the j[th] direction due to forces at the k[th] direction. The j index indicates the direction of the fluid force and the k index refers to the mode of motion (i.e. surge, sway, heave, roll, pitch and yaw, respectively). The body-inertia coefficient can be obtained by Newton's Second Law of Motion, which defines the force vector as

$$\vec{F} = \frac{d}{dt} \iiint_V \rho_B (\vec{v} + \vec{\omega} \times \vec{r}) dV \tag{2-26}$$

From the conservation of angular momentum, the moment vector is defined as

$$\vec{M} = \frac{d}{dt}\iiint_V \rho_B \vec{r} \times (\vec{v} + \vec{\omega} \times \vec{r})\, dV \tag{2-27}$$

where $\vec{M}$ is the moment vector, and M_{jk} is the body-inertia coefficient and as appropriate element of the mass matrix. The quantity ρ_B is the body density and is assumed constant. The velocity vector in the previous equations can be expressed in the form

$$(\vec{v} + \vec{\omega} \times \vec{r}) = \sum_{k=1}^{6} v_k \vec{e}_k \tag{2-28}$$

where $\vec{e}_j$ vectors are the normal unit vectors and defined as

$$(\vec{e}_1, \vec{e}_2, \vec{e}_3) = (\vec{\imath}, \vec{\jmath}, \vec{k}) \tag{2-29}$$

$$(\vec{e}_4, \vec{e}_5, \vec{e}_6) = (\vec{\imath}, \vec{\jmath}, \vec{k}) \times \vec{r} \tag{2-30}$$

Substituting equations (2-29) and (2-30) into equations (2-26) and (2-27) we have

$$F_j = \sum_{k=1}^{6} \dot{v}_j \iiint_V \rho_B \vec{e}_j \bullet \vec{e}_k dv \quad ; \text{j = 1,2,3} \tag{2-31}$$

$$F_j = \sum_{k=1}^{6} \dot{v}_j \iiint_V \rho_B \vec{e}_j \bullet \vec{r} \times \vec{e}_k dv \quad ; \text{j = 4,5,6} \tag{2-32}$$

Equation (2-32) is related to equation (2-31) such that

$$F_j = \sum_{k=1}^{6} \dot{v}_j \iiint_V \rho_B \vec{e}_j \bullet \vec{e}_k dv \quad ; \text{j = 1,2,..,6} \tag{2-33}$$

Comparing equations (2-33) and (2-25) yields

$$M_{jk} = \iiint_V \rho_B \vec{e}_j \bullet \vec{e}_k dv \tag{2-34}$$

As the structure is assumed to have longitudinal symmetry and with no trim, the centre of the gravity of the structure can be assumed at (0, 0, z_G). Hence, the mass matrix [M] of the structure can be written as

$$[M] = \begin{bmatrix} M & 0 & 0 & 0 & Mz_G & -My_G \\ 0 & M & 0 & -Mz_G & 0 & -Mx_G \\ 0 & 0 & M & My_G & -Mx_G & 0 \\ 0 & -Mz_G & My_G & I_{44} & I_{45} & I_{46} \\ Mz_G & 0 & -Mx_G & I_{54} & I_{55} & I_{56} \\ -My_G & Mx_G & 0 & I_{64} & I_{65} & I_{66} \end{bmatrix} \tag{2-35}$$

in which the three moments of inertia of the body about the origin are defined by

$$I_{jk} = \iiint_V \rho_B \left[r_j^2 \delta_{jk} - \left(1 - \delta_{jk}\right) x_{j-3} x_{k-3} \right] dv \quad ; \text{ j, k = 4,5,6} \tag{2-36}$$

where δ_{jk} is the Kronecker delta function such the $\delta_{jk} = 1$ if $j = k$ and $\delta_{jk} = 0$ if $j \neq k$. r_j is the distance of the mass element to the corresponding axis of rotation about the origin and (x_1,x_2,x_3) is (x,y,z) . For a body with one longitudinal plane of symmetry, $y_G = 0$ and $I_{45} = I_{54} = I_{56} = I_{65} = 0$.

In addition, when the vessel is assumed to have one longitudinal axis of symmetry then the linearized problem is divided into two independent groups; the linear couple surge-heave –pitch equation and the sway-roll-yaw equation. Equating the inertia force given by equation (2-25) to the hydrodynamic forces as given by equation (2-6), we obtain the equations of the six rigid body motions in the frequency domain as

$$F_j^W = \sum_{k=1}^{6} \left\{ \left(M_{jk} + A_{jk} \right) \ddot{\zeta}_k + B_{jk} \dot{\zeta}_k + C_{jk} \zeta_k \right\} \tag{2-37}$$

For a regular harmonic wave train the preceding equation can be written as

$$F_j^W = \sum_{k=1}^{6} \left\{ -\omega^2 \left(M_{jk} + A_{jk} \right) - i\, \omega B_{jk} + C_{jk} \right\} \zeta_k \tag{2-38}$$

These are six simultaneous linear equations, which can be solved for the body motion of amplitude ζ_k by the employment of standard numerical techniques. The presence of the water free surface renders the amplitude ζ_k a complex quantity that exhibits a phase difference between the incidence wave and the rigid body motion. The complex amplitude ζ_k of the body motion is the kth mode in response to the incident wave of unit amplitude and is known as the transfer function or the response amplitude operator (RAO). Once the added masses A_{jk}, the damping coefficients B_{jk} and the wave exciting forces F_j^W are determined by direct integration of both the corresponding radiation potential and the diffraction potential due to the incident wave, then the motion response amplitudes in regular waves are easily obtained.

2.3.6 Second-order forces and moments

(Chan, 1990) presented a mathematical model of the calculations of the second-order forces and moments acting on a marine structure advancing in regular waves. The same method is applicable on a fixed or moored structure and with the forward speed being replaced by the current velocity. The second-order forces and moments are estimated based on a method that combines the three-dimensional source distribution technique

with the near-field method. Current velocity computations are conducted using the three-dimensional translating pulsating source modelling method.

The near-field method estimates the second-order forces and moments by the direct integration of the fluid pressures over the mean wetted body surface, and that is calculated from Bernoulli's equation. The advantage of this method is that it allows for the investigation of the components of the second-order forces and moments separately. This results in a better understanding of phenomena such as the effects of wave elevation, velocities and pressures. The near-field expressions for the second-order forces and moments acting on a structure in regular waves and current are introduced briefly herein.

The total velocity potential $\Phi(\vec{x};t)$ due to the incident wave system and the current velocity is expressed as

$$\Phi(\vec{x};t) = \bar{\Phi}(\vec{x}) + \widetilde{\Phi}(\vec{x};t) \tag{2-39}$$

The potentials $\bar{\Phi}(\vec{x})$and $\widetilde{\Phi}(\vec{x};t)$ are the steady and unsteady parts respectively. The steady potential $\bar{\Phi}(\vec{x})$ is due to the current speed modelled as uniform stream potential (Ux) and a steady perturbation potential $\bar{\varphi}(\vec{x})$. On the other hand, the unsteady potential $\widetilde{\Phi}(\vec{x};t)$ consists of the incoming wave potential φ_o and the body potential φ_B. The fluid motion is assumed to be harmonic in time with the frequency of encounter ω_o. The unsteady velocity potential $\widetilde{\Phi}(\vec{x};t)$ and the free surface elevation $\zeta(\vec{x};t)$ can be written using the perturbation analysis as

$$\widetilde{\Phi}(\vec{x};t) = \varepsilon\,\widetilde{\Phi}^{(1)} + \varepsilon^2\,\widetilde{\Phi}^{(2)} + \ \ldots \tag{2-40}$$

$$\zeta(\vec{x};t) = \zeta(\vec{x}) + \varepsilon\,\zeta^{(1)} + \varepsilon^2\,\zeta^{(1)} + \ \ldots \tag{2-41}$$

Here the steady perturbation potential $\bar{\Phi}(\vec{x})$ is assumed to be small and neglected in both the linearized free surface condition and the linearized body boundary condition for the unsteady forward motion/current velocity problem. Thus, the fluid pressure on the instantaneous wetted body surface S_w is given by Bernoulli's equation in terms of the unsteady velocity potential $\widetilde{\Phi}(\vec{x};t)$ as:

$$p(\vec{x};t) = -\rho\left\{\widetilde{\Phi}_t + \frac{1}{2}\nabla\widetilde{\Phi}\bullet\nabla\widetilde{\Phi} + \vec{W}\bullet\nabla\widetilde{\Phi} + \frac{1}{2}\left(\vec{W}\bullet\vec{W} - U^2\right) + gz\right\} \tag{2-42}$$

on S_w

Hence, the forces and moments acting on the body can be obtained by the direct integration of pressure over the instantaneous wetted body surface S_w as follows:

$$\vec{F} = -\iint_{S_w} p\,\vec{n}\,ds \tag{2-43}$$

$$\vec{M} = -\iint_{S_w} p\,(\vec{r}\times\vec{n})\,ds \tag{2-44}$$

The integral over the instantaneous wetted surface S_w is then transformed into an integral over S_o the mean wetted surface of the body in its equilibrium position in calm water and the pressure p is expanded using Taylor series expansion. Subsequently, the integration on S_w is divided into two parts: the mean wetted surface S_o and the instantaneous time-dependent part ΔS_o. Hence, the second-order forces and moments are expressed as:

$$\vec{F} = -\left(\iint_{S_o} + \iint_{\Delta S_o}\right)(p + \vec{\alpha} + \ldots)\vec{n}\,ds \tag{2-45}$$

$$\vec{M} = -\left(\iint_{S_o} + \iint_{\Delta S_o}\right)(p + \vec{\alpha}\bullet\nabla p + \ldots)\vec{r}\times\vec{n}\,ds \tag{2-46}$$

where the vector $\vec{\alpha}$ is the local displacement of a point on S_w due to translational and rotational motions with respect to S_o. Gauss's theorem is then applied on both equations (2-45) and (2-46) in order to transform the surface integral into a volume integral V. The final expressions of the mean second-order force and moment are

$$\begin{aligned}\vec{F}^{(2)} = {} & -\tfrac{1}{2}\rho g \oint_{L_o}\zeta_r^{(1)2}\,\vec{n}\,dl + \tfrac{1}{2}\rho\iint_{S_o}\left(\nabla\widetilde{\Phi}^{(1)}\bullet\nabla\widetilde{\Phi}^{(1)}\right)\vec{n}\,ds + \\ & \rho\iint_{S_o}\left(\vec{\alpha}\bullet\nabla\widetilde{\Phi}_t^{(1)}\right)\vec{n}\,ds + \vec{\Omega}^{(1)}\times\vec{F}^{(1)} - \rho U\iint_{S_o}\left(\vec{\alpha}^{(1)}\bullet\nabla\widetilde{\Phi}_x^{(1)}\right)\vec{n}\,ds \\ & -\rho g\,\zeta_4^{(1)}\zeta_6^{(1)}S_{10}\,\vec{k}\end{aligned} \tag{2-47}$$

$$\begin{aligned}\vec{M}^{(2)} = {} & -\tfrac{1}{2}\rho g \oint_{L_o}\zeta_r^{(1)2}\,\vec{r}\times\vec{n}\,dl + \tfrac{1}{2}\rho\iint_{S_o}\left(\nabla\widetilde{\Phi}^{(1)}\bullet\nabla\widetilde{\Phi}^{(1)}\right)\vec{r}\times\vec{n}\,ds \\ & + \rho\iint_{S_o}\left(\vec{\alpha}\bullet\nabla\widetilde{\Phi}_t^{(1)}\right)\vec{r}\times\vec{n}\,ds + \vec{\delta}^{(1)}\times\vec{F}^{(1)} + \vec{\Omega}^{(1)}\times\vec{M}^{(1)} \\ & -\rho U\iint_{S_o}\left(\vec{\alpha}^{(1)}\bullet\nabla\widetilde{\Phi}_x^{(1)}\right)\vec{r}\times\vec{n}\,ds \\ & -\rho g\left(\zeta_2^{(1)}\left(\zeta_3^{(1)}S_{00} - \zeta_5^{(1)}S_{10}\right) + \zeta_3^{(1)}\zeta_6^{(1)}S_{10} + \zeta_5^{(1)}\zeta_6^{(1)}(S_{02} - S_{20})\right. \\ & \left.-\zeta_1^{(1)}\left(\zeta_3^{(1)}S_{00} - \zeta_5^{(1)}S_{10}\right) + \zeta_4^{(1)}\zeta_6^{(1)}(S_{02} - S_{20})\right)\end{aligned} \tag{2-48}$$

where S_{ij} is the property of the waterplane at $z = 0$ and defined as

$$S_{ij} = \iint_A x^i y^j \, dx \, dy|_{z=0} \tag{2-49}$$

The first-order relative wave elevation $\zeta_r^{(1)}$ and the steady wave elevation $\bar{\zeta}$ are defined as

$$\zeta_r^{(1)} = \zeta^{(1)} - \zeta_3^{(1)} - y\,\zeta_4^{(1)} + x\,\zeta_5^{(1)} \text{ on z = 0} \tag{2-50}$$

$$\bar{\zeta} = -\frac{1}{2g}\left(\vec{W} \bullet \vec{W} - U^2\right) \text{ on z = 0} \tag{2-51}$$

The second-order forces and moments, given in equations (2-47) and (2-48) are formed from six components and which are:

i. **The relative wave elevation**: this represents the first-order pressure field acting between the mean waterline and the instantaneous free surface. Since the square of the relative wave elevation is always a positive value, the pressure due to the relative wave elevation is acting inward on the wetted surface.

ii. **The pressure drop due to the first-order velocity field**: this is a quadratic term in Bernoulli's equation and is evaluated over the mean wetted surface. This pressure is acting outward on the wetted surface.

iii. **The product of the first-order motion and the gradient of the first-order pressure field**: in response to wave excitation, the body oscillates about its mean position. The oscillatory motions change the wetted surface of the first-order pressure field. Thus this term corrects the first-order pressure on the mean surface to that on the instantaneous surface.

iv. **The cross product of the first-order motion and the first-order force**: this term makes a correction to the direction of the first-order force during the oscillatory motion. The first-order force is the direct integration of the first-order pressure normal to the mean wetted surface, so that the force vector rotates as the body oscillates.

v. **The contribution due to the forward speed or current speed**: this is the product of the forward speed or the current speed, first-order motion and the x-component of the gradient of the unsteady velocity field. Thus this term corrects the convective effect of the unsteady velocity field due to the forward speed on the mean surface to that on the instantaneous surface.

vi. **The contribution due to the second-order motions**: this term represents changes in the buoyancy force due to second-order motions. For the mean second-order forces and moments, the second-order motions are the second-order effects of the first-order motion responses.

2.3.7 Viscous damping effects

The solving of the equations of motions, using the potential theory involved neglecting the viscous effects of the fluid on the wave forces by using the assumption that the fluid is inviscid. Chan (1992) stated that this assumption is acceptable for motions of small amplitudes and large inertia due to the neglect of the viscous effects on these motions. However, this may be of importance for surge, sway and yaw motions, where restoring forces do not exist for a moving, or relatively moving structure. Hence, to consider the viscous damping effects on the wave forces, Chan (1992) presented an empirical approach to take the viscous effect on the wave forces into account by combining the three-dimensional linearized potential technique, as described previously, with a cross – flow approach. The equation of motion using this approach, after taking into account the viscous effect can be written as

$$F_j^W + F_j^V = \sum_{k=1}^{6}\left\{\left(M_{jk} + A_{jk}\right)\ddot{\zeta}_k + B_{jk}\dot{\zeta}_k + C_{jk}\zeta_k\right\} \tag{2-52}$$

in which

F_j^W Wave exciting force in jth direction, and

F_j^V Viscous excitation force in jth direction.

The hydrodynamic coefficients in the equations of motion may be considered as having a linear dependence on the fluid forces due to the potential flow and viscous effects such as $B_{jk} = b_{jk} + \hat{b}_{jk}$ where b_{jk} and $\hat{b}_{jk}$ are the potential and the viscous damping coefficients. This approach was applied via assuming the value of the viscous damping and computing the corresponding forces and responses. The results of the application of this method are presented later in Chapter Five.

2.4 Mathematical model based on Morison's approach

In this section, a mathematical method that is based on Morison's approach (Morison et al., 1950) is used to predict the dynamic surge motion loading on and responses of a semisubmersible platform. This approach is based on Morison's equation and was presented in (Incecik, 1993), where it was applied to a Tension Leg Platform (TLP).

The approach takes into account large amplitude displacements of the platform in its responses due to steady waves, winds and currents. In addition, the approach predicts the responses due to first-and second-order forces for different approaching angles.

In the present study, the wind effect is neglected and only the head sea wave condition is examined. This is due to the limitations that the main objective of this study is the analysis of wave and current loadings and their effect on surge motion responses.

The first-order wave induced forces consist of dynamic pressure forces, acceleration forces and drag forces. The dynamic pressures and accelerations may be combined together and known as the inertia force term. In this mathematical model, the inertia and drag forces terms are calculated using the linear wave theory equations (Faltinsen, 1993).

(Incecik, 1993) used a model that consists of circular columns and pontoons while the basic model used in this study consists of a rectangular shaped deck, four square columns with round corners connected by four rectangular under-water pontoons.

Hence, in the following sections, two case studies are presented for these two structural models. The dimensions of the model with rectangular cross sections are chosen to be similar to that of the scale model used in the ocean basin experiments conducted. Additionally, the dimensions of the model with circular cross section are chosen to give same water plane areas as the rectangular model. The model experiments and test programme are presented in details in Chapter Three.

The formulas that are presented in this section are for the estimation of the surge loading and corresponding body responses for the first case study model with circular columns and pontoons. Moreover, modifications are needed in order to modify the approach in order to estimate the loading and responses of the second case study model.

2.4.1 Definition of the coordination system

In this section, a different coordination system is used than that presented in Section 2.2.1. This coordination system (o-xyz) is the structure's fixed reference system and its axes are related to each other by the right hand rule and defined as follows:

x-direction in the horizontal plane with origin $x = 0$ at the centre of the structure.

y-direction directed vertically upward (positive) with the origin $y= 0$ at the still water level

z-direction in the horizontal plane with origin $z = 0$ at the centre of the structure.

2.4.2 First-order surge wave induced forces and responses

In this section, the total dynamic wave loading on a moored semisubmersible platform with circular columns and pontoons is examined. The total wave forces are estimated as being the summation of the forces acting on the columns and pontoons members separately. The wave-induced forces consist of the dynamic pressure, acceleration forces and the drag forces. The dynamic pressure and acceleration forces are combined as one term and that is known as inertia force. In the following sub-sections, the calculations for both surge wave induced loading on the columns and on the pontoons are given.

2.4.3 First-order surge wave induced forces on circular columns

The surge wave-induced forces acting on all of the four circular columns are the inertia and the drag terms that are given in details as follows

$$F_{WC}^{S} = \sum_{i=1}^{4} \int_{-D_R}^{0} C_m \rho A_s a_x dy + \int_{-D_R}^{0} \sum_{i=1}^{4} \frac{1}{2} \rho C_D D_C \left(\frac{1}{2} H_w \omega\right)^2 e^{2\nu y} *$$

$$\cos^2(\beta)\cos(\nu x - \omega t)\,|\cos(\nu x - \omega t)|$$

$$F_{WC}^{S} = \sum_{i=1}^{4} C_m \rho \frac{\pi D_C^2}{4} \frac{1}{\nu} \left[1 - e^{-\nu D_R}\right] \sin(\nu x_i - \omega t) \cos(\beta) \left(\frac{1}{2} H_w \omega^2\right) \qquad (2\text{-}53)$$

$$+ \sum_{i=1}^{4} \frac{1}{2} \rho C_D D_C \cos(\nu\, x_i - \omega t)\,|\cos(\nu\, x_i - \omega t)| \cos^2(\beta)\, \frac{1}{2\nu} *$$

$$\left[1 - e^{-2\nu D_R}\right] \left(\frac{1}{2} H_w \omega\right)^2$$

where

A_s	Cross sectional area of the column,
a_x	Acceleration of the fluid particle,
C_D	Wave drag coefficient,
C_m	Wave inertia coefficient ,
D_R	Draft ,
H_w	Wave height ,
i	Column number,
β	Wave heading angle with x-axis,

v Wave number ,

ρ Water density,

sp Spacing between pontoons,

x_o and z_o Rigid body displacements due to current forces (and wind forces if taken into consideration), and

$$\left.\begin{aligned} X_1 &= \left(\frac{sp}{2}+x_0\right)\cos(\beta)+\left(\frac{sp}{2}+z_0\right)\sin(\beta) \\ X_2 &= \left(\frac{sp}{2}+x_0\right)\cos(\beta)+\left(-\frac{sp}{2}+z_0\right)\sin(\beta) \\ X_3 &= \left(-\frac{sp}{2}+x_0\right)\cos(\beta)+\left(\frac{sp}{2}+z_0\right)\sin(\beta) \\ X_4 &= \left(-\frac{sp}{2}+x_0\right)\cos(\beta)+\left(-\frac{sp}{2}+z_0\right)\sin(\beta) \end{aligned}\right\} \quad (2\text{-}54)$$

x_o and z_o are the total rigid body displacements in the surge and sway directions due to both steady current and wind forces if existing. Thus, in the present study, as the wind forces are neglected, and the sea states considered are for head seas only with no sway motion, then z_o vanishes and x_o to be due to the current forces only. The estimation of x_o is presented later in Section 2.4.10. The expression in equation (2-53) neglects the change in the flow around the columns due to the existence of other columns in the wave field.

2.4.4 First-order surge wave induced forces on circular pontoons

In this sub-section, the calculations for surge wave-induced forces acting on the circular pontoons are presented. Only the two pontoons parallel to y –axis would contribute to the surge forces. The first pontoon will be referred to as (LHS) and the second as (RHS) in the following calculations.

$$F_{WH}^{S} = \sum_{\mathrm{i}} C_m \rho A_s a_x \Delta x_i + \sum \frac{1}{2}\rho C_D D_H \left(\frac{1}{2}H_w\,\omega\right)^2 e^{2\nu y} * \cos^2(\beta)\cos\left(\nu x_i^{LHS,RHS} - \omega t\right)\left|\cos\left(\nu\, x_i^{LHS,RHS} - \omega t\right)\right| \Delta x_i \quad (2\text{-}55)$$

After conducting the integration, the previous equation can be re-written as follows

$$F_{WH}^{S} = \sum_{i=1}^{9} C_m \rho \frac{\pi D_H^2}{4} e^{-\nu\left(D_R - \frac{D_H}{2}\right)} \left(\sin\left(\nu x_i^{LHS} - \omega t\right) + \sin(\nu x_i^{RHS} - \omega t) \cos(\alpha)\right)\left(\frac{1}{2} H_w \omega^2\right) + \sum_{i=1}^{9} \frac{1}{2} \rho C_D D_H \cos^2(\alpha) e^{-2\nu\left(D_R - \frac{D_H}{2}\right)} \left(\frac{1}{2} H_w \omega\right)^2 * \left\{\cos\left(\nu x_i^{LHS} - \omega t\right) * \left|\cos\left(\nu x_i^{LHS} - \omega t\right)\right| + \cos\left(\nu x_i^{RHS} - \omega t\right)\left|\cos\left(\nu x_i^{RHS} - \omega t\right)\right|\right\} \quad (2\text{-}56)$$

The summation in equation (2-56) is conducted by subdividing the length of each pontoon into eight sections of equal length and by applying the Simpson's integration rule. Thus, the total surge force on the structure is calculated as follows

$$F^S = F_{WC}^S + F_{WH}^S \quad (2\text{-}57)$$

2.4.5 First-order surge wave responses

The surge response of the platform about a displaced position due to steady sinusoidal wave can be obtained from the solution of the surge equation of motion as a single degree of freedom system and that is written as follows

$$(M + M_{AVM})\ddot{X} + C\,\dot{X} + K\,X = F^S \quad (2\text{-}58)$$

Hence, solving the previous equation results in the surge response is as follows

$$X_{wave} = \frac{F^S}{K_X} * Q \quad (2\text{-}59)$$

where

$$Q = \frac{1}{\sqrt{\left(1 - r_s^2\right)^2 + (2 r_s d)^2}} \quad 2\text{-}60)$$

$$r_S = \frac{\omega}{\omega_{n\,surge}} \quad (2\text{-}61)$$

X_{wave} The rigid body displacements due to wave forces, and

d damping ratio ($d = \frac{C}{C_{cr}}$ and $C_{cr} = \sqrt{2\,K_x\,M}$)

2.4.6 Surge response spectrum

The formulas given in the previous section are for the wave loading and body responses for platforms in regular waves. As for structures in irregular waves, the corresponding surge response is estimated by means of spectral analysis, which depends on the

irregular wave spectrum *S(ω)*. Response Amplitude Spectrum $R_S(\omega)$ is estimated as follows

$$R_S(\omega) = S(\omega) * RAO^2 = S(\omega) * \left(\frac{X}{\frac{1}{2}H_w}\right)^2 \quad (2\text{-}62)$$

2.4.7 Steady and dynamic responses to second-order wave forces

The second-order forces consist of two components; the steady and the slowly varying components. In this sub-section, both of these components and the corresponding body responses are presented. The importance of the second-order forces is that due to the very low damping at the low frequency region near the surge natural frequency, these forces would result in large motion amplitudes.

The peak of the low frequency force spectrum coincides with the surge natural frequency and the hydrodynamic damping in the natural frequency region is very low. Thus the oscillations due to the second-order waves contribute significantly to the total lateral displacement of these platforms.

2.4.8 Steady drift forces and responses

The steady component of the second-order drift force of the surge motion mode $\overline{F_R}$ is calculated via an approached that was presented in (Remery and Hermans, 1971). This approach estimated the drift forces as a function of a reflection function, cylinder diameter, and wave height as follows

$$\overline{F_R} = \frac{1}{2}\,\rho\, g(D_C)\left(\frac{1}{2}H_w\right)^2 R^2(\omega) \quad (2\text{-}63)$$

In addition, the corresponding steady surge response x_{SD} is estimated as

$$\mathrm{X_{SD}} = \frac{\overline{F_R}}{\mathrm{K_X}} \quad (2\text{-}64)$$

where the drifting force (reflection) coefficient is estimated by (Chakrabarti, 1984) as

$$R^2(\omega) = \frac{1}{\pi^2\left(\frac{k\,D_C}{2}\right)^3}\sum_{n=0}^{\infty}\frac{1}{A_n A_{n+1}}\left[1 - \frac{n(n+1)}{k\,\frac{D_C}{2}}\right]^2 \quad (2\text{-}65)$$

in which

$$A_n = \acute{J}_n^2\left(k\frac{D_C}{2}\right) + \acute{Y}_n^2\left(k\frac{D_C}{2}\right) \quad (2\text{-}66)$$

$$2\acute{J}\left(k\frac{D_C}{2}\right) = J_{n-1}\left(k\frac{D_C}{2}\right) - J_{n+1}\left(k\frac{D_C}{2}\right) \quad (2\text{-}67)$$

$$2\acute{Y}_n\left(k\frac{D_C}{2}\right) = Y_{n-1}\left(k\frac{D_C}{2}\right) - Y_{n+1}\left(k\frac{D_C}{2}\right) \quad (2\text{-}68)$$

where J_n and Y_n are Bessel functions of the First and Second kind respectively.

2.4.9 Slowly varying drift force spectrum and response

For irregular waves, the slowly varying drift force spectrum $S_F(\mu)$ at a specific frequency μ is estimated based on the wave spectrum of the irregular wave environment $S(\omega)$ as follows

$$S_F(\mu) = 2\,\rho^2 g^2 * 4{D_C}^2 \int_0^\infty S(\omega)S(\omega+\mu)R^4\left(\omega+\frac{\mu}{2}\right)d\omega \quad (2\text{-}69)$$

$$R_S(\mu) = S_F(\mu)(RAO)^2 \quad (2\text{-}70)$$

As seen from the previous equations (2-69) and (2-70) , the slowly varying drift force spectrum depends on the wave spectrum of the irregular wave environment. Different irregular wave spectra were generated using the JONSWAP spectrum (Faltinsen, 1993). The waves used in this study are (H6, T12), (H12, T12), (H7.5, T15) and (H15, T15). The JONSWAP spectra for these waves are shown in Figure 2-2.

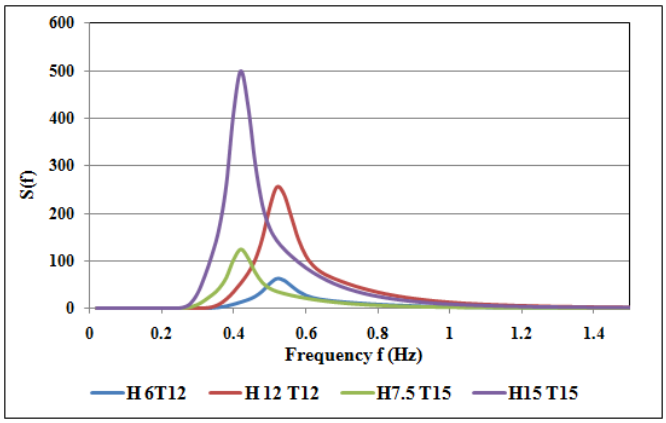

Figure 2-2 Irregular wave JONSWAP spectra

Alternative way to estimate the slowly varying drift force spectrum $S_F(\mu)$ is defined as

$$S_F(\mu) = 8\int_0^\infty S_\zeta(\omega)S_\zeta(\omega+\mu)\left[\frac{F^{(2)}(\omega,\omega+\mu)}{\zeta_a^2}\right]^2 d\omega \quad (2\text{-}71)$$

where the term in brackets represent the second-order forces per wave amplitude squared in regular waves.

2.4.10 Current surge forces and responses

The current may affect the marine structure from any direction. Hence, the current forces may induce steady force components in both the surge and sway directions. In this study, the current is assumed to approach the semisubmersible with angle of zero degrees. For other values of approaching angles, the current forces can be simply converted into surge and sway components.

The value of the surge force component depends on the current velocity, the dimensions of the underwater pontoons and it can be estimated as follows:

$$F^{s}_{current} = \frac{1}{2}\rho C_D \,(4\, D_c\, d + 4\, D_H\, L)\mathrm{U}^2 \tag{2-72}$$

Moreover, the steady surge displacement due to current force $x^{s}_{current}$ which is the only components of x_o is calculated as:

$$x^{s}_{current} = \frac{F^{s}_{current}}{\mathrm{K_x}} \tag{2-73}$$

2.4.11 Viscous drift forces on vertical columns

(Standing and Dacunha, 1982) and (Chakrabarti, 1984) gave a formula to be used in order to estimate the steady wave induced component of the viscous drift forces acting on vertical circular section cylinders of radius *a* , in the absence of a current as follows

$$\bar{F}_D = \frac{4\pi}{3}\, C_D \rho g\, \nu\, a\, \zeta_a^3 \tag{2-74}$$

The above expression shows that the steady component is proportional with the cube of the wave particle amplitude and it may be used as an approximation for the calculation of the viscous drift forces on the rectangular columns of the test example semisubmersible by use of the rectangular breadth as the characteristics dimension of the column instead of the diameter. Subsequently, the value of the drag coefficient would change to match the shape of the column cross sectional area.

The same expression was also given in (Pinkster and Van Oortmerssen, 1977). This expression was obtained via direct pressure integration from z = 0 to the instantaneous

free surface elevation gives the mean value of the horizontal drag force on a vertical column while the integration from $z = -\infty$ to the mean water surface vanished.

2.5 Summary

This chapter presented the two mathematical methods that are to be employed in this thesis order to estimate the first and second-order forces acting on a semisubmersible structure. The results obtained from these methods are to be presented later in Chapter Five. In addition, these results are to be compared as well with the results obtained from experimental tests.

Chapter 3. Model Experiments

3.1 Introduction

One of the main objectives of this study is to investigate the slowly varying forces and the corresponding rigid body motion responses of a moored semisubmersible platform in high sea states. To achieve this, a series of model scale experimental tests at different sea states and using different model mooring set-up arrangements were conducted. A description of the employed model, set-up of the experiments, analysis methods of measurements and of the results are presented in this chapter.

The experiments were conducted in the ocean basin in MARINTEK, Trondheim, Norway. The ocean basin dimensions are 80 m x 50 m and maximum depth is 10m. A sketch of the ocean basin and location of the wave makers is shown in Figure 3-1.

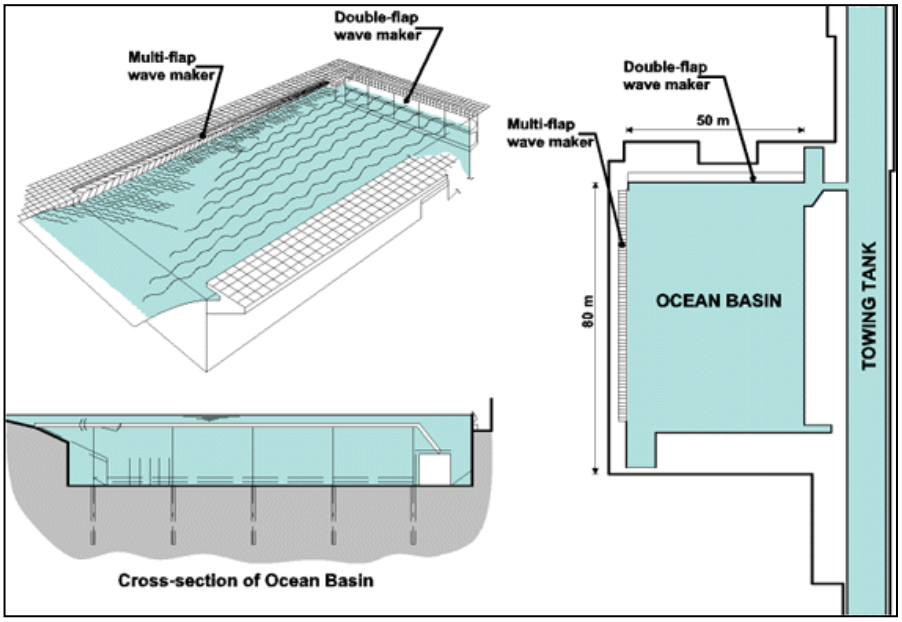

Figure 3-1 MARINTEK ocean basin (MARINTEK, 2011)

The ocean basin has two wave makers. The first wave maker is a multi-flap device, and which is electronically driven. It consists of 144 individually controlled flaps and is installed on the long side of the basin. The second device is a double-flap wave maker, which is hydraulically driven and can generate regular waves of maximum height of 0.9 m, and having a wave period of 0.8 s and above, and also produce a maximum current velocity of approximately 0.2 m/s at a water depth of 5 m. The second wave maker is the one that was used in the experiments described here.

3.2 Model description

The employed model is of a semisubmersible platform with four square columns with rounded corners and rectangular four pontoons. The tests were thus conducted with a 1/50 scale model in the equivalent of 250 m water depth (full-scale). The main full-scale geometrical characteristics of the actual semisubmersible are given below in Table 3-1 and a photograph of the scale model is shown in Figure 3-2.

Table 3-1 Geometrical Characteristics of the semisubmersible (full-scale values)

Length /breadth outside pontoons(m)	84.48
Height to upper deck(m)	54.8
Breadth of pontoons(m)	16.64
Height of pontoons(m)	8.4
Column length (m)	16.64
Column breadth(m)	16.64
Column corner radius (m)	4.8
Draught (m)	21
Displacement (tonne)	55867
Water depth (m)	250

Figure 3-2 The semisubmersible scale model

3.3 Test programme

The main scope of the experiments was to study the model responses in several sea states using two different mooring systems; namely alternatively horizontal and catenary mooring lines. Horizontal mooring system is where the structure is moored using horizontal springs that are attached to the structure above the water surface level. Such a system does not have practical usage. However, the investigation of the responses of the structure moored with horizontal springs can be studied as being influenced by the damping of only the hull. Hence, differences between the responses of the semisubmersible model when moored via horizontal springs to those when moored using catenary mooring system are considered due to the mooring lines.

Thus, the first part of the calibration tests is to calibrate the characteristics of the artificially generated waves and currents used in the experiments before installing the model in water. The second part of the calibration tests was aimed to identify the main

characteristics of the two behaviour of the mooring system. The first part was conducted by calibration tests for regular and irregular waves and for the currents. The second part was achieved by conducting static-pull out tests and decay tests. Afterwards, the test programme focused on measuring the model responses in regular and irregular waves, in both cases both with and without a current.

The test programme can be thus classified into the following groups: environmental calibration tests (for current and both regular and irregular waves), decay tests, static pullout tests, the effects of regular waves (with and without current), and the effects of irregular waves (with and without current).

3.3.1 Location of wave and current gauges

Three wave gauges and one current gauge were installed in the ocean basin in order to be able to measure the time variation of the waves and the current during the calibration tests. Each test duration time was equivalent of three hours in the full scale. The locations of these gauges are illustrated in Figure 3-3 . As for the model, four relative wave height gauges were attached to the hull columns. The relative wave height gauges measure the wave height with respect to the mean water surface level. Their locations in the horizontal (X-Y) plane are illustrated in Figure 3-4. In addition to the measurements from the four relative wave heights gauges, the restoring force, mooring line tensions, and the six degrees of freedom motions at the model's centre of gravity were recorded as well.

3.3.2 Definition of the coordinate system

A fixed co-ordination system origin at the basin's centre is used for the data collected. The definitions of the positive axes of the co-ordination system are as follows:

X-direction orthogonal to the axis of the wave generators, with x=0 at the basin centre and with the positive x-direction from the basin centre towards the generators.

Y-direction in the horizontal plane parallel to the axis of the generators with the origin y=0 at the basin centre and with the positive y direction to the left when looking from the basin centre along the x-axis opposite to the multi-flap wave generators.

Z-direction directed vertically downward (positive) with z=0 located at the still water surface.

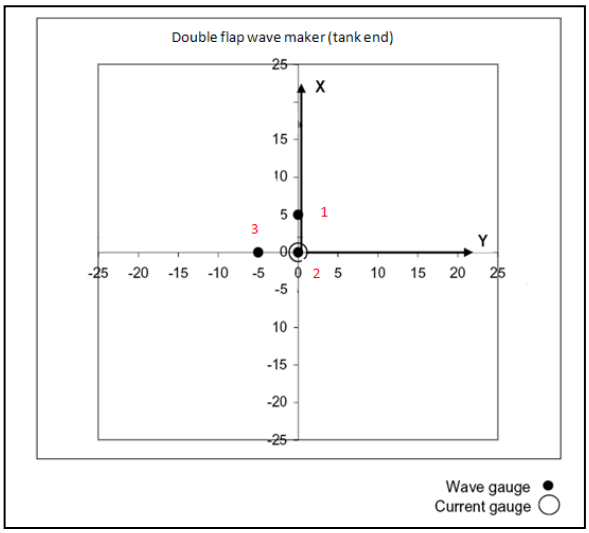

Figure 3-3 Locations of wave and current gauges

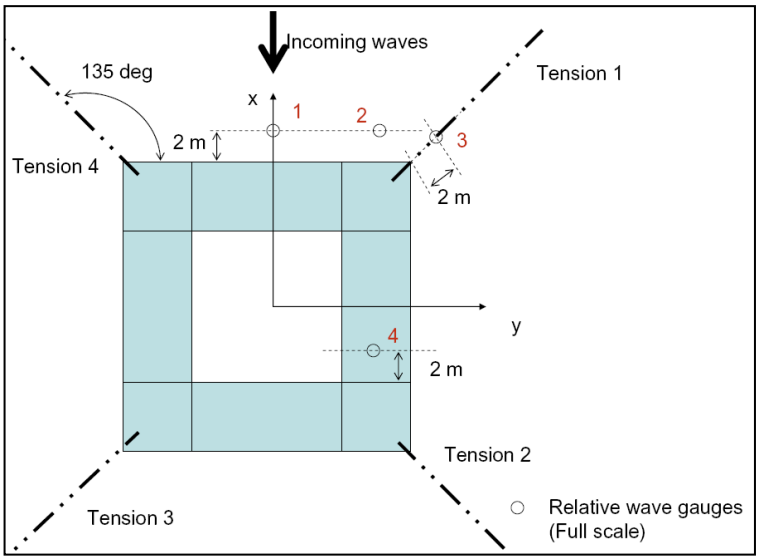

Figure 3-4 Location of relative wave height gauges

3.3.3 Mooring systems

The tests were conducted using two different mooring systems; a horizontal mooring system (HOR MOR) and a catenary mooring system (CAT MOR). In both systems, the model was held in position using four mooring lines, which were attached to the corner of each column. The attachment points are at the still water surface level. The tests with horizontal and catenary mooring lines aimed at identifying the effect of damping due to the mooring lines on the motions of the semisubmersible in waves and in waves and current. The horizontal mooring system was designed so that stiffness of the whole system was k= 144.8 kN/m leading to a natural surge period of 146 s which is determined via the surge decay test. The characteristics of each of the two mooring

systems were determined by the static pullout tests, which will be presented in a separate section later in this chapter. The vertical profile of the full scale catenary mooring lines is shown in Figure 3-5. This figure shows the true shape in the plane of each mooring line. For the catenary mooring system, each of the mooring lines consisted of three segments of wires and chains. The characteristics of these segments such as; diameter, length are given later in Chapter Four.

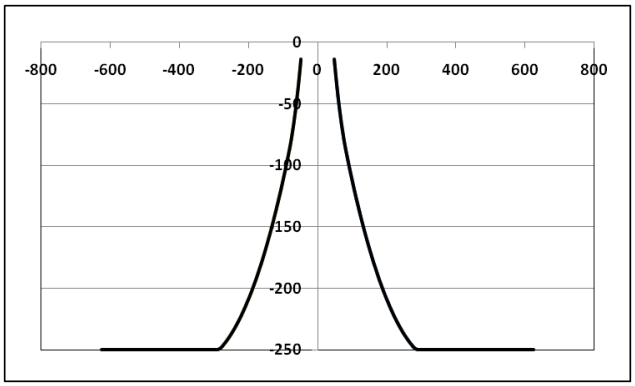

Figure 3-5 The vertical profile of the catenary mooring system

3.3.4 Environmental calibration

Environmental calibration tests were conducted to verify the repeatability of the basin's capability and to check the characteristics of the waves/current generated by the wave maker (while the model is not in the basin yet and thus not affected by the physical presence of the model). The calibration tests were for current only, for the regular wave (REG), and for the irregular (IRR) wave.

3.3.4.1 Current calibration

Two current speeds U were created and used in the tests, which are 0.6 and 1.2 m/s. The calibration tests numbers for these speeds are Test 8304 and Test 8313, respectively. For each of these tests, the current speed was recorded by the current gauge shown in Figure 3-3. The mean values and standard deviations of the recorded current velocity for the tests 8304 and 8313 are 0.63, 0.07, 1.23, and 0.13 respectively.

3.3.4.2 Regular waves calibration

Several regular waves were used either alone or combined with one of the current velocities (0.6 and 1.2 m/s). These waves were calibrated before installing the model to check their fundamental characteristics. Two wave heading angles were used; zero and 45 degrees. The 45 degrees case study was obtained by rotating the semisubmersible model and the mooring system. A summary of the regular wave tests with zero wave heading is given in Table 3-2. The following notation is used to describe the sea state conditions: H for wave height for regular waves and significant wave height for irregular waves, T for average mean zero crossing wave period and U for current velocity.

Table 3-2 Regular waves calibration tests

Test	H (m)	T (sec)	U (m/sec)	Test	H (m)	T (sec)	U (m/sec)	Test	H (m)	T (sec)	U (m/sec)
8212	5	10	0	8251	5	10	0.6	8291	5	10	1.2
8220	10	10	0	8261	10	10	0.6	8300	10	10	1.2
8230	11	15	0	8271	11	15	0.6	8410	11	15	1.2
8241	22	15	0	8280	22	15	0.6	8421	22	15	1.2
8430	33	15	0								

During each of the these tests, the wave gauges as specified and shown in Figure 3-3 and named wave 1, wave 2 and wave 3, recorded the time variation of the wave that was generated by the wave maker at the three points in the ocean basin.

The recorded times series of the calibration tests were analyzed using Fourier analysis and which gave the minimum value, the maximum value, the amplitude and period of zero harmonic motion, the amplitude and period of first harmonic motion, and the amplitude and period of second harmonic motion. From the Fourier analysis, it was found that the second harmonic motions were small and almost zero while the amplitude of the first harmonic motion equalled half the wave height and the period of the first harmonic equals the period of the wave.

3.3.4.3 Irregular wave calibration

Four main irregular sea states were used in this study in combination with two different current velocities. A summary of the fundamental characteristics of the irregular waves is given in Table 3-3, where IRR stands for irregular waves.

Table 3-3 Irregular waves calibration tests

Test	H (m)	T (sec)	U (m/sec)	Test	H (m)	T (sec)	U (m/sec)	Test	H (m)	T (sec)	U (m/sec)
8010	7.5	15	0	8030	7.5	15	0.6	8050	7.5	15	1.2
8020	15	15	0	8040	15	15	0.6	8060	15	15	1.2
8071	6	12	0	8090	6	12	0.6	8111	6	12	1.2
8081	12	12	0	8101	12	12	0.6	8121	12	12	1.2

The calibration process of the irregular waves that was performed by the MARINTEK team was conducted by converting the measured wave time series into spectra plots in frequency domain. The obtained spectra plots are shown in Figures 3-6 to 3-17 inclusive.

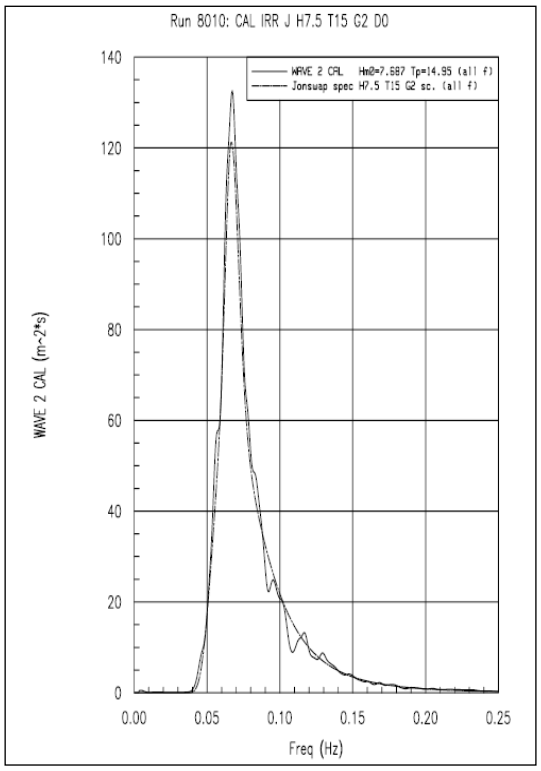

Figure 3-6 Test 8010 CAL IRR (H7.5, T15)

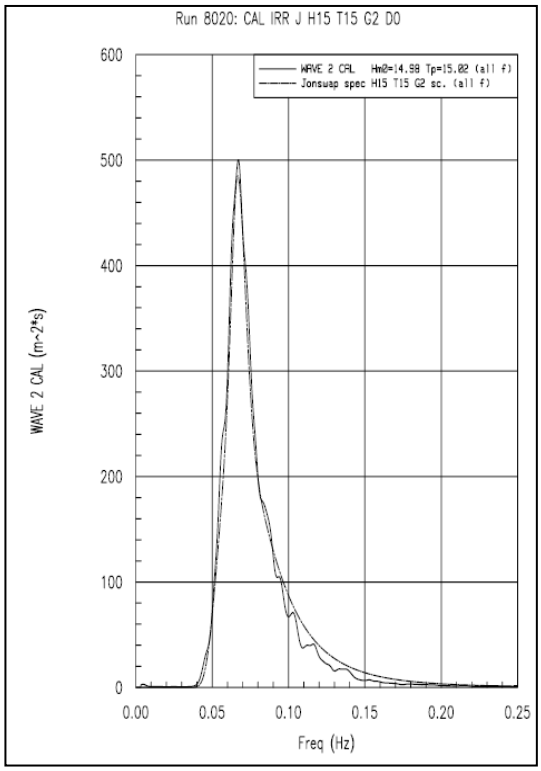

Figure 3-7 Test 8020 CAL IRR (H15, T15)

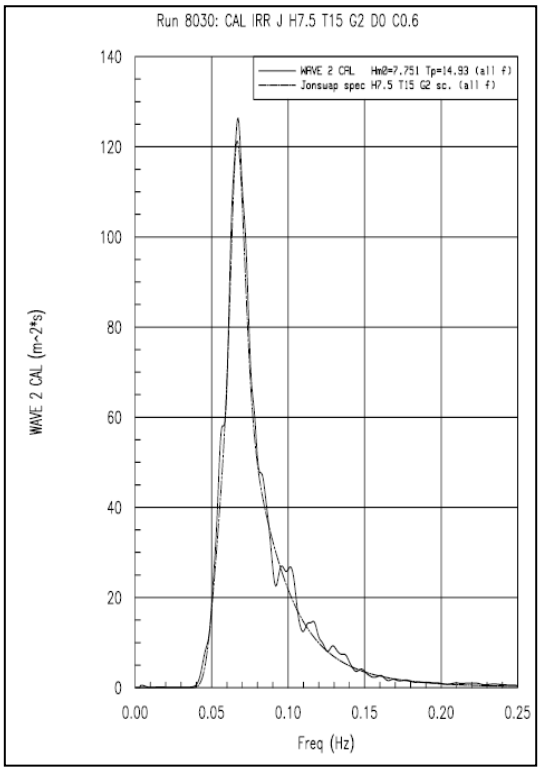

Figure 3-8 Test 8030 CAL IRR (H7.5,T15,U 0.6)

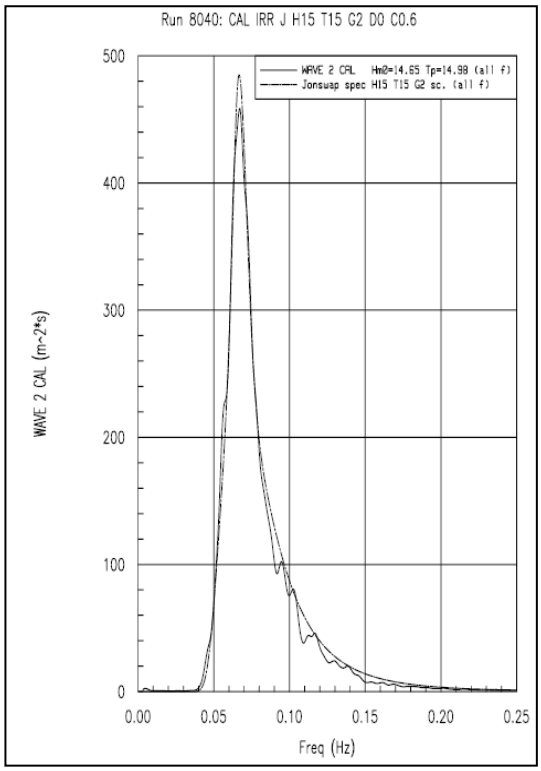

Figure 3-9 Test8040 CAL IRR (H15, T15, U 0.6)

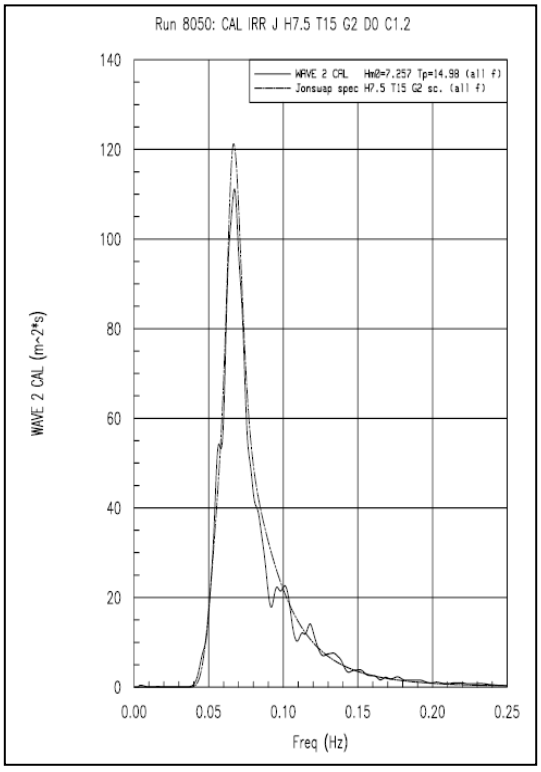

Figure 3-10 Test8050 CAL IRR (H7.5,T15,U1.2)

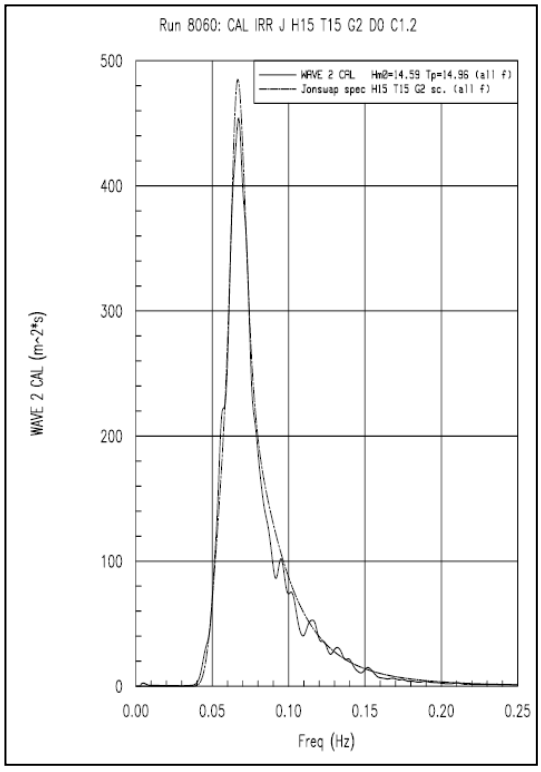

Figure 3-11 Test8060 CAL IRR (H15,T15,U 1.2)

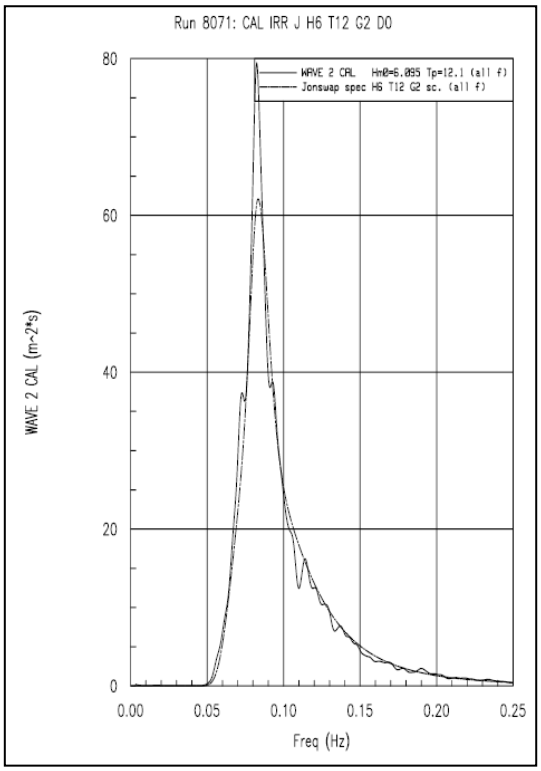

Figure 3-12 Test 8071 CAL IRR (H6, T12)

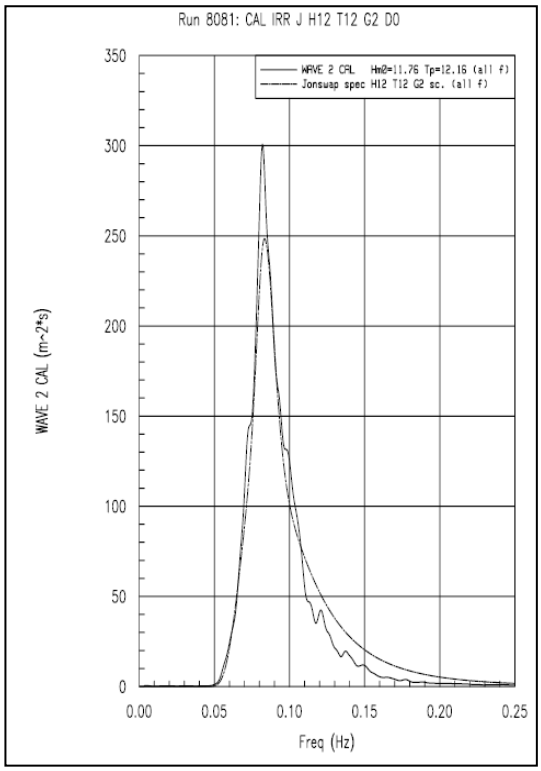

Figure 3-13 Test 8081 CAL IRR (H12, T12)

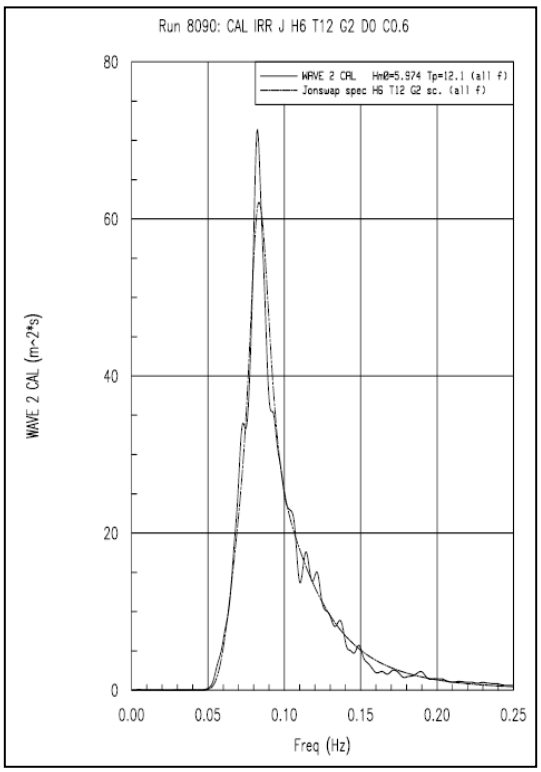

Figure 3-14 Test 8090 CAL IRR (H6, T12,U 0.6)

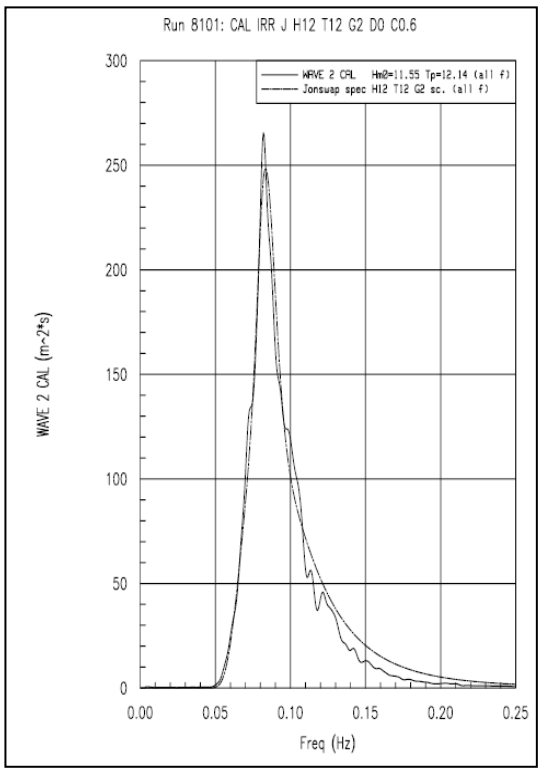

Figure 3-15 Test8101 CAL IRR (H12,T12, U0.6)

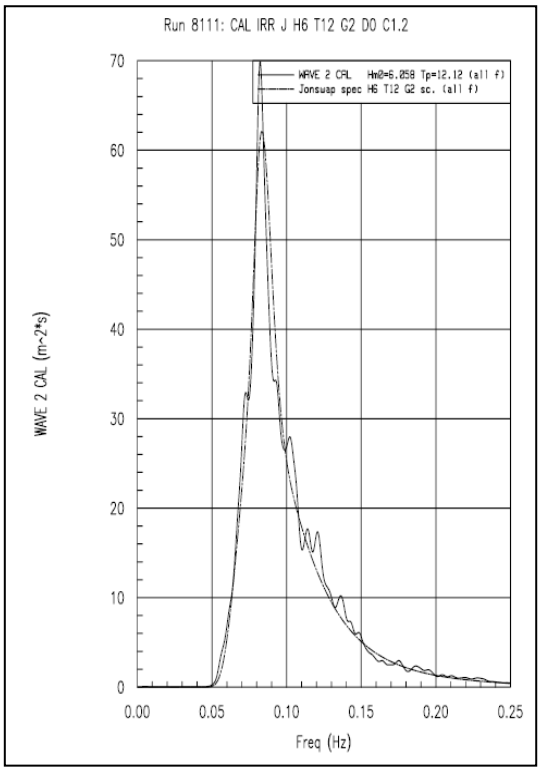

Figure 3-16 Test 8111 CAL IRR (H6,T12,U 1.2)

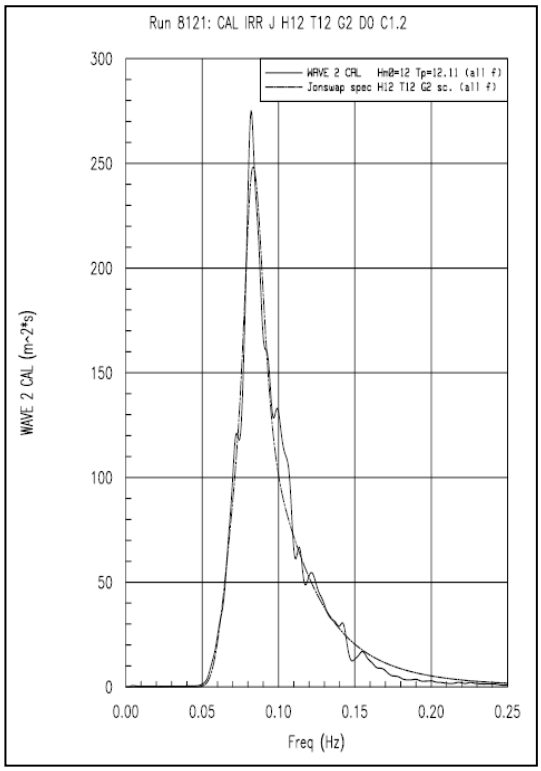

Figure 3-17 Test8121 CAL IRR (H12,T12,U 1.2)

3.3.4.4 Static pull-out tests

Static pull-out tests were performed after the placement of the structure in the basin. The purpose of these tests was to identify the characteristics of the two mooring systems that were investigated (horizontal and catenary mooring lines) and undertaken by moving the model a specific distance and measuring the corresponding restoring force in the same direction. This test was carried out in three cases; a static pull-out test in the surge direction using the catenary mooring system (Test 1010), a static pull-out test in the surge direction using the horizontal mooring system (Test 1310), and due to the symmetry of the semisubmersible structure, one static pull-out test in a diagonal 45-degree direction using the horizontal mooring system (Test 1320). Figure 3-18 shows the results of the measurements of the restoring force versus the surge displacement for both the horizontal and catenary mooring systems.

The horizontal system was designed so that the stiffness of the horizontal mooring system would match that of the catenary system as closely as possible. However, there is a difference due to the non-linear nature of the stiffness of the catenary mooring system. The effect of the different stiffnesses of the two systems is taken into consideration in the calculations presented in Section 3.5.4.

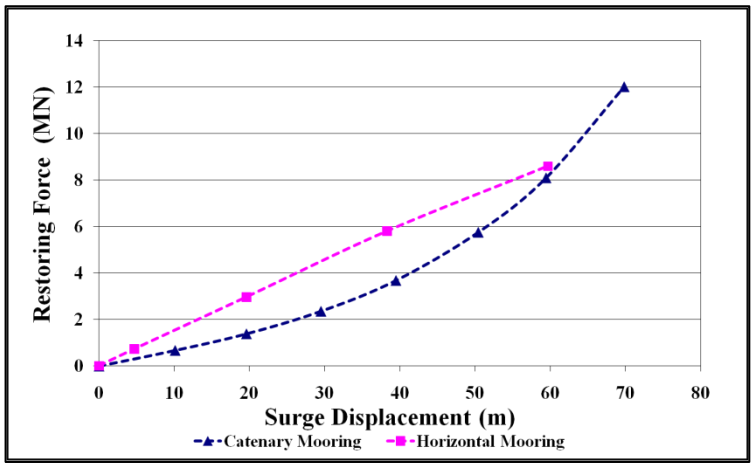

Figure 3-18 Restoring force versus surge displacement for horizontal and catenary mooring system

3.3.4.5 Decay tests

Several decay tests were conducted in both still water and in current conditions in order to determine the natural frequencies and relative damping coefficients for both mooring systems and that will be experienced in different sea conditions and in several motion directions. A list of the decay tests that were performed is given in Tables 3-4 and 3-5. Decay tests of sway and roll motions were not needed due to the symmetry of the model hull and the fact that only wave conditions were limited to only following seas.

Table 3-4 List of the decay tests with horizontal mooring system

Test number	Test Description
1410	Decay surge diagonal 45 degree
1420	Decay surge
1430	Decay heave
1440	Decay pitch
1450	Decay yaw
1510	Decay surge in mean current velocity of 1.2 m/s
1520	Decay pitch in mean current velocity of 1.2 m/s
1530	Decay yaw in mean current velocity of 1.2 m/s
1610	Decay surge in mean current velocity of 0.6 m/s

Table 3-5 List of the decay tests with catenary mooring system

Test number	Test Description
1110	Decay surge
1120	Decay heave
1130	Decay pitch
1140	Decay yaw
1210	Decay surge in mean current velocity of 1.2 m/s
1220	Decay pitch in mean current velocity of 1.2 m/s
1230	Decay yaw in mean current velocity of 1.2 m/s

Figure 3-19 to Figure 3-33 inclusive show the recorded time series of the decay tests. Some of the tests were repeated two times or more in order to ensure the accuracy of the measurements. These time series measurements are used in Section 3.3.5 in order to estimate the relative damping ratios

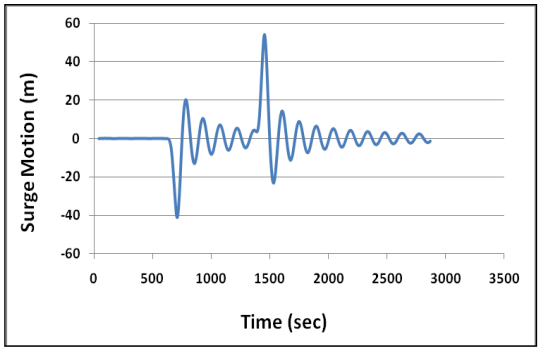

Figure 3-19 Surge decay in still water with horizontal mooring system

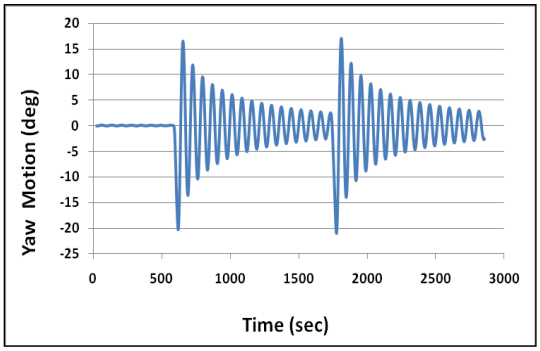

Figure 3-22 Yaw decay test in still water with horizontal mooring system

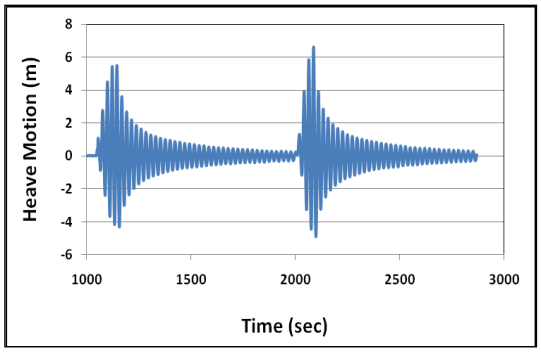

Figure 3-20 Heave decay test in still water with horizontal mooring system

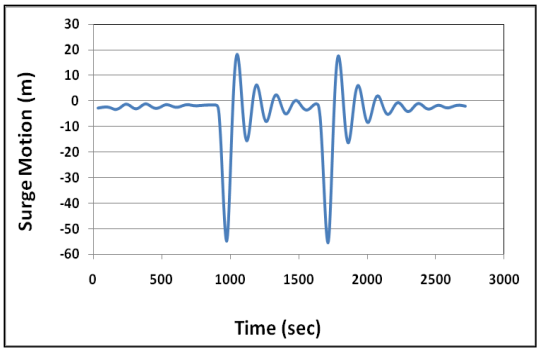

Figure 3-23 Surge decay test in current U = 0.6 m/s with horizontal mooring system

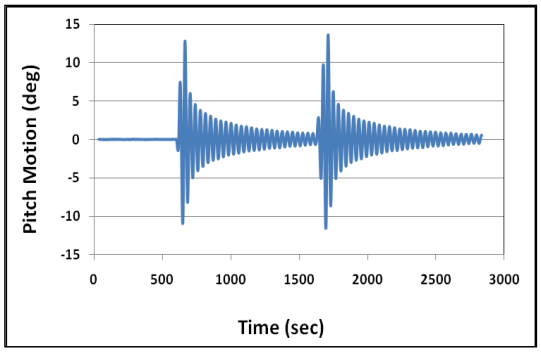

Figure 3-21 Pitch decay test in still water with horizontal mooring system

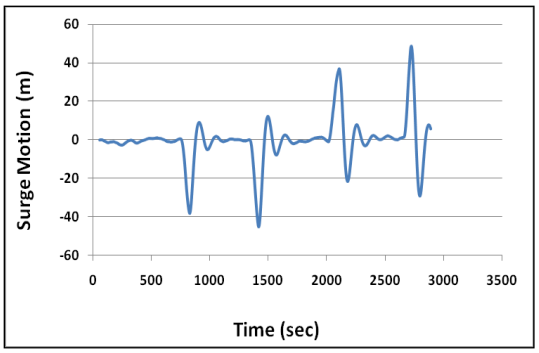

Figure 3-24 Surge decay test in current U= 1.2 m/s with horizontal mooring system

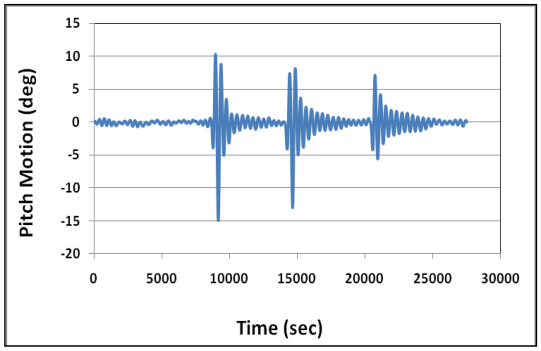

Figure 3-25 Pitch decay test in current U= 1.2 m/s with horizontal mooring system

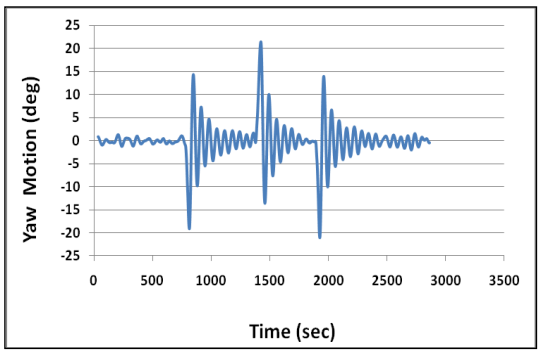

Figure 3-26 Yaw decay test in current U= 1.2 m/s with horizontal mooring system

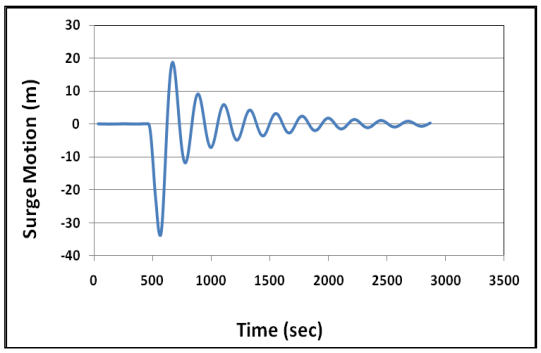

Figure 3-27 Surge decay test in still water with catenary mooring system

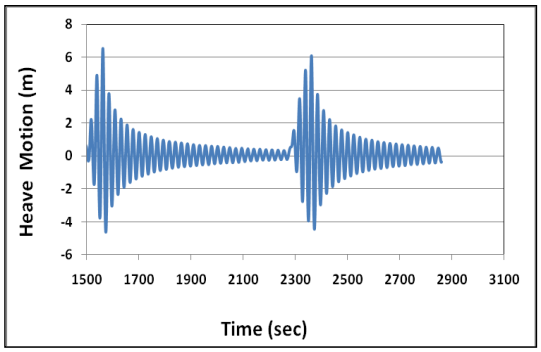

Figure 3-28 Heave decay test in still water with catenary mooring

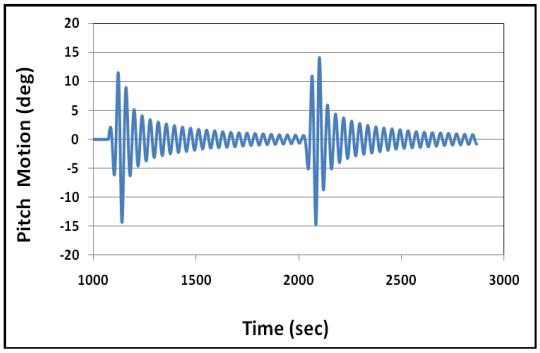

Figure 3-29 Pitch decay motion in still water with catenary mooring system

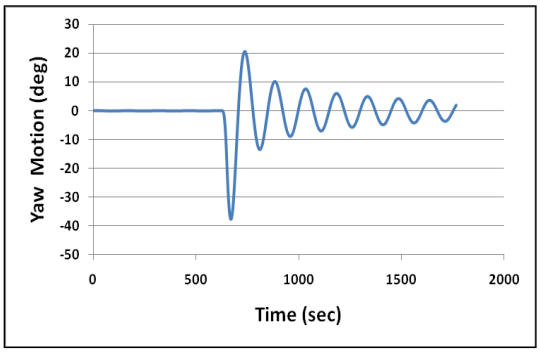

Figure 3-30 Yaw decay in still water with catenary mooring system

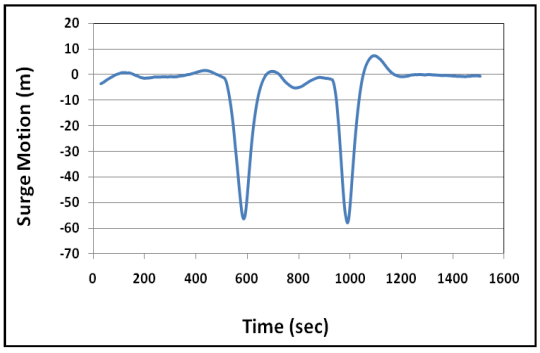

Figure 3-31 Surge decay test in current U= 1.2 m/s with catenary mooring system

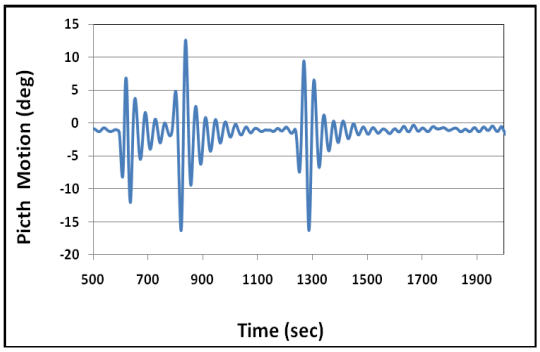

Figure 3-32 Pitch decay test in current U= 1.2 m/s with catenary mooring system

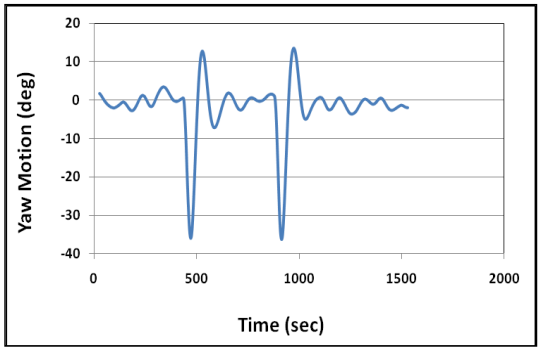

Figure 3-33 Yaw decay test in current U= 1.2 m/s with catenary mooring system

3.3.5 Relative damping calculations

The relative damping is the ratio between the damping to the critical damping at which the resonance phenomena occurs. In this section, two numerical methods that can be employed to estimate the damping ratios are presented. The first method is based on the logarithmic decrement method and is used to calculate the damping ratios as a function of the motion amplitude. In the second method, a single value of the damping ratio is calculated based on the peaks of the decay motion time series.

3.3.5.1 The logarithmic decrement method

The time series data obtained from the decay tests previously described was analyzed using the logarithmic decrement method in order to obtain the damping ratio. This method was presented in (Hearn and Tong, 1989) and was used to calculate the wave drift damping of tankers, barges and semisubmersibles. However, only the results for the tankers and barges were presented. This method defines the damping ratio as

$$\kappa = \frac{P}{P_{cr}} = \frac{\delta}{\sqrt{\pi^2 + \delta^2}} \quad , \quad \delta = \ln\left(\frac{Y_i}{Y_{i-1}}\right) \tag{3-1}$$

where

κ damping ratio,

P linear damping coefficient,

P_{cr} critical damping coefficient,

Y_i *and* Y_{i-1} two succeeding amplitudes at a time interval of $T_d/2$ and

Td zero-crossing period of oscillations.

Thus, the damping ratios can be estimated as a function of the motion amplitude (Y_{mean}) which is defined as the mean of amplitudes of two successive half cycles. A detailed study of the results of this method and a discussion of the current speed effect on the values of the damping rations is presented later in this chapter in Section 3.5.4.

3.3.5.2 Exponential approximation method

In this method, a single value of the damping ratio is calculated for each sea state. The peaks of the decay motion are approximated as an exponential function. The constant value of the exponential is $\eta\ \omega$. Thus, η can be calculated after estimating the damping frequency. This exponential function is defined as follows

$$X(t) = a\, e^{-\zeta \omega_d t} \tag{3-2}$$

where

X(t) decay motion amplitude,

a motion amplitude,

η damping ratio, and

ω_d damping natural frequency.

3.3.5.3 Natural Frequencies and damping ratios

From the time series of the decay tests, previously shown in Figure 3-19 to Figure 3-33 inclusive, the period of motion of each test is estimated. In addition, the damping ratios are calculated based on the exponential method previously described in Part 3.3.5.2 of the current section. Results for both horizontal and catenary mooring systems are summarized in Table 3-6 and Table 3-7.

.

Table 3-6 Motion periods and damping ratios using horizontal mooring system

Test number	Motion	Motion period	Damping ratio
1420	Surge HOR M	146 seconds	0.02
1610	Surge U 0.6 HOR M	145 seconds	0.138
1510	Surge U 1.2 HOR M	145 seconds	0.23
1430	Heave HOR M	23 seconds	0.029
1450	Yaw HOR M	72 seconds	0.023
1530	Yaw U1.2 HOR M	67 seconds	0.064
1440	Pitch HOR M	37 seconds	0.024
1520	Pitch U1.2 HOR M	36.5 seconds	0.068

Table 3-7 Motion periods and damping ratios using catenary mooring system

Test number	Motion	Motion period	Damping ratio
1110	Surge CAT M	220 seconds	0.07
1210	Surge U 1.2 CAT M	not enough data points available	
1130	Pitch CAT M	39 seconds	0.055
1220	Pitch U 1.2 CAT M	36 seconds	0.149

3.4 Main Experiments

The main experiments in the test programme can be classified in different ways. Two mooring systems were examined; namely horizontal and catenary mooring lines. Two current speeds (0.6 and 1.2 m/s) were used in combined wave-current tests in addition to tests with no current and current only tests. The waves used were both regular and irregular. During all main experiments the following measurements are recorded: relative wave height at four points on the model hull (the locations of relative wave gauges are shown in Figure 3-4, tension force in each of the four mooring lines, and the six degrees of freedom motions. Summaries of the set-ups in the main tests in currents, regular waves and irregular waves are given in Table 3-8 to 3-10 inclusive, respectively.

Table 3-8 Current only tests

Test number	Current speed (m/s)	Mooring system
5110	1.2	CAT MOR
6110	0.6	HOR MOR
6210	1.2	HOR MOR
7120	1.2	HOR MOR at wave heading 45-degrees

Table 3-9 Regular wave tests in following seas

Catenary Mooring				Horizontal Mooring			
Test	H	T	U	Test	H	T	U
2010	5	10	--	3010	5	10	--
2022	10	10	--	3020	10	10	--
2030	11	15	--	3030	11	15	--
2040	22	15	--	3040	22	15	--
2050	33	15	--	3050	33	15	--
2110	5	10	1.2	3110	5	10	0.6
2120	10	10	1.2	3120	10	10	0.6
2130	11	15	1.2	3130	11	15	0.6
2140	22	15	1.2	3140	22	15	0.6
				3210	5	10	1.2
				3220	10	10	1.2
				3230	11	15	1.2
				3240	22	15	1.2
				4010	10	10	--
				4020	22	15	--
				4110	10	10	1.2
				4120	22	15	1.2

Table 3-10 Irregular waves tests

Catenary Mooring				Horizontal Mooring			
Test	H	T	U	Test	H	T	U
5010	6	12		6010	6	12	--
5020	12	12		6020	12	12	--
5021	12	11		6030	7.5	15	--
5030	7.5	15		6040	15	15	--
5040	15	15					
5120	6	12	1.2	6120	6	12	0.6
5130	12	12	1.2	6130	12	12	0.6
5140	7.5	15	1.2	6140	7.5	15	0.6
5150	15	15	1.2	6150	15	15	0.6
				6220	6	12	1.2
				6230	12	12	1.2
				6240	7.5	15	1.2
				6250	15	15	1.2
				7010	15	15	D45
				7130	15	15	D45 C1.2

3.5 Results and Discussion

3.5.1 Time series results

During the experiments in irregular waves, the six degrees of freedom motion responses and corresponding mooring line tensions were recorded. The test programme can be classified into two main groups according to the wave-heading angle, which were zero (i.e. following seas) and 45 degrees. In the case of the 45 degrees, it does not matter whether the 45 degrees angle is with starboard or port side of the vessel due to the symmetry of the structure and the mooring system arrangements. The recorded data was first low-pass filtered at 20 Hz using an analogue filter and afterwards it went through a low-pass filter at 15 Hz using a digital filter to remove any noise from the readings. Figure 3-34 to Figure 3-37 inclusive show the time series of surge responses in waves alone, and with combined waves and current made using both horizontal and catenary mooring lines, as a sample of the large amount of the recorded time series data. In the next sections, these time series data from the regular wave tests are analyzed in order to estimate the wave drift coefficients.

In addition, the irregular wave time series data was used to investigate the effects of the mooring lines on motion forces and responses, on mooring line damping, and the effect of current velocity on system damping in different sea states. Furthermore, a study of the contribution of the mooring system to the low-frequency motions of a semisubmersible in combined irregular wave and current is presented in Section 3.5.5 . Since the main part of the test programme was undertaken in following seas, this study

focuses on the surge motion and responses in different sea states. The data from other motions is used as and when needed. For the tested sea states, the time series of the motion responses were filtered into both low frequency and high- frequency motions and it was found that the low-frequency motions are the more dominant.

3.5.2 Surge wave drift coefficients

The drift coefficient is defined as the force per unit wave amplitude squared. In this section, the surge wave drift coefficients are calculated based on the mean value of the surge responses in regular waves. The results for horizontal mooring system in following sea are shown in Table 3-11 where F_{Hor} is the surge drift force in the horizontal plane in the direction of positive x-axis. F_{Hor} is estimated via the force-displacement relationship of the system which is obtained from the static-pullout test and shown previously for both horizontal and catenary mooring system in Figure 3-18. A more detailed study and discussion of the values shown in Table 3-11 is given later in Chapter Five.

Table 3-11 Surge wave drift coefficients in regular waves with horizontal mooring system

Test number	H (m)	T (s)	U (m/s)	Surge motion mean value (m)	F_{HOR} (kN)	Drift Coefficient $F_{HOR}/\left(\frac{H}{2}\right)^2$ kN/m^2	f (Hz)
3010	5	10	-	6.17	972.30	155.57	0.1
3020	10	10	-	27.66	4084.19	163.37	0.1
3030	11	15	-	1.02	226.36	7.48	0.067
3040	22	15	-	9.16	1404.90	11.61	0.067
3050	33	15	-	39.97	5866.55	21.55	0.067
3110	5	10	0.6	9.82	1500.73	240.12	0.1
3120	10	10	0.6	29.92	4410.63	176.43	0.1
3130	11	15	0.6	2.33	416.01	13.75	0.067
3140	22	15	0.6	15.04	2255.83	18.64	0.067
3210	5	10	1.2	6.75	1056.21	168.99	0.1
3220	10	10	1.2	29.33	4325.51	173.02	0.1
3230	11	15	1.2	1.84	345.37	11.42	0.067
3240	22	15	1.2	15.88	2377.64	19.65	0.067

3.5.3 Comparisons of the statistical parameters in waves, in a current and in combined waves and a current

In this section, the time series of the irregular waves experiments are analyzed by investigating their statistical characteristics, such as the minimum, maximum, mean value and standard deviation values. In this section, the mean values and standard deviations of the low-frequency surge motion responses in different sea states with irregular waves with both horizontal and catenary mooring systems are also presented.

The time series of the surge motion responses, samples of which were shown previously in Figures 3-34 to 3-37 inclusive, have transition parts at the start of each of the experiments. These transition parts were removed in order to study the motions after the disturbance from the initial start up of the waves generated by the wave generator. Afterwards, the mean and standard deviation values are calculated. The test programme consisted of four different irregular sea states, which will be identified as follows: Case 1 (H6, T12), Case 2 (H12, T12), Case 3 (H7.5, T15), and Case 4 (H15, T15). For each of these sea states, the experiments were first conducted in waves only (W), and then in combined waves and current field (W+ U). In addition to these tests, further tests in current only (U) for the two current speeds (0.6 and 1.2 m/s) were examined.

A comparison was then carried out between the measured surge motion responses in combined wave and current field (W+ U) versus superimposed responses (S) resulting from the separate wave (W) and current (U) tests being added together. The superimposed response (S) is the algebraic summation of the mean values of the responses due to wave and current. On the other hand, for the standard deviation values, the superimposed value is estimated as a vector sum which is the root sum of squares of the standard deviation values of the individual sea sates.

Firstly, for the model moored with the horizontal mooring system, Figure 3-38 to Figure 3-41 show the comparisons of the mean values and standard deviations in the four sea states including the two current speeds (0.6 and 1.2 m/s). For the horizontal mooring system, it is assumed that the interaction between the mooring lines and wave and/or the current is ignored. Thus, any difference between the measured motion responses and calculated combined superimposed responses is assumed to be due to the wave- current flow interaction only. Figure 3-38 shows that the mean values of the low-frequency surge motion responses due to waves only, in Case 1 and Case 3; both moderate sea states, are similar to that due to the current speed (0.6 m/s). In this

situation, the combined superimposed value of the motion responses due to the wave and current acting separately is found to be agreeing well with that measured from the combined wave-current test. On the other hand, in Case 2 and Case 4; both high sea states the mean values of the low frequency surge motion responses due to waves only are dominating and are much higher than that due to the current only (0.6 m/s). It is observed that in this situation, that the actual responses in the wave-current field are larger than the combined superimposed responses from waves and current separately. Figure 3-40 shows that the above observations are still valid at current speed 1.2 m/s.

As for the standard deviation comparisons, it is observed that the standard deviation of the responses in the current only case is less than that obtained for waves acting alone. Figure 3-39 and Figure 3-41 show that in combined wave-current field with horizontal mooring system, the measured standard deviations in moderate sea states (Case 1 and Case 3) agree well with those obtained from the superposition of the separate wave and current results. However, in Case 2 and Case 4 (high sea states) where the waves are dominating the wave-current field, the measured standard deviations exceed those obtained from the superposition of the responses due to waves and current separately for the two current speeds.

The measured mean values of the surge responses of the semisubmersible moored with catenary mooring shown in Figure 3-42 are found to correlate well with those obtained from the superposition of the responses due to waves and current separately. The standard deviations of the measured responses shown in Figure 3-43 are seen to be less than the superposition values. The difference between the measured and calculated through superposition standard deviation is more pronounced in the moderate sea states (Case 1 and Case 3) than in the high sea states (Case 2 and Case 4). This section was published by the author in summary form in (Hassan et al., 2009) which can be found in Appendix A. A second paper of the author was published in (Berthelsen et al., 2009) , which investigated the viscous effect via numerical time domain simulations in regular and irregular sea states. The viscous forces and damping were included in the numerical model by Morison's equation drag term using a total relative velocity approach that is integrated up to the free surface elevation. It was found that drag coefficient in waves with current is lower than in waves only. This study was applied on a semisubmersible that is moored with horizontal mooring system in order to study the hydrodynamics of hull only.

Run 5010: IRR (H6, T12, U0)

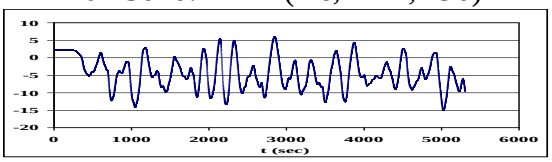

Run 5020: IRR (H12, T12, U0)

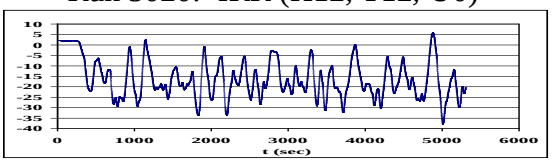

Run 5030: IRR (H7.5, T15, U0)

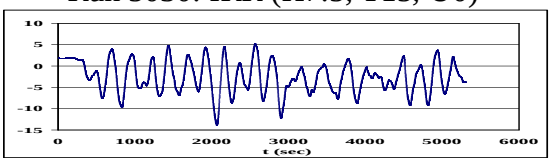

Run 5040: IRR (H15, T15, U0)

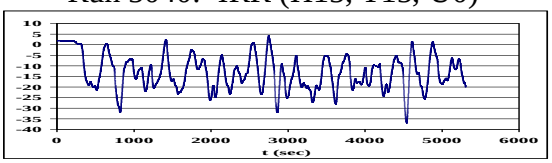

Figure 3-34 Surge responses in irregular waves only, catenary mooring(m)

Run 6010: IRR (H6, T12, U0)

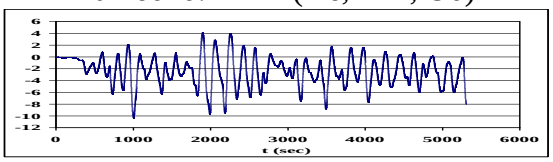

Run 6020: IRR (H12, T12, U0)

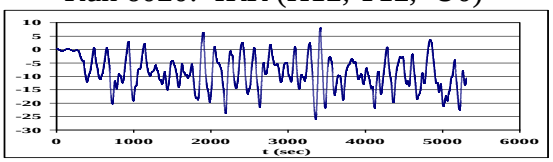

Run 6030: IRR (H7.5, T15, U0)

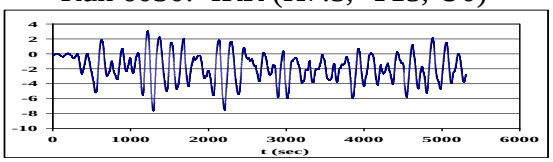

Run 6040: IRR (H15, T15, U0)

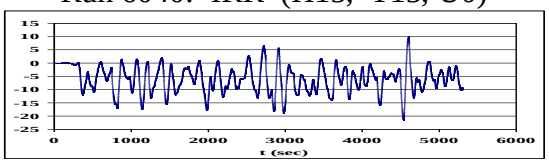

Figure 3-35 Surge responses in irregular waves only, horizontal mooring(m)

Run 5120: IRR (H 6, T12, U1.2)

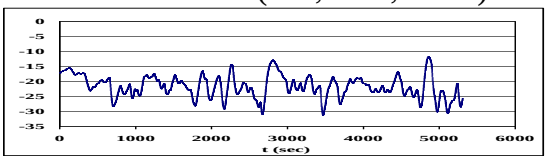

Run 5130: IRR (H 12, T12, U1.2)

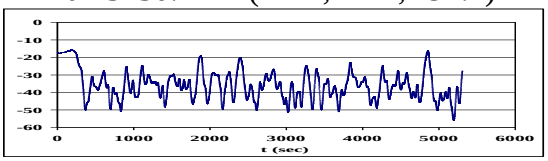

Run 5140: IRR (H7.5, T15, U1.2)

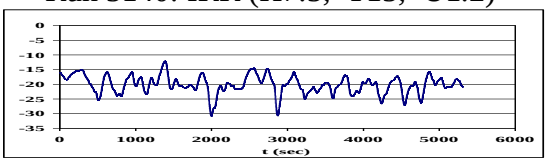

Run 5150: IRR (H15, T15, U1.2)

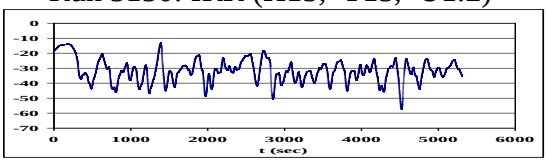

Figure 3-36 Surge responses in irregular waves and current, catenary mooring(m)

Run 6220: IRR (H6, T12, U1.2)

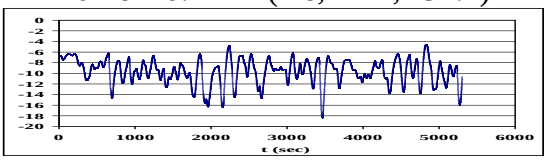

Run 6230: IRR (H12, T12, U1.2)

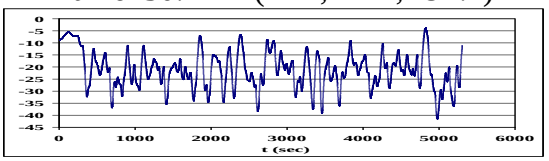

Run 6240: IRR (H7.5, T15, U1.2)

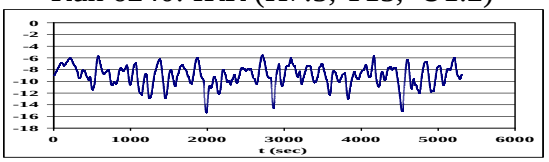

Run 6250: IRR (H15, T15, U1.2)

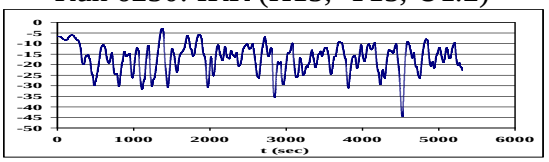

Figure 3-37 Surge responses in irregular waves and current, horizontal mooring(m)

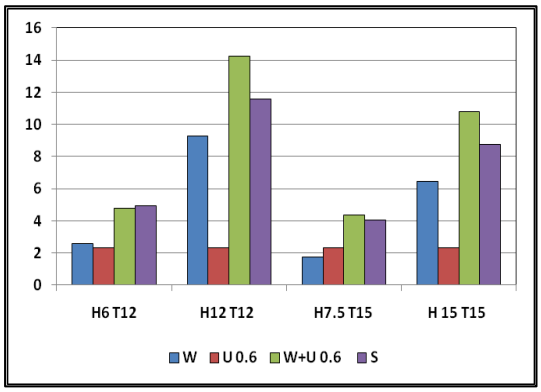

Figure 3-38 Mean values of low-frequency surge motion, horizontal mooring (U =0.6 m/s)

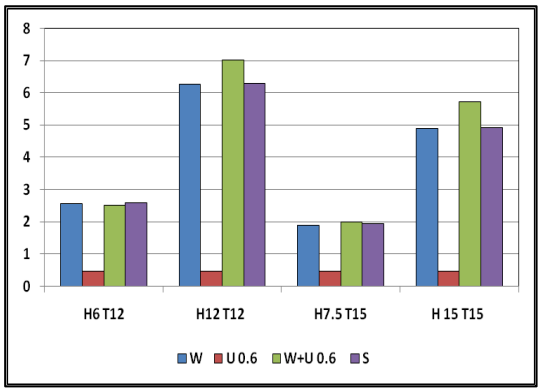

Figure 3-39 Standard deviation of low-frequency surge motion, horizontal mooring (U= 0.6 m/s)

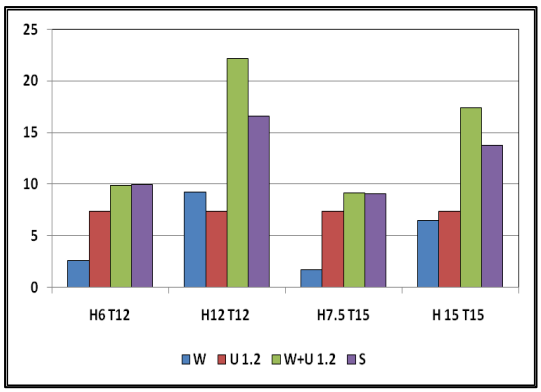

Figure 3-40 Mean values of low-frequency surge motion, horizontal mooring (U= 1.2 m/s)

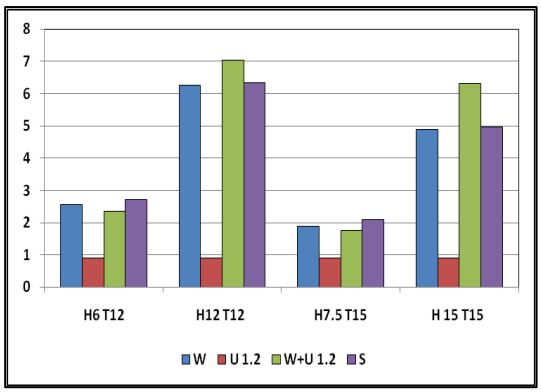

Figure 3-41 Standard deviation of low-frequency surge motion, horizontal mooring (U =1.2 m/s)

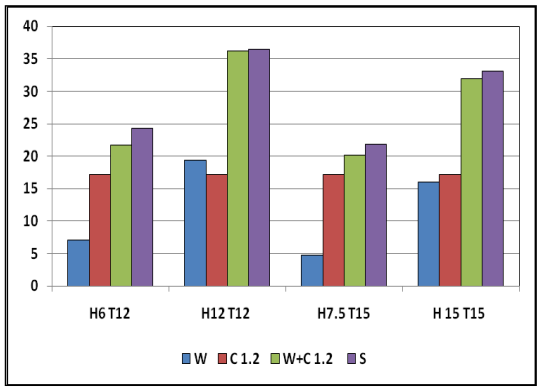

Figure 3-42 Mean values of low-frequency surge motion, catenary motion (U= 1.2 m/s)

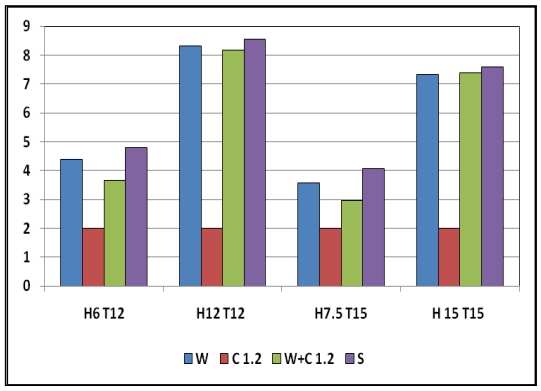

Figure 3-43 Standard deviation of low-frequency surge motion, catenary mooring (U =1.2 m/s)

3.5.4 Effect of mooring lines and current on system damping

Several decay tests were conducted in both still water and in currents using both the horizontal and the catenary mooring lines. The decay response in each of these physical tests depends on both the damping of the hull and of the mooring lines.

In this study, it is assumed that, the mooring line damping for the horizontal mooring line is neglected. Hence, the damping is assumed to be due to hull only. Therefore, the

difference between the responses of the semisubmersible moored with the horizontal and catenary moored systems is assumed to be due to the catenary mooring lines only.

The damping of the system is estimated via calculating the relative damping ratio/ coefficient with respect to the critical damping. The relative damping coefficients are calculated as previously explained in Section 3.3.5.1 as a function of the mean amplitude of the decay motion. Decay motion time series were shown in Section 3.3.4.5. In these tests, the semisubmersible scale model was given an initial displacement and afterwards is left to oscillate freely. Those free oscillations decay with time and their amplitudes are reduced due to the effect of the system damping. The analysis of the rate of the decaying motion is a measure of the damping of the system.

Figure 3-46 shows a comparison between the relative overall system damping coefficients in still water with the alternative horizontal and catenary mooring line arrangements. It is clearly observed that the relative damping when using the catenary mooring system is higher than that for horizontal mooring system which agrees with the same observation for the damping ratios that were calculated using the exponential method and illustrated in Tables 3-6 and 3-7. It can be seen from Figure 3-44, that the existence of a current increases the damping when using horizontal mooring lines. A similar comparison of the damping ratios in currents with catenary mooring lines is shown in Figure 3-45 however due to the high damping and the low number of decay cycles, only one point could be plotted. This section was published by the author in summary form in (Hassan et al., 2009) which can be found in Appendix A.

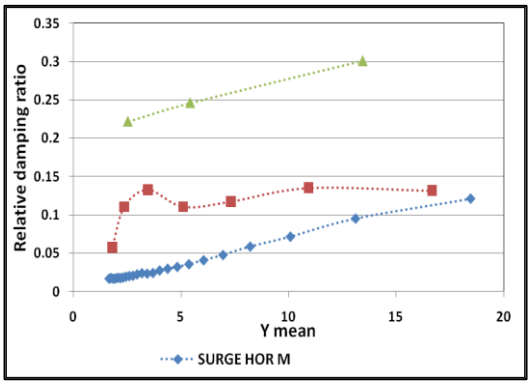

Figure 3-44 Relative damping ratios for overall model at different current speeds, horizontal mooring

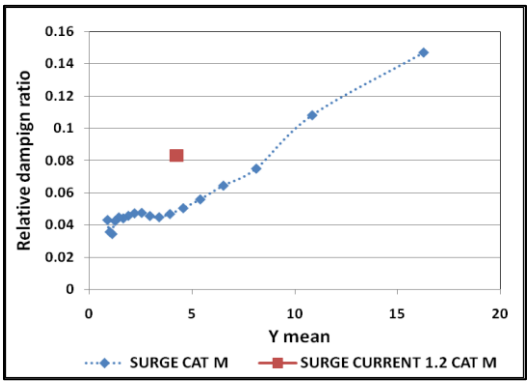

Figure 3-45 Relative damping ratios for overall model at different current speeds, catenary mooring

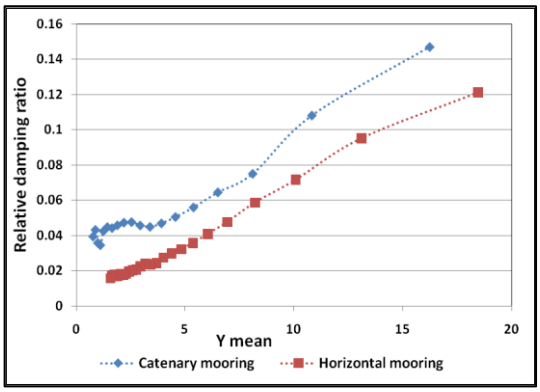

Figure 3-46 Relative damping ratios for overall model in still water for horizontal and catenary mooring systems

3.5.5 Contribution of the mooring system to the low-frequency motions of a semisubmersible in combined waves and current

The statistical comparisons presented in Section 3.5.3 were carried out for each mooring system separately. Figure 3-18 showed that the horizontal mooring system has linear relationship between the force and corresponding displacement unlike the catenary mooring system. Thus, in order to compare the characteristics of the two mooring systems and the responses of the semisubmersible with both of the two systems, it was necessary to eliminate the effect of the different stiffnesses of the two systems.

This was achieved by a simple procedure that is sketched briefly in Figure 3-47. The procedure employs the measured surge mean motion response when the semisubmersible is moored with the horizontal mooring system (X_{Hor}). Then the corresponding loading force (F_{Hor}) is estimated via the force-displacement relationship shown in Figure 3-18. This loading force emerges from the environmental condition and is not mooring system dependant. Thus, the surge loading force (F_{Hor}) is the same for the catenary mooring system and the corresponding mean surge motion response($X_{cal\ Cat}$) is estimated according to the force-displacement relationship. The final step is to compare the calculated surge response with the catenary mooring system ($X_{cal\ Cat}$) with the actual measured responses from the experiments ($X_{M\ Cat}$).

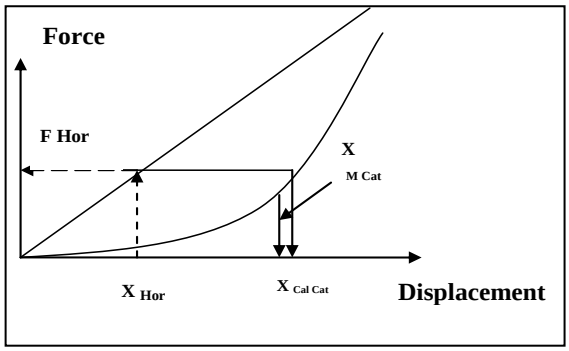

Figure 3-47 Sketch of the procedure of the elimination of stiffness effect

Four cases for comparison were carried out in order to separate the effects of mooring lines damping, considering waves, current and wave-current interaction, on the mean values of the surge responses. These four comparisons are as follows

Case A: Effect of mooring lines in waves only,

Case B: Effect of mooring lines in current only,

Case C: Wave-Current interaction, Horizontal Mooring, and

Case D: Wave-Current interaction, Catenary Mooring.

In these cases, the measured mean values of the low frequency surge responses with the horizontal mooring system are used as a reference in order to investigate the effect of the catenary mooring lines which is the system that is used in practical applications.

3.5.5.1 Case A: Effect of mooring lines in waves

Table 3-12 shows the values of measured surge responses with horizontal mooring lines (HOR), and both the calculated forces that correspond to the measured responses (in meters) and surge responses with catenary mooring lines (CAT).

Table 3-12 Waves- mooring Lines interaction

Sea State	X_{Hor} (m)	F_{Hor} (kN)	$X_{Cal\ Cat}$ (m)	$X_{m\ Cat}$ (m)	Difference (%)
H6, T12	2.48	438.20	6.53	6.69	2.45
H12, T12	8.99	1381.03	19.49	18.27	-6.25
H7.5, T15	2.01	369.70	5.51	4.42	-19.78
H15, T 15	6.74	1054.71	15.34	15.16	-1.17

where

X_{Hor} measured surge responses with horizontal mooring,

F_{Hor} calculated surge forces corresponding to X Hor,

$X_{cal\ cat}$ calculated surge responses with catenary mooring at F_{Hor},

$X_{m\ Cat}$ measured surge responses with catenary mooring, and

Difference $= X_{\text{measured catenary}} - X_{\text{calculated Catenary}}$.

It is found that in the waves only conditions, that the measured motion responses with catenary mooring lines are found, in three sea states out of four, to be less than those expected when the same force acts on the model with horizontal mooring lines. In the fourth sea state (H6, T12) a slight increase is found.

3.5.5.2 Case B Effect of mooring lines in current

Table 3-13 shows the interaction effect between current and mooring lines by comparing the responses in current with the horizontal and the catenary moorings. It is found that the measured body mean surge response in the current only is larger than that anticipated as a result of the different value of the stiffness.

Table 3-13 Current -mooring lines interaction

Sea State	X_{Hor} (m)	F_{Hor} (kN)	$X_{Cal\ Cat}$ (m)	$X_{m\ Cat}$ (m)	Difference (%)
U1.2	7.35	1143.89	16.51	17.19	4.11

The relative damping ratios values were estimated from the decay tests and results were given using exponential method in Table 3-6, Table 3-7. Results obtained via algorithmic decrement method were shown in Figure 3-44 and Figure 3-45.

These two sets of results show that the damping is larger in current with catenary mooring lines than with horizontal mooring lines in current case. Thus, the increase in responses may be explained by the fact that the mooring lines themselves would be subject to forces from the current.

3.5.5.3 Case C: Wave-Current Interaction, Horizontal Mooring

In this case, a comparison is carried out between the actual mean values of surge responses due to wave-current field and the superimposed responses due to waves and current those were examined separately. In this case, it is assumed that there is no interaction between waves or current with the mooring lines and the parameters studied

show only the effects of wave-current interaction on the body mean surge low-frequency responses.

Table 3-14 Wave-current interaction, horizontal mooring

Sea State	X_W (m)	X_C (m)	X_{W+C} (m)	X_S (m)	Difference (%)
H6, T12	2.48	7.35	9.86	9.84	0.2
H12, T12	8.99	7.35	21.45	16.35	-23.77
H7.5, T15	2.01	7.35	9.21	9.36	1.63
H15, T15	6.74	7.35	17.35	14.09	-18.79

It is seen in Table 3-14 that the superposition approach gives a good agreement with the measured values in moderate sea states ((H6, T12) and (H7.5, T15)) while in high sea states ((H12, T12) and (H15, T15)), there is a large increase in the measured values compared with the superposition obtained values and which is considered to be due to the wave - current interaction.

3.5.5.4 Case D: Wave-Current interaction, Catenary Mooring

In this case, the measured mean surge responses in a wave-current field with catenary mooring ($X_{m\ Cat}$) are compared to those in a wave-current field with ($X_{Cal\ Cat}$) after eliminating the effect of using different mooring configurations with different stiffness than that of the horizontal mooring system.

Table 3-15 shows that in all sea states, the responses in a wave-current field are larger than anticipated. This increase is the net combined effect of the wave-current interaction with each other (increasing the responses as stated in Case C) and their interaction with the mooring lines (reduction due to waves and increase due to current). This section was published by the author in summary form in (Hassan et al., 2009) which can be found in Appendix A

Table 3-15 Wave-current interaction, catenary mooring compared with horizontal Mooring

	X_{Hor} (m)	F_{Hor} (kN)	$X_{Cal\ Cat}$ (m)	$X_{m\ Cat}$ (m)	Difference (%)
H6, T12, U1.2	9.86	1506	19.76	22.15	12.09
H12, T12, U1.2	21.4	3185	32.74	36.14	10.38
H7.5, T15, U1.2	9.21	1413	18.78	20.71	10.27
H15, T15, U1.2	17.3	2592.	29.09	32.66	12.27

3.6 Summary

This chapter presented the description of the conducted experimental tests and the results obtained from them. The presented results included the damping ratios in both still water and in current, the effects of both mooring lines and current on damping, investigation of the effect of the catenary mooring lines system on the low frequency surge motion responses. In addition, the effect of the wave-current interaction for both horizontal and catenary mooring systems in different sea states on the mean values of the surge low frequency motion responses was presented. Surge wave drift coefficients estimated from the measurements were presented and are to be compared versus the numerical calculated coefficients later in Chapter Five.

Chapter 4. Mooring lines damping model

4.1 Introduction

The main function of a mooring system of floating structures such a Semisubmersible is in keeping the moored structure located within defined bounds above a sea bed position where the function of the platform such as drilling, from the platform, is taking place. However, the mooring lines themselves would also affect the body motions of the platform in two ways. The first effect is through line stiffness, which determines the platform resonant periods. The second effect is due to the motion damping of the mooring lines.

For moored offshore structures, the second-order wave forces are more dominant than are first-order forces and their assessment are important in order to determine the peak offsets, mooring line peak loads, and riser movement design requirements. Several works in the literature have been carried out to investigate the mooring lines damping effects on both the wave induced and low-frequency motions.

One of the more important works concerning mooring line damping was introduced by Huse in (Huse, 1986). Before this publication, it was normal to neglect the mooring line drag based on the inference that the drag area of a line is very small relative to the drag area of the vessel itself. However, Huse in (Huse and Matsumoto, 1988; Huse, 1986) showed that the motion amplitude of the line can be many times larger than the corresponding floating body surge amplitude. It was shown that energy dissipation due to line drag force is proportional to the third power of the line motion amplitude. Thus in spite of their small drag area, the mooring lines may still represent a significant contribution to the total surge damping. The same possibility can also be postulated regarding the sway motion damping.

Later in this chapter, Huse's energy dissipation approach, as mentioned earlier, is used to calculate the damping due to the mooring lines themselves. This approach is initially applied on a simple model of a single mooring line with characteristics that are similar to those examined by Huse for method verification purposes. Following this, the approach is applied to a semisubmersible model whose characteristics are the same as the model that was studied in the previous chapters of this thesis.

The approach that is used calculates the energy that is dissipated by the mooring line or lines during one surge cycle of movement at the fairlead point. The calculations and results of these two studies are given in detail in Sections 4.3.2 and 4.3.4. In addition, a

study of the effect of water depth on mooring line dissipated energy is introduced and discussed in Section 4.3.3.

4.2 Catenary Mooring Lines

The shape of the vertical profile in its own two-dimensional plane of the individual mooring line used in calculations is approximated as an inelastic cable line following the catenary equations which are fully described in (Faltinsen, 1993). The main equations describing the catenary lines are summarized as follows

$$Z - Z_O = \frac{T_O \cos(\theta_o)}{w}\left[\frac{1}{\cos(\theta)} - \frac{1}{\cos(\theta_o)}\right] \quad (4\text{-}1)$$

$$Z + h = \frac{T_o}{w}\left[cosh\left(\frac{wx}{T_o} - 1\right)\right] \quad (4\text{-}2)$$

$$\tan(\theta) = \sinh\left(\frac{wx}{T_o}\right) and \ \frac{1}{\cos(\theta)} = \cosh\left(\frac{wx}{T_o}\right) \quad (4\text{-}3)$$

$$X = l - l_s + x \ = l - h\sqrt{\left(1 + \frac{2a}{h}\right)} + \text{acosh}^{-1}\left(1 + \frac{h}{a}\right), where\ a = \frac{T_o}{w} \quad (4\text{-}4)$$

where $a = \frac{T_H}{w}$, h is the water depth to fairlead point, and *To* is the horizontal component of mooring line tension in reference position. The variables and parameters used in the above equations (4-1) to (4-4) inclusive are based on the coordination system illustrated in Figure 4-1. *A*, *B* and *C* are the anchoring point, lift-off and fair lead attachment point on the floating body, respectively.

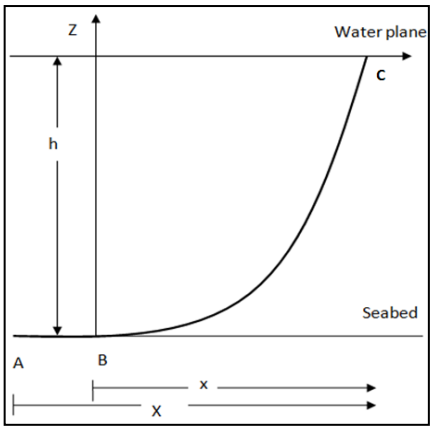

Figure 4-1 Catenary line coordination system

For the experimental tests (see Chapter Three), real typical in service- type mooring lines were represented with a set of four equivalent suitable modelled mooring lines attached to the corners of the semi submersible model. Each of these four lines consisted of three line segments of different diameters, and material, and hence having different weight per unit length. However, in order to simplify the actual numerical

analysis of such a mooring lines system, each mooring line is approximated to consist of only one segment. The value of the weight per unit length of this segment is estimated and adjusted so that the shapes of the line satisfies the catenary lines equations and give the same shape as the lines in experimental tests.

Table 4-1 shows the full scale diameters of the mooring line segments used in the experiments and the average diameter. Table 4-2 shows the full scale length and weight per unit length of each of the three segments of the assumed typical actual mooring line. The average weight per unit length based on the data in Table 4-2 is found to be 10.33 kN/m. It is to be noticed that such a value is much higher than a typical standard mooring line weight per unit length used in real life. This is due to the assumption that the mooring system used in the experiments consisted of only four mooring lines while a real mooring system for an offshore platform generally consists usually of 12 or 16 mooring lines.

4.2.1 Calculation of the average weight per unit length of the three segments of the employed mooring line

As mentioned earlier, the investigation of catenary mooring lines required the knowledge of the value of the weight of the mooring line per unit length in sea water.

The usage of an average value of buoyant weight per unit length of w = 10.33 kN/m, that is estimated from the values given in Table 4-2, produced mooring lines with catenary vertical profiles that did not match those of the lines used in the experimental tests. Thus, an alternative value was obtained through a trial and error process. A good agreement was found at value of w = 15 kN/m. The mooring line orientation angles of the four mooring lines are shown later in this chapter in Figure 4-22.

The catenary vertical profiles of the experimental line number 1 and calculated lines are shown in Figure 4-2 at values of w = 10.33 and 15 kN/m. The modified line represents the measured mooring line after shifting so that its axes match those used in catenary equations given in Section 4.2. Similar vertical profiles for mooring lines 2, 3 and 4 were found to agree with the theoretical line obtained at w= 15 kN/m.

Table 4-1 Average diameter of the cable line (full scale)

Segment number	Diameter (m)
1	0.29
2	0.272
3	0.29
Average diameter	0.284

Table 4-2 Mooring line segments data

Segment number	length of segment (m)	unit weight in sea water (kN/m)
1	350	14.4
2	252	3.064
3	84.63	15.12

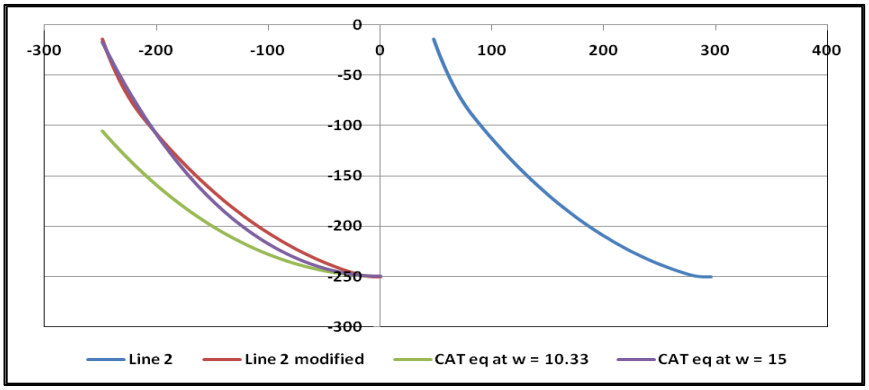

Figure 4-2 Theoretical and experimental vertical profiles of mooring line 1

Generally, there are three different mooring line configurations employed in mooring structures that were given and examined by (Haug and Greiner, 1999) which are named: steel catenary, steel semi-taut leg, and polyester taut leg. Each of these configurations may be fabricated from wire, chain, or polyester. The corresponding break strength and wet weight per unit length for each configuration is given in the cited reference. For the polyester, the wet weight values are typically 7.77 kg/m, while for the wire it ranges between 51.5 and 68.1 kg/m and for the chain it ranges between 172 and 234 kg/m.

It is observed that the calculated value of the weight per unit length based on the experimental data is much higher than the typical values in real life applications shown in (Haug and Greiner, 1999). This is due to that the mooring system in the experiments consisted of four mooring lines while most real systems usually consist of twelve or sixteen mooring lines.

4.3 Huse Mooring Line Damping Mathematical Model (Energy Dissipation Method)

The energy dissipation approach was introduced by Huse in (Huse, 1986) as a theoretical method to calculate the energy dissipated by the drag force on the mooring line. The method calculates the energy dissipated by the mooring lines during one surge cycle (one period T) of the fairlead point using the positions of the fairlead and lift-off

points of each mooring line at extreme points of the motion. Afterwards, in (Huse and Matsumoto, 1988) , the method was applied in conjunction with the energy dissipated by the velocity term in the equation of motion to calculate the mooring line damping.

The following assumptions are made in the energy method:

a. Calculations include drag forces that are normal to the line at all points.

b. Motion components of the line are within the vertical plane of the line.

c. Motions are slow enough that the catenary shape is retained all the time.

In the following sections, a brief summary of the calculations that are made within the energy dissipation method is given and followed by three study cases for verification and illustration.

4.3.1 Energy Calculations

In this section, the formulas that are used to calculate the mooring line dissipated energy and the energy dissipated by the velocity term in the equation of motion are given.

4.3.1.1 Energy dissipated by a mooring line

The energy dissipated ΔE by an element of the line ΔS_L is defined as follows

$$\Delta E = 2 \int_{-\eta_o}^{\eta_o} \Delta F_D \, d\xi \tag{4-5}$$

where ΔF_D is the drag force on an element of the line ΔS_L and is defined as

$$\Delta F_D = \frac{1}{2} \rho \, D \, C_D \, |\dot{\xi}| \dot{\xi} \Delta S_L \tag{4-6}$$

in which ρ is the water density, D is the mooring line diameter, and C_D is the drag coefficient of the mooring line which would vary with line type in a real mooring line such as chains and wires. In addition, C_D is assumed to remain constant along all the length of the mooring line.

ξ is the assumed moved distance by the mooring line fairlead point horizontally in the plane of the line. In addition, this motion is assumed to be sinusoidal and ξ is defined as

$$\xi = \xi_o \sin(\omega t) \tag{4-7}$$

where ω is the frequency of the structure oscillations. In addition, the horizontal component of mooring line tension T_H is assumed to be

$$T_H = T_o + \tau \tag{4-8}$$

where *To* is the horizontal component of mooring line tension in reference position and τ is defined as

$$\tau = \tau_o \sin(\omega t) \tag{4-9}$$

Hence, the energy dissipated is estimated as

$$\Delta E = \frac{4}{3}\rho_w D C_D \omega^2 \xi_o^3 S_L \tag{4-10}$$

The estimation of the energy dissipated by the whole mooring line requires the integration of equation (4-10) along the line. Hence,

In order to get the energy dissipated by the whole line it is now necessary to integrate Eq. (4-5) along the line. For this purpose we need to know no as a function of *s* or *x*.

$$\text{Let } \Delta Z = Z_U - Z_L \tag{4-11}$$

where Z_U and Z_L are the highest and lowest *z* values during the surge period. Then, the moved distance by the structure in the reference position ξ_o can be approximated as

$$\xi_o = \frac{1}{2}\Delta Z \cos(\phi) \tag{4-12}$$

where $$\cos(\phi) = \frac{T_o}{T_t} = \frac{T_O}{\sqrt{{T_O}^2 + \left(T_O \sinh\left(\frac{w}{T_O}(X - X_O)\right)\right)^2}} \tag{4-13}$$

Hence, by conducting the integration in equation (4-5) the energy dissipated can be written as

$$E = \frac{1}{6}\rho_w D_L C_D \omega^2 \int_{X_o}^{X_{max}} \frac{|(\Delta Z)^3|}{1 + \sinh^2\left(\frac{w}{T_o}(x - x_0)\right)} \tag{4-14}$$

4.3.1.2 Energy dissipated by the velocity term in the equation of motion

Assuming that the equation of the surge motion of the vessel in the vertical plane where the catenary mooring line lies is given by $M\ddot{S} + B\dot{S} + CS = F_O \sin(\omega t)$, and then the energy that is dissipated by the velocity term in the motion equation for one mooring line is calculated as follows

$$E = 4 \int_0^{S_o} B\dot{S_L} dS_L \tag{4-15}$$

where *B* is the linearized damping coefficient of the mooring line, *M* is the mass of the structure, and Fo is the excitation force amplitude. Thus, the total energy dissipated by the mooring line during one period cycle is defined as

$$E_{tot} = \pi\omega S_{L_0}^{\ 2}\, B \tag{4-16}$$

The previous equation estimates the energy dissipated by one mooring line and needs to be multiplied by the number of mooring lines that have similar oscillation characteristics. It is to be noted that not all mooring lines in the same system would dissipate identical amount of energy and it may be needed to estimate the dissipated energy for each line individually. Then, equating energy dissipated by all the lines in the mooring system to that dissipated by the velocity term in equation of motion results in equation (4-16) , the damping coefficient *B* is found to be $\frac{E_{tot}}{\pi\omega S_{L_o}^{\ 2}}$ and the relative damping would equal$\frac{B}{2\omega M}$.

Huse introduced a simplified procedure in (Huse and Matsumoto, 1988) that can be employed to calculate the dissipated energy by introducing three non-dimensional groups of parameters namely π_1, π_2, and π_3 so that $E = \frac{1}{6}\rho D_L\, C_D \omega^2\, I$ where

$$I = \int_{X_o}^{X_{max}} \frac{|(\Delta Z)^3| dX}{1+\sinh^2\left(\frac{w}{T_o}(X-X_o)\right)}. \tag{4-17}$$

The three non-dimensional parameters are $\pi_1 = \frac{S_o}{H}, \pi_2 = \frac{w\,H}{T_o}\ and\ \pi_3 = \frac{EA}{T_o}$. By conducting a systematic variation of π_1, π_2, and π_3, simple diagrams of $\frac{I}{H^4}$ for different values of the three parameters were given by Huse. These diagrams are easy to use for the energy calculations assuming that the used mooring line characteristics are within the plotted range.

In the following two sections, the Huse energy dissipation method is applied on two examples. The first example is for a vessel moored with a single mooring line and the second is for a more realistic semisubmersible arrangement that is moored with four mooring lines, similar to those used in the model experiments.

4.3.2 Single mooring line study

In this section, a numerical example is presented that is based on Huse's energy dissipation method. The mooring line characteristics used are as shown in Table 4-3 and are the same characteristics given by Huse in his work for verification purpose within

this study. The model is for a vessel that is moored with one single line and that is given a sinusoidal horizontal motion at the top vessel attachment end. The energy dissipated is calculated for different values of peak-to-peak surge motion amplitudes.

Table 4-3 Mooring line characteristics

Type of line	steel chain
Outer diameter of the mooring line(D_L)	0.084 m
Total length of line (S_L)	1200 m
Horizontal tension at the fairlead point at reference position (T_O)	1000 kN
Fairlead height above sea bed (h)	136 m
Drag coefficient (C_D)	3.5
Angular wave frequency (ω)	0.0494 rad/S
Weight per unit length in water (w)	1 and 0.8 kN/m

In (Huse, 1986) Huse did not actually provide the value of the weight per unit length of the submerged line that was used in his calculations. Thus, two values were assumed, for these calculations, to be 0.8 and 1 kN/m and trial values and their results were then compared with Huse's results. A good agreement of the calculated energy was found with Huse's results at a weight per unit length of 0.8 kN/m.

In order to conduct the calculations, the stiffness of the system (force-displacement relationship) was needed as well. Since it was not provided by Huse, it was estimated by using the following procedure which is based on the catenary line shape equations provided by (Faltinsen, 1993) and that are given in the Section 4.2. A full description of the procedure that was followed is given in the next section.

4.3.2.1 Force-displacement relationship estimation

The procedure starts with calculating the characteristics of the maximum displaced position of the structure, where the suspended length of the line equals the total line length (L_S= L). Afterwards, solving the catenary equation for suspended length $L_S = \sqrt{h^2 + 2ha}$, where $a = \frac{T_O}{w}$, provides the value of T_O at the maximum possible displaced position of the vessel. The corresponding horizontal position of the vessel (x) measured from the lift-off point is calculated as$a\cosh^{-1}\left(1+\frac{h}{a}\right)$. Subsequently, lift off point would coincide with the anchor point. Maximum displacement δ_{max} of the vessel is thus the difference between the horizontal position in maximum position and the still water start position. This value is thus the absolute upper limit of the surge motion amplitude value that can be used in the study. Different values of vessel displacement δ in the range 0 and $\delta_{max,}$ are chosen and by setting $X= X_{static} + \delta$ and by using equation

(4-4), the corresponding new value of the horizontal tension exerted by the mooring line now can be calculated. The previous procedure was applied for two values of mooring line weight per unit length; that is w = 0.8 and 1 kN/m. The calculated tension-horizontal position relationships are shown in Figure 4-3.

The floating structure is affected by both wave and current forces. The energy dissipation method takes into account the steady displacement of the structure due to the combined effect of the waves and current. The new position of the structure due to these combined forces becomes new temporary position offset by a distance S from the original position. The semisubmersible then oscillates; in the same surge direction about the new temporary position with amplitude of δ.

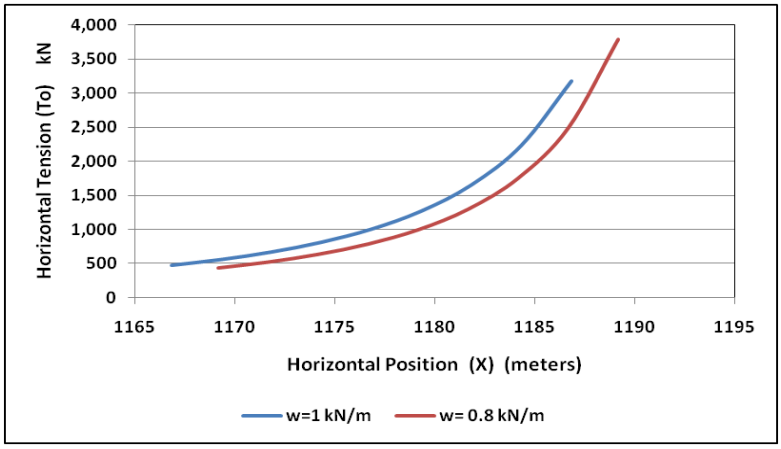

Figure 4-3 Horizontal tension force- position relationship

After conducting the previous procedure and estimating the horizontal force- position relationship, at the fairlead point the dissipated energy can be estimated by conducting the integration of the energy element between the far end and near end positions of the line for a surge motion cycle and repeated at different values of motion amplitudes. Between each of these two positions, the length of the line is divided into horizontal sections of equal length and the energy is integrated section by section over the whole length of the line. The calculations of the energy dissipation procedure were conducted for three different arbitrary values of surge motion amplitude (δ), which were 2.5, 5 and 7.5 m. In addition, two values of effective weight per unit length of the submerged line, namely w = 1 and 0.8 kN/m, were used.

The vertical profiles of the mooring lines assuming w= 1 kN/m determined at the different values of the surge motion amplitude (δ) are shown in Figure 4-4 to Figure 4-8 inclusive and those at w = 0.8 kN/m are shown in Figure 4-5 to Figure 4-9 inclusive. Each figure shows the vertical profiles of the mooring line in three positions; the

reference position, near end and far end positions. The near and far end positions represent the positions of the motion amplitude range of the structure. It is observed from these figures it is seen that at higher value of weight of line per unit length results in a larger value of horizontal position (measured from the anchor point) of the lift-off points at the same surge motion amplitude in the studied cases. The dissipated energy values given by Huse are compared to those calculated at w = 0.8 and 1 kN/m in Figure 4-10 . A good agreement with Huse's values was found at w = 0.8 kN/m , thus confirming a correct understanding of Huse's method.

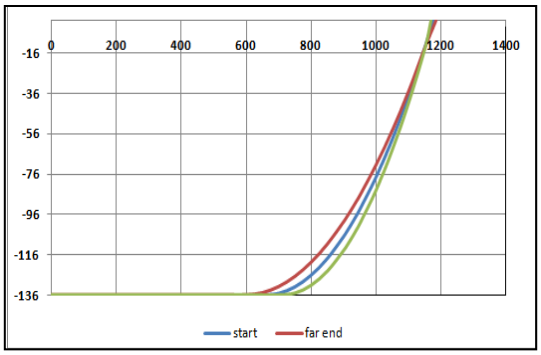

Figure 4-4 Vertical profiles of mooring line 1 at mid, near, far positions when w = 1kN/m and δ= 2.5 m

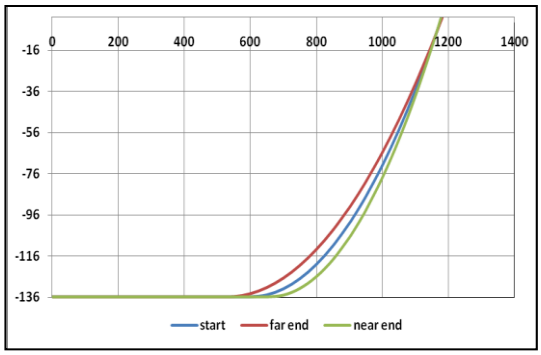

Figure 4-5 Vertical profiles of mooring line 1 at mid, near, far positions when w = 0.8 kN/m and δ= 2.5 m

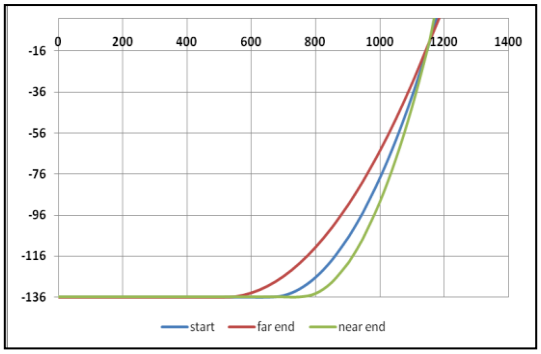

Figure 4-6 Vertical profiles of mooring line 1 at mid, near, far positions when w = 1kN/m and δ= 5 m

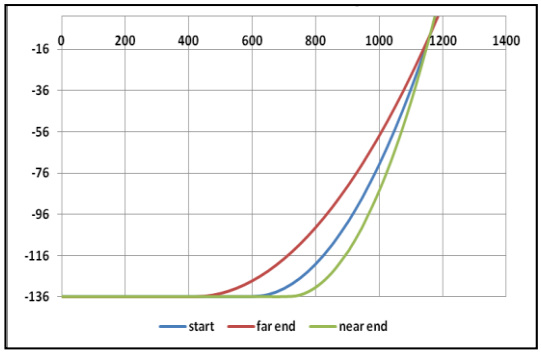

Figure 4-7 Vertical profiles of mooring line 1 at mid, near, far positions when w = 0.8 kN/m and δ= 5 m

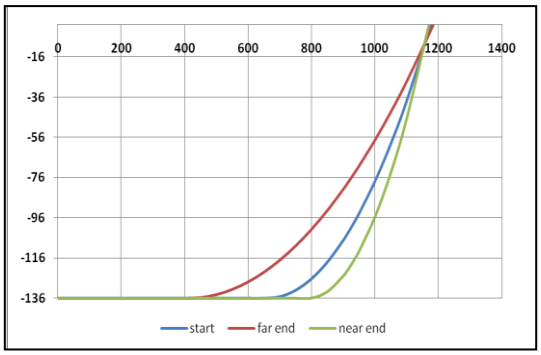

Figure 4-8 Vertical profiles of mooring line 1 at mid, near, far positions when w = 1kN/m and δ = 7.5 m

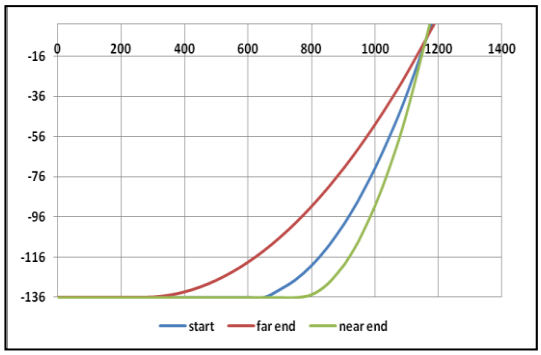

Figure 4-9 Vertical profiles of mooring line 1 at mid, near, far positions when w = 0.8 kN/m and δ= 7.5 m

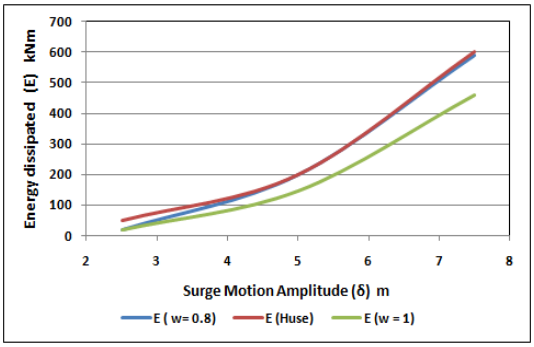

Figure 4-10 Comparison between Huse's dissipated energy to calculated energy when *w* = 0.8 and 1 kN/m

4.3.3 Effect of water depth on the energy dissipation

In this section, the energy dissipation approach is applied to a semisubmersible platform moored using a single mooring line as before but at different values of the water depth. In this study and at all of the selected values of the water depth the total horizontal distance between anchor and vessel and the distance between anchor point and lift off point are kept constant. Hence, the total length of cable, the suspended length and required pretension would consequently be different for each selected water depth.

At the initial water depth h = 250 m, the cable length is assumed to be 1000 m. Afterwards the suspended length, distance between vessel and anchor point and distance between vessel and lift off point are calculated. These distances X, x, and AB are then kept constant at the other values of the water depth. From this, the corresponding cable length and the suspended length are each estimated at the other water depth values. At a submerged weight per unit length = 15 kN/m, the calculated values of cable length, suspended length, horizontal position of the vessel and pretension force corresponding to several values of water depth are shown in Table 4-4. In addition, Figure 4-11 shows the vertical profiles of the mooring lines at the chosen water depth values.

For each of the water depth cases shown in Table 4-4, various arbitrary values of the surge motion (mean value and amplitude) of the fairlead point were chosen in order to carry out the energy calculations. The same set of the arbitrary values are applied to all water depth cases. The pretension in each of these cases was calculated by solving the catenary shape equation (4-4). Another method that can be used to estimate the value of the mooring line tension is from the static pull out test (see Chapter Three). Figure 4-12 shows a comparison between the static pull out test measurements and the calculated tension obtained by the author from the above equation and where a good agreement

between the two methods is observed. In the current case study, the tension is calculated using the first method as it is suitable at any displaced position of the structure.

Table 4-4 Mooring line characteristics at different water depths

Water depth (h) (m)	Pretension (T_O) (kN/m)	Suspended length (m)	x(m)	L(m)	X(m)	AB(m)
250	2410	377.93	255.61	1000	877.68	622.07
300	2126.66	418.41	255.61	1040.48	877.68	622.07
400	1779.04	504.86	255.61	1126.93	877.68	622.07
500	1572.61	595.68	255.61	1217.75	877.68	622.07
600	1434.59	689.03	255.61	1311.10	877.68	622.07
700	1334.95	783.96	255.61	1406.03	877.68	622.07
1000	1150.00	1073.93	255.61	1696.00	877.68	622.07

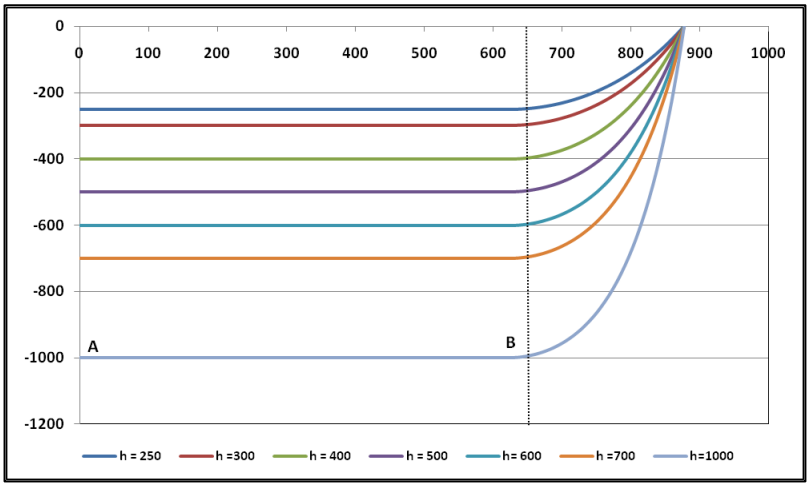

Figure 4-11 Vertical profiles of the mooring line at different water depths

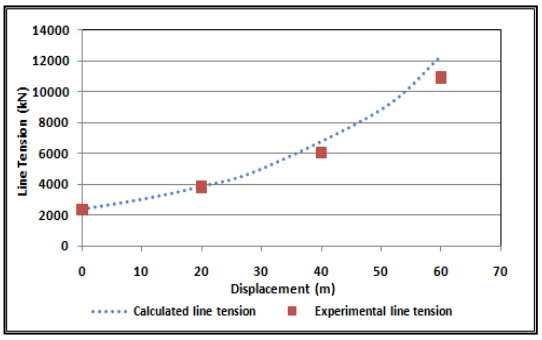

Figure 4-12 Experimental and calculated mooring horizontal line tension force

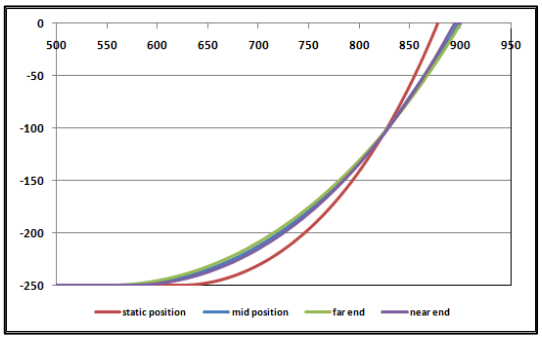

Figure 4-13 Vertical profile of mooring line at different positions at S= 20 and δ = 3m

Assuming mean surge motion movement *S* values of 10 and 20 metres and motion amplitude δ of values of 1 to 6 metres about the mean position of the structure, the corresponding new shifted position of the platform (mid position), near end and far end positions of the platforms are calculated at each of the water depth values shown

previously in Table 4-4. An example of the mooring line catenary shape at the original static position, and at a shifted mean position with corresponding near end and far end positions at a water depth 250 m is shown in Figure 4-13 at S= 10 m and δ= 3m .

4.3.3.1 Results

The following Figures Figure 4-14 and Figure 4-15 show comparisons of the energy dissipated by the mooring line at two values of mean displaced distance in the direction of the surge motion (S= 10 and 20 m) and various amplitudes. These two figures show the effect of the surge motion amplitude δ on the energy dissipated as well which ranges between 1 and 6 metres. It is observed that the energy increases with the increase of the surge motion amplitude and goes down with increase in the displacement of the position in the direction of the surge motion.

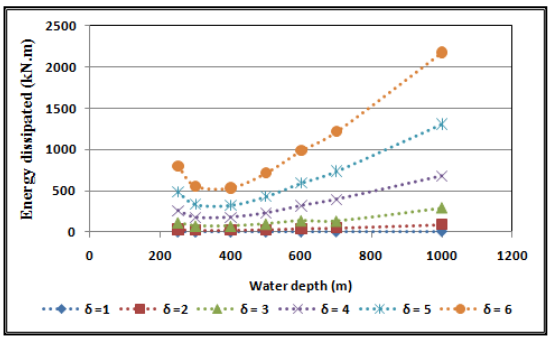

Figure 4-14 Effect of water depth on dissipated energy at S= 10 m

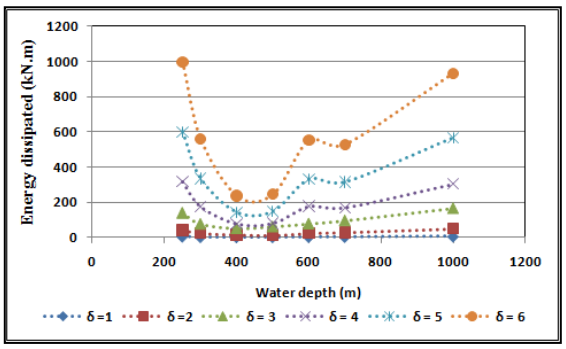

Figure 4-15 Effect of water depth on dissipated energy at S= 20 m

The date plotted in Figure 4-14 and Figure 4-15 can be presented differently by comparing the effect of the two mean surge motion S values at each of the different values of the surge motion amplitudes. Figure 4-16 to Figure 4-21 inclusive show that at all of the six assumed values of the surge motion amplitude, there is an obvious decrease in the dissipated energy when increasing the mean surge displacement from 10 to 20 m.

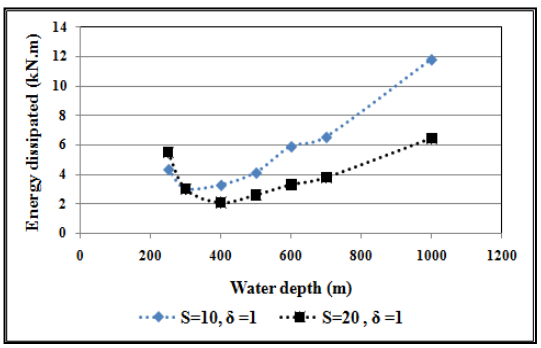

Figure 4-16 Effect of water depth and mean surge displacement on energy dissipated at δ = 1m

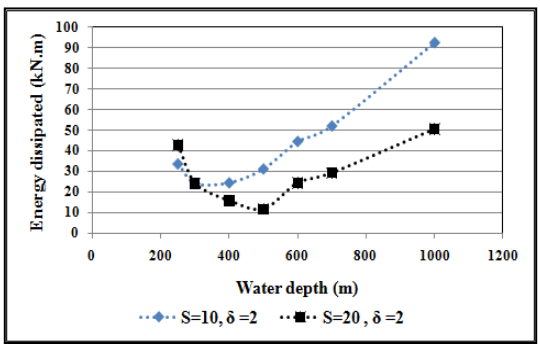

Figure 4-17 Effect of water depth and mean surge displacement on energy dissipated at δ = 2m

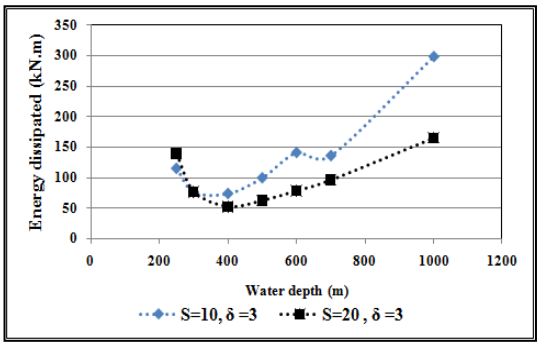

Figure 4-18 Effect of water depth and mean surge displacement on energy dissipated at δ = 3 m

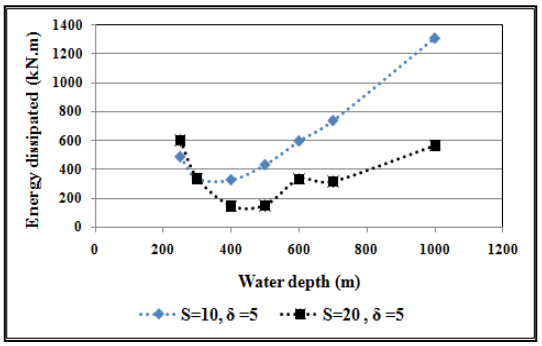

Figure 4-20 Effect of water depth and mean surge displacement on energy dissipated at δ = 5 m

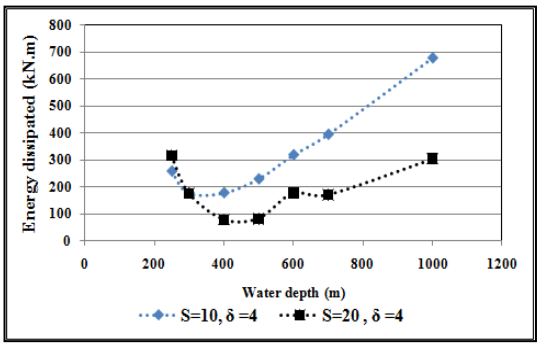

Figure 4-19 Effect of water depth and mean surge displacement on energy dissipated at δ = 4m

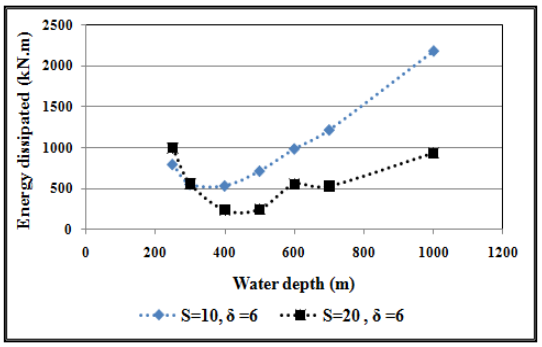

Figure 4-21 Effect of water depth and mean surge displacement on energy dissipated at δ = 6 m

4.3.4 Semisubmersible model study

In the previous section, a study of the motions and damping of a vessel moored with a single mooring line was presented. In this section a more practical case is studied with a symmetrical arrangement of four mooring lines. The semisubmersible model that was used in the experimental tests and employed in the current study is moored using four cables with orientation angles of 45,135,225, and 315 degrees as shown in Figure 4-22 .

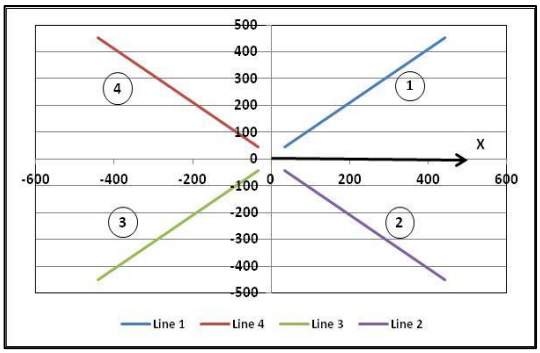

Figure 4-22 X-Y plan of the mooring lines orientation angles

The original as-installed measured coordinates of the mooring lines in the still water static position were recorded in a three-dimensional format. In order to be able to study the motion of each of these lines individually, the coordinates are converted into 2D coordinates. Figure 4-23 shows the vertical profile of the 3D coordinates of two of the

mooring lines. The other two lines are coinciding with these two. The plotting of the 2D data of the mooring lines is shown in Figure 4-24.

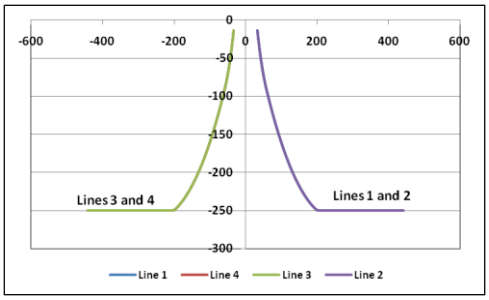

Figure 4-23 Vertical profile of the 3D data of the mooring lines

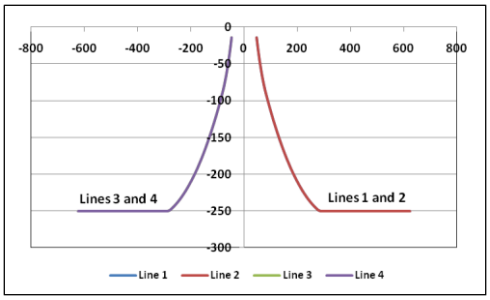

Figure 4-24 Vertical profile of the 2D data of the mooring lines

The Huse energy dissipation approach is applied to the four mooring lines and the total energy of the system is the sum of each of the separate lines dissipated energy. The current study is for the surge motion in the direction of the global X- axis. For each mooring line, the analysis is applied in the vertical plane of the line itself. Thus the mean displaced distance in the surge direction of the vessel S_O is used to estimate the mean displaced distance s_O in the in-plane direction of each line as $s_O = S_O * |\cos(\alpha)|$ where α is the angle between vessel surge motion and mooring line direction. As the vessel moves to the right (positive X-axis) with surge displacement *S*, two mooring lines are stretched by the motion while the other two are compressed by the same amount. This effect of the motion on the position of the vessel is taken into consideration while conducting the energy dissipation calculations for this mooring system.

4.3.4.1 Results

Table 4-5 shows the calculated energy dissipated by the two slacking and by the two stretching mooring line pairs and the combined (four lines) total energy in different regular wave sea conditions. The mean surge displaced distance *S* and the amplitude of the motion δ values given in Table 4-5 are for the motion of the semisubmersible. These values are estimated as being the mean and standard deviation values of the surge motion time series data in regular sea states, previously discussed in Chapter Three. The corresponding values for the mooring lines in the directions of the lines themselves are estimated using the values of the angles between mooring line directions and vessel surge motion direction. The value of the mooring line diameter that is used in the

calculation is D_L = 0.284 m, which is calculated as being the average for the three segments as shown previously in Table 4-1.

In Section 4.3.3.1 , it was shown that the increase of the mean surge motion displacement value results in a decrease in the dissipated energy. On the other hand, the increase in the cyclic amplitude of the motion results in an increase in the dissipated energy. Table 4-5 shows the dissipated energy at different values of the mean surge displacement and cyclic amplitude. It is observed that when comparing the results from the two waves REG (H10, T10) and REG (H22, T15), though the first wave induced almost double the mean surge displacement, but the total dissipated energy is less.

Table 4-5 Energy dissipated of catenary mooring lines in regular waves

Wave	Mean surge displaced distance S (m)	Amplitude of the oscillating motion δ (m)	Slacking lines energy (kN.m)	Stretching lines energy (kN.m)	Total energy (kN.m)	Damping (tonnes/s)
(H5, T10)	12.07	1.64	171.36	52.92	224.3	0.78
(H10, T10)	42.47	2.10	10086.96	803.89	10891	3.06
(H11, T15)	3.72	2.63	887.33	1149.64	2037	111.71
(H22, T15)	23.48	5.60	13643.76	4489.76	18134	24.99
(H33, T15)	56.76	7.18	N/A	N/A	N/A	N/A

This can be explained by the observation that one of the main parameters affecting the energy is the vertical difference of the mooring line position in the near and far end positions ΔZ that was introduced in equation (4-11). In Figure 4-25 to Figure 4-28 inclusive, it can be seen that ΔZ changes dramatically depending on the vertical profile of the mooring line for the near and far end positions of the surge oscillation. The mid positions, which form the centre location between the near and far positions, depend on both the mean surge displacement and the cyclic amplitude. Hence, the higher dissipated energy that is observed is seen to be where the near and far end positions result in higher ΔZ values. This is found in Figure 4-28 for the wave (H22, T15).

As for the wave (H33, T15), the energy dissipated was not calculated due to that the surge mean displacement being higher than the known range of the force-displacement relationship of the platform so it was excluded from the analysis.

In summary, an increase in the mean surge displacement S results in decreasing the energy dissipated, while an increase in the cyclic motion amplitude δ results in an increase in the energy. This can be explained by the effect of such changes on the vertical profile of the catenary mooring lines in both the near end and far end surge oscillation induced positions. The dissipated energy is proportional with the cube of the difference of the vertical coordinates ΔZ of these two positions. Thus any slight increase in ΔZ values would contribute to a large increase in the energy dissipated. On the other hand, from observations of the studied cases using the selected values of (S and δ) obtained from regular waves measurements, it is found that both of (S and δ) would affect the vertical profile of the mooring lines and thus control the change in (ΔZ) and consequently , the dissipated energy and damping.

The dissipated energy in different sea states largely varies according to the changes in the mean surge displacement and the oscillations amplitude. Thus, in order to compare the effects of the different sea states, the dissipated energy levels in the different sea states are compared to the surge mean displacements and to the corresponding relative damping, as shown in Figure 4-29 and Figure 4-30.

Figure 4-29 and Figure 4-30 show that it is not necessary that high-dissipated energy levels will lead to high damping. As for the studied cases, the highest amount of dissipated energy was obtained at the waves (H22, T15) and (H10, T10). On the other hand, these two waves also caused a large mean value of the surge displacement and hence smaller relative damping than that produced by the wave (H11, T15) where it produced a smaller mean surge displacement and a larger relative damping value.

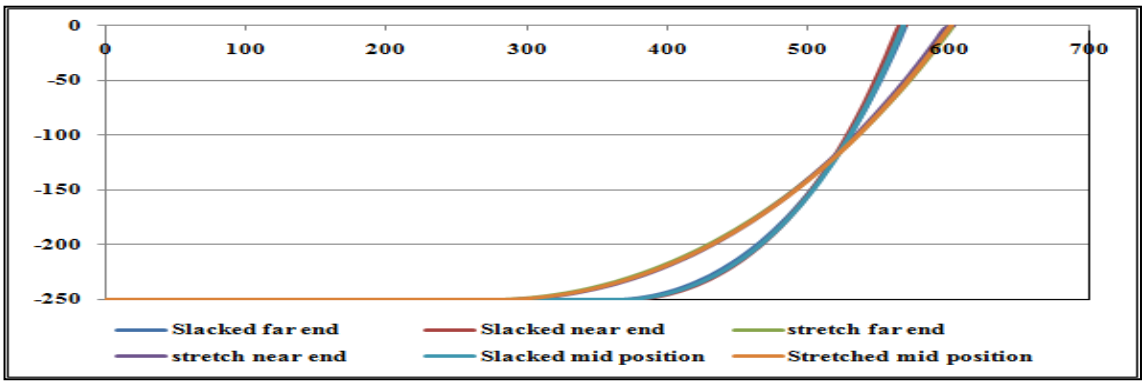

Figure 4-25 Vertical profiles of mooring lines in wave REG (H5, T10)

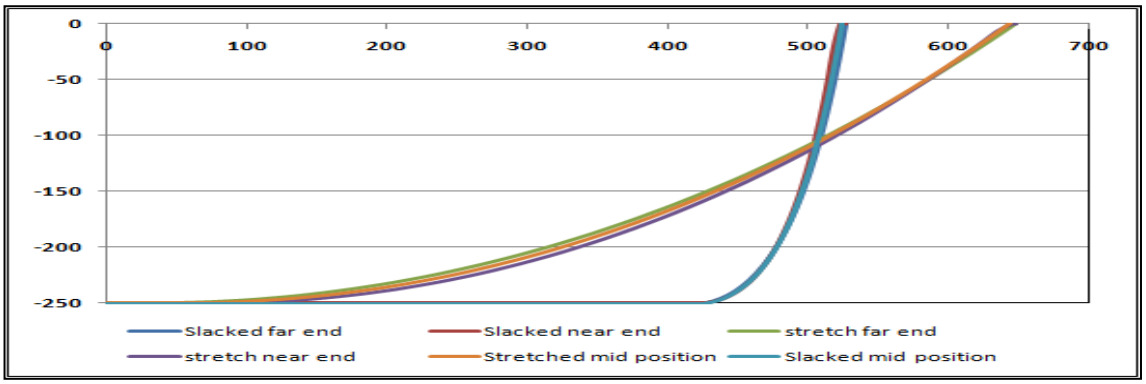

Figure 4-26 Vertical profiles of mooring lines in wave REG (H10, T10)

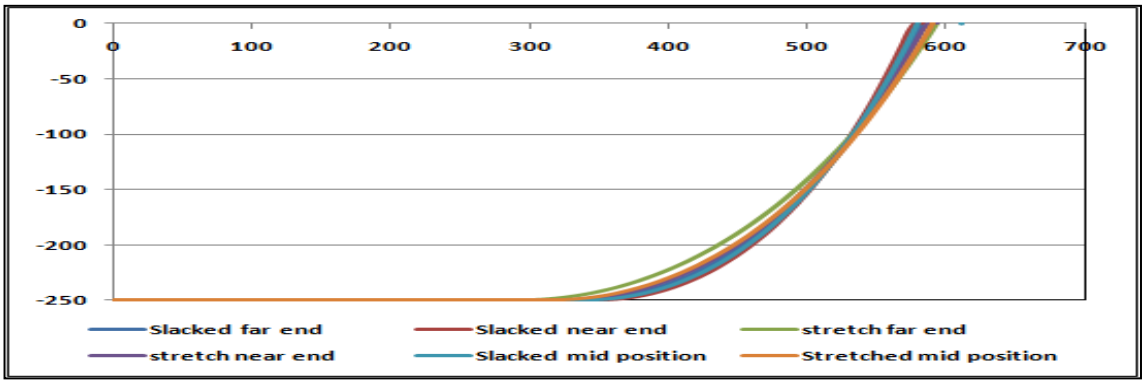

Figure 4-27 Vertical profiles of mooring lines in wave REG (H11, T15)

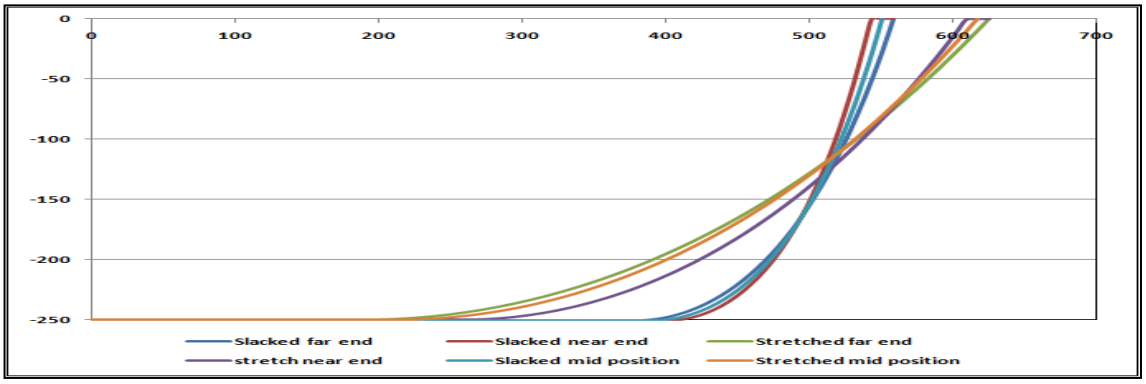

Figure 4-28 Vertical profiles of mooring lines in wave REG (H22, T15)

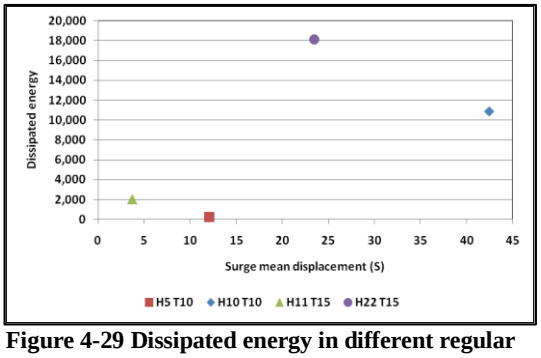

Figure 4-29 Dissipated energy in different regular sea states

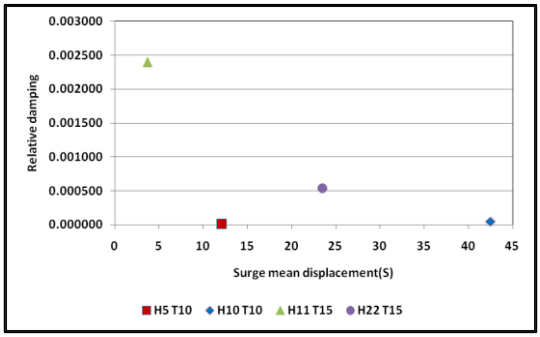

Figure 4-30 Relative damping in different sea states

4.3.5 Effect of superposed high-frequency motion

In addition, Huse's approach takes into account the effect of high frequency motion on the drag force and hence on the energy dissipated. Such an effect is studied by introducing a new parameter that is the velocity amplitude ratio (VAR) which is given $\frac{E_m}{E_O} = \frac{\omega_m \eta_m}{\omega_O \eta_O}$, provided that $\frac{\omega_m}{\omega_O} \gg 1$. VAR is approximated by quasi-stationary approach to be $\frac{\omega_m S_m}{\omega_O S_O}$ where S_O, and S_m are the low-and high-frequency motion amplitudes respectively at the fairlead point. The values of $\frac{E_m}{E_O}$ as a function of VAR are given in Figure 4-31.

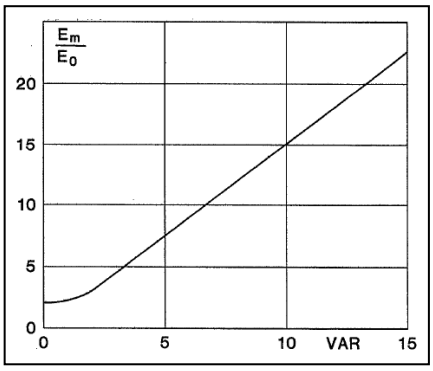

Figure 4-31 Correction factor for the influence of the superposed high-frequency line motions (Huse and Matsumoto, 1988)

However, the actual VAR value would be less than $\frac{\omega_m S_m}{\omega_O S_O}$ due to that the observed line shape would have deviated from the original catenary shape in the initial stationary position. A computer program developed by MARINTEK was used by Huse to study VAR based on application of the finite element method. The program considers the following factors: line material tensile elasticity, seabed friction, line mass force, and quadratic fluid drag force on the line. The program calculated the ratio between the high-frequency line motion amplitude obtained by dynamic analysis to that from a quasi-stationary approach. This ratio depends on line construction type, degree of pretension, surge amplitude and surge frequency. Thus an approximate was found to be: $VAR = K_D \frac{\omega_m S_m}{\omega_O S_O}$ where K_D is a correction factor due to the line dynamics and which ranges normally between 0.2 and 1 for typical moored offshore structures.

The damping coefficients were calculated from decay tests in still water and in a current flow. As shown earlier in Chapter three, a single value of damping may be estimated using either the exponential approximation method or as a function of the motion

amplitude using the logarithmic decrement method. On the other hand, the energy dissipation method depends on both the mean surge displacement and the cyclic surge amplitude (S and δ) in order to calculate the damping and the corresponding relative damping coefficient.

The experimental test programme that was conducted during this study, and that was previously introduced in Chapter Three, did not include any decay tests in the regular waves. Thus it is not possible to compare damping coefficients from experiments with those that were obtained from the energy dissipation method.

As for conditions in irregular waves, the wave spectra are generally known from experimental data and thus the low and high frequencies can be identified. In addition, the time series data can be filtered into low and high frequency time series components and hence the corresponding low and high frequency mean surge motions may be estimated. If decay tests are available in irregular waves and by using the low and high frequencies and corresponding mean surge motions, then the corresponding values of VAR may be estimated. In this way, it would have been possible to compare the damping coefficients estimated from decay tests with those that were estimated from the energy dissipation method. Unfortunately, this is not available in the current study because data from decay tests in irregular waves are not available.

4.4 Summary

In this chapter, the energy dissipation method was investigated in details and was applied on a Semisubmersible in two cases. In the first case the platform is moored with a single line and in the second case was moored with four lines. The single mooring line case was used to investigate the effects of both the water depth, mean value of surge displacement of the platform, the amplitude of the surge motion fluctuation on the dissipated energy and damping. On the other hand, the four mooring lines case showed that the sea state effect on the damping cannot be determined via estimating only the dissipated energy as the value of the mean surge displacement contributes to the damping as well.

Chapter 5. Results and Correlations

5.1 Introduction

In Chapter Two, two numerical simulation methods were presented in order to estimate the wave loading forces and response of a semisubmersible platform; namely a three-dimensional linearized diffraction – radiation technique and the Morison's approach. In the current chapter, numerical results are presented and comparisons between the two methods are made versus the results from the experimental tests that are presented in Chapter Three in cases where enough data is available.

In addition, a discussion of the estimation of the mooring line relative damping ratios estimated from the decay tests and from the mooring line energy dissipation method is presented.

5.2 Three-dimensional technique numerical computations

The estimation of the wave loading on and responses of a semisubmersible platform in regular waves was carried out using a software packages that is based on the three dimensional technique shown in (Chan, 1990) and mentioned in the previous chapters. The first program is HullSUR3D.exe, which uses the coordinates of the platform points/nodes in order to generate the faceted hull surface panels on which integration is conducted. In the current study, the points/nodes were chosen to form the external surface of a semisubmersible hull whose geometric characteristics are the same as the full scale dimensions of the model that was used in the experiments that were discussed in detail previously in Chapter Three. The model used is of a semisubmersible platform with four square columns with rounded corners and rectangular section ring pontoons. The semisubmersible platform thus was modelled by 4044 panels. The generated mesh of these panels at draught of 21 metres is plotted and shown in Figure 5-1.

The next step was to define the mooring system characteristics into the second program that is named LossMoor.exe. These characteristics include the number of mooring lines, co-ordinations of the attachment points, orientation angles, inclining angles, stiffness and pretension of each of the mooring lines.

After defining the geometric characteristics of the platform and the characteristics of its mooring system, the final program Motion3D.exe is applied in order to estimate the wave first-order forces and the corresponding phase angles, second-order force, added mass, damping, motion response amplitudes and the corresponding phase angles in the

frequency domain. The Motion3D program requires data about both the environmental sea conditions and of the platform geometry below the still water line.

The environmental conditions used are: water density, water depth, and current velocity, number of wave heading approaching angles to be examined and their values, and the range of values of wave frequencies at which motion loadings and response would be estimated. The waves are assumed to be of a regular nature and at unit amplitude of wave height. Thus, the obtained values of the first-order variables are per unit of wave amplitude and those of second-order are per wave unit amplitude squared.

In addition, more information about the platform geometry such as the vertical position of its centre of gravity and the hull moments of inertia must be provided in order to carry out the motion calculations. It is assumed that the structure is doubly symmetric such that the centre of gravity is at the simple geometric centre as shown in a plan view at the centre of X and Y coordinates as shown in Figure 5-2. To ensure that the chosen panel size and dimensions are sufficient to provide accurate results, the individual panel size was chosen so that the width of the panel should not exceed half of the minimum wavelength to be examined. In addition, both the panel width and height dimensions should result in a reasonable aspect ratio of around a value of unity (i.e. keeping all panels to be reasonably square shaped).

5.3 Mooring systems characteristics

In this section, the alternative sets of characteristics of both a horizontal and a catenary mooring systems of specific arrangements are presented. For both the horizontal and the catenary mooring systems, the platform is moored using four lines, which are at orientation angles of 45, -45, 225 and 135 degrees (i.e. a symmetrical 45 degrees spread) and the corner attachment points (fairleads points) are at height of 21m above the base plane. The main specifications for the two mooring systems are shown in Table 5-1 and Table 5-2. The basic mooring lines layout in plan view is sketched in Figure 5-2. The static pull out test previously presented in Chapter Three, showed that the stiffness of the individual lines in the system is 144.8 kN/m. The horizontal stiffness of the catenary mooring lines mentioned in Table 5-1 and Table 5-2 is defined as the horizontal stiffness at zero- displacement or the still water condition of the model and is determined by the slope of the force-displacement relationship which is known from the static pullout test. In addition, for the catenary mooring system, the inclining angles are

determined as being the local slope of the catenary vertical profile of the mooring lines arrangement at the attachment point in the static position.

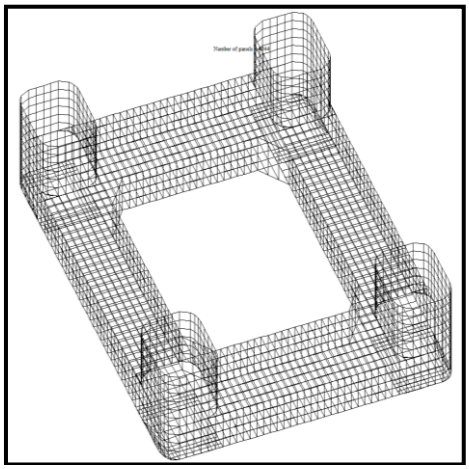

Figure 5-1 Platform surface mesh

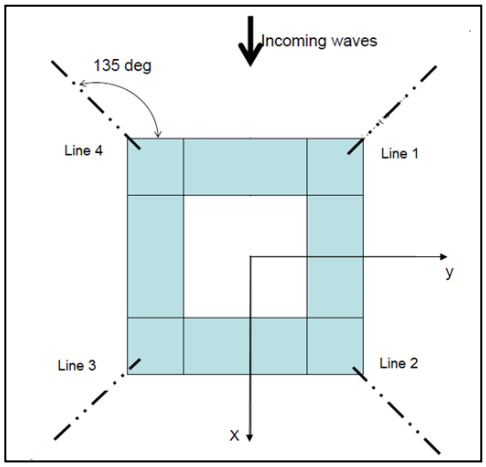

Figure 5-2 Orientation angles and locations of the mooring lines

Table 5-1 Horizontal mooring system specifications

	Cable 1	Cable 2	Cable 3	Cable 4
X to Aft Perpendicular (m)	75.84	75.84	8.64	8.64
Y From CL (m)	42.24	-42.24	-42.24	42.24
Z above base line (m)	21			
Orientation angle (degree)	45	-45	225	135
Inclining angle from free surface(degree)	0			
Horizontal cable stiffness (kN/m)	72.405			
Pretension (kN)	2410			

Table 5-2 Catenary mooring system specifications at water depth h = 250 m

	Cable 1	Cable 2	Cable 3	Cable 4
X to Aft Perpendicular (m)	75.84	75.84	8.64	8.64
Y From CL (m)	42.24	-42.24	-42.24	42.24
Z above base line (m)	7.2			
Orientation angle (degree)	45	-45	225	135
Inclining angle from free surface (degree)	70			
Horizontal cable stiffness (kN/m)	76.553			
Pretension (kN)	2410			

In the following sections, the calculated wave loading forces and system motion responses are presented for both the horizontal and the catenary mooring systems. For both mooring systems, the main calculated variables are the six D.O.F motion responses, wave first-order excitation forces, mean second-order forces, components of the mean second-order forces, added mass, and the potential damping. The previous mentioned variables were calculated at water depth values of 250, 500, 750 and 1000 m. For the horizontal mooring system, the properties of the mooring lines are kept constant at the different values of the water depth. On the other hand, for the catenary mooring

system, the characteristics of the lines are modified to ensure that the shape of the mooring lines satisfy the catenary shape equations at each value of the water depth.

5.4 Results

In this section, the first-order forces, added mass values and potential damping that are estimated using the three-dimensional technique are presented. These variables are all estimated at different values of water depth of 250, 500, 750 and 1000 m and are the same for both horizontal and catenary mooring systems. Subsequently, another study was made with two values of current speed of 0.6 and 1.2 m/s in order to investigate the effect of the current velocity on the semisubmersible model using both the horizontal and catenary mooring systems.

The numerical results of the three-dimensional technique have showed few irregular values of the first-order forces and the added mass presented in the next sub-sections. These irregular values are due to the singularity of the Green's function.

5.4.1 First-order wave forces

In this section, the amplitudes of the first-order wave forces and moments are presented for the semisubmersible model in following regular sea waves in the direction of the X-axis of the platform and at different values of water depth. After solving the coupled equations of motion, it is found that the first-order wave forces of sway, roll and yaw motions vanish, while those of surge, heave and pitch motions, which do occur, are not affected by the values of the water depth, as shown in Figure 5-3 to Figure 5-5 inclusive.

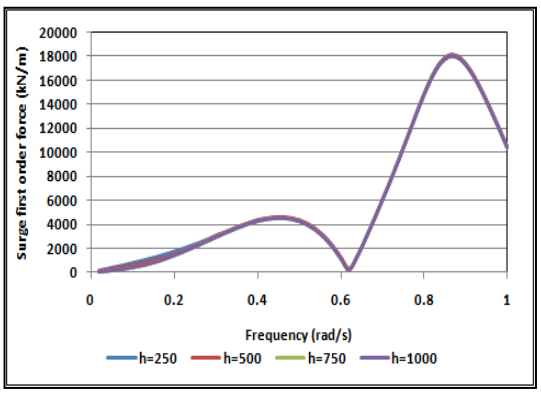

Figure 5-3 Surge wave excitation forces with horizontal mooring system

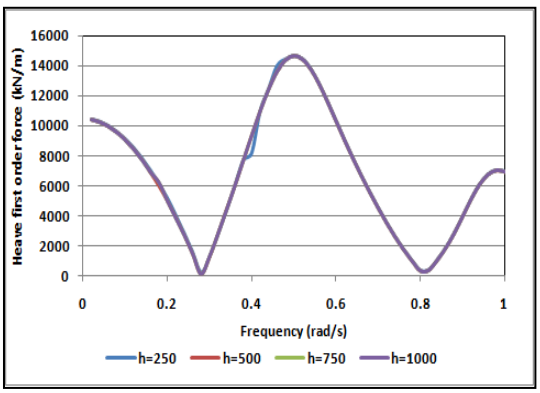

Figure 5-4 Heave wave excitation forces with horizontal mooring system

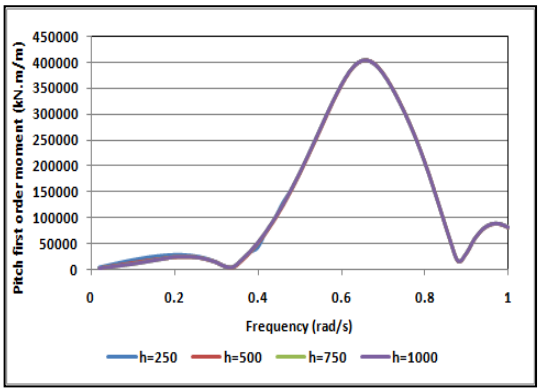

Figure 5-5 Pitch wave excitation forces with horizontal mooring system

5.4.2 Added mass

In this section, the six degrees of freedom added mass values are presented. It is found that the water depth has a very small or no effect on the added mass predicted. The most important area of concern in the current study is in the low frequency region near to the natural frequency of the system where the system experiences large motions at resonance frequency.

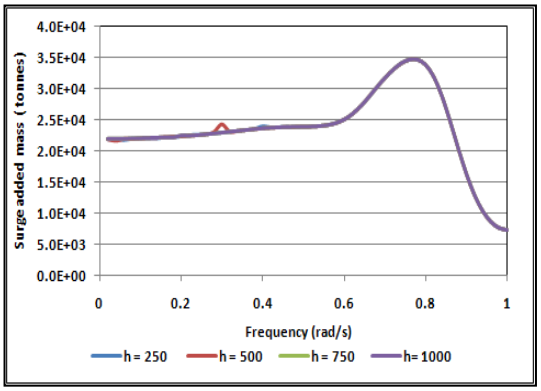

Figure 5-6 Surge added mass at four water depths

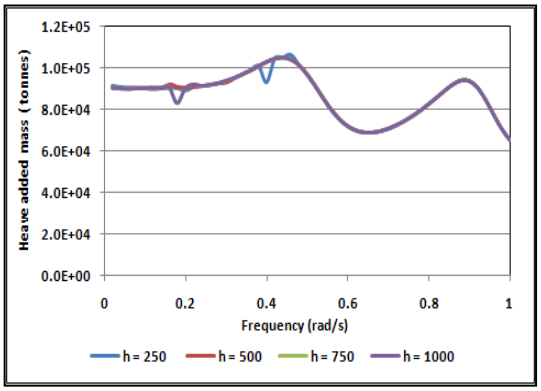

Figure 5-8 Heave added mass at four water depths

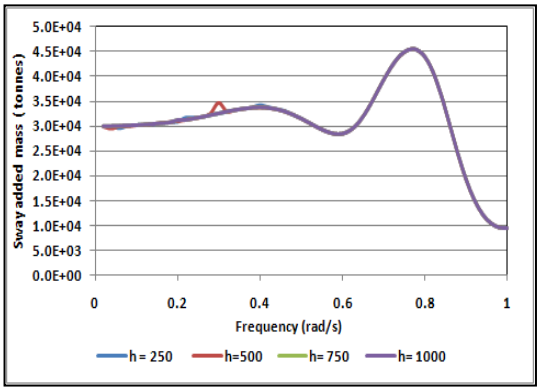

Figure 5-7 Sway added mass at four water depths

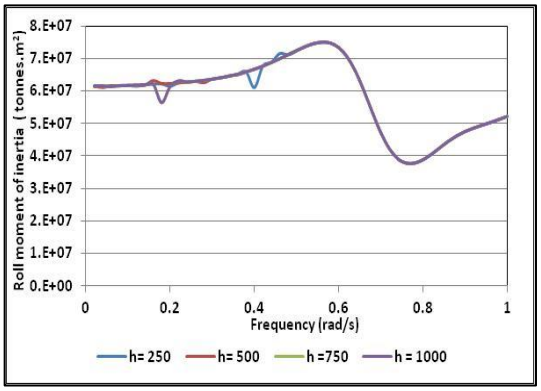

Figure 5-9 Roll moment of inertia at four water depths

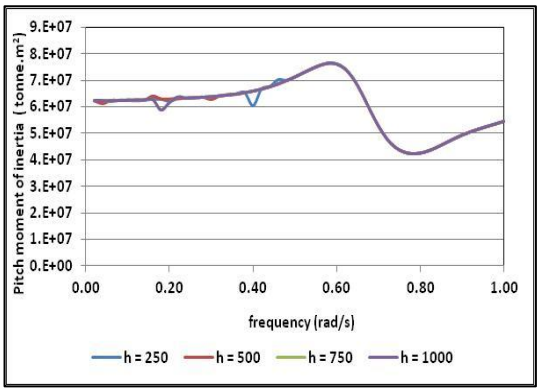

Figure 5-10 Pitch moment of inertia at four water depths

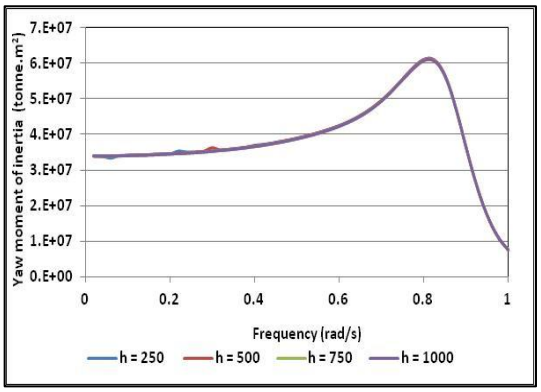

Figure 5-11 Yaw moment of inertia at four water depths

5.4.3 Potential damping

In this section, the calculated damping values for the semisubmersible platform are presented in Figure 5-12 and Figure 5-13. Figure 5-12 shows the damping for the surge, sway and heave motions and Figure 5-13 shows those for the roll, pitch and yaw motions.

It is observed from the two figures that at the low frequency region (around the various motions resonance frequencies) the potential damping vanishes which agrees with what was mentioned previously regarding the importance of low frequency motions response near to the resonance frequency.

In addition, same results for the damping values for the six degrees of freedom were estimated at different values of the water depth of 250, 500, 750 and 1000 m and where no effect of water depth was found. Thus, there was no need to present diagrams of these results.

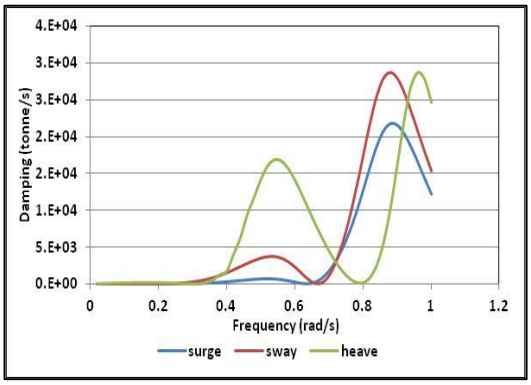

Figure 5-12 Surge, sway and heave damping

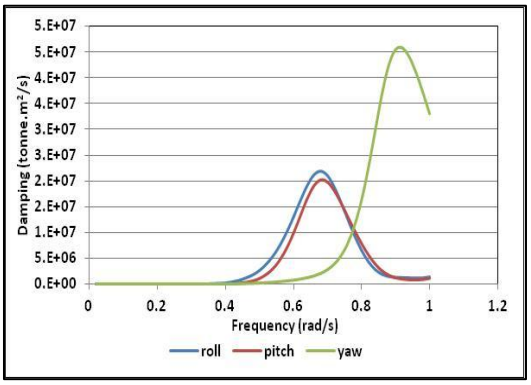

Figure 5-13 Roll, Pitch and yaw damping

5.4.4 Effect of current velocity on first-order forces

In this section, the effect of a current on the first-order wave forces was investigated at two current velocities of 0.6 and 1.2 m/s and compared with the results obtained for no current. It was found that for the surge first-order forces, that the current velocity has no effect at overall system frequencies that are below 0.8 rad/s (which represents the frequency of the second high peak of the forces). At frequencies that are larger than 0.8 rad/s, it was observed that the surge forces increase as the current velocity increases for the studied values of velocity. For the heave and pitch motions, a similar phenomenon was observed but at the different frequencies at which their peaks occurred. In addition, a change in the peak frequency was observed and this may be explained by the change of the effective wave encounter frequency due to the current velocity in the same direction of travel as the waves.

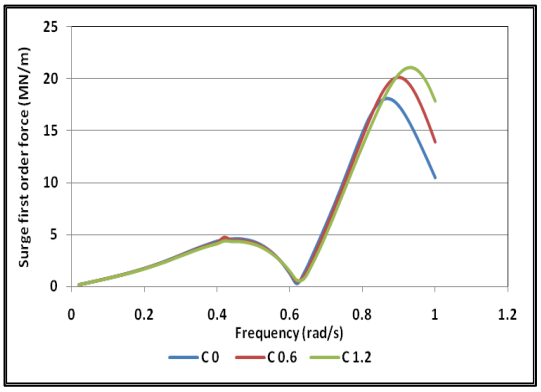

Figure 5-14 First-order surge wave forces at U = 0, 0.6 and 1.2 m/s

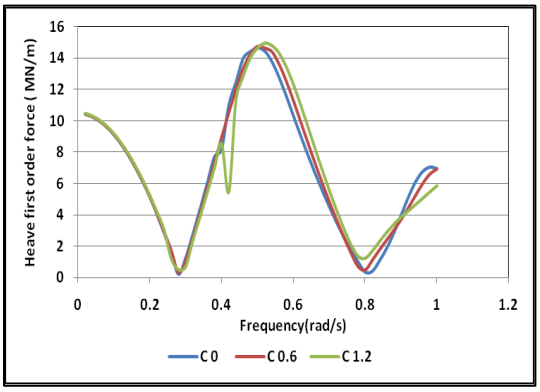

Figure 5-15 First-order heave wave forces at U = 0, 0.6 and 1.2 m/s

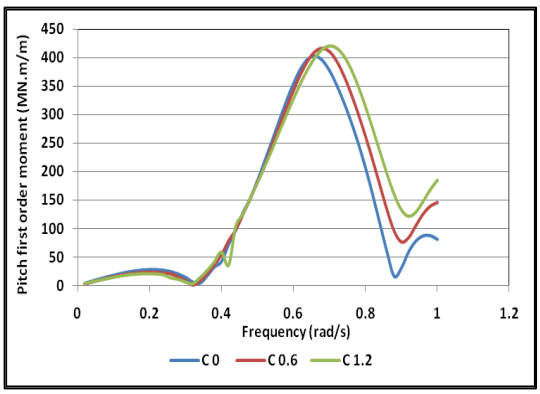

Figure 5-16 First-order pitch wave moments at U= 0, 0.6 and 1.2 m/s

5.4.5 Effects of current velocity on added mass

The magnitude of the added mass affects the value of the natural frequency of the rigid body structure. Therefore, any change in the magnitude of the added mass must be taken into consideration during an investigation of the peaks of the forces and motion

responses and of their corresponding frequencies. It was found that there was no effect due to the current velocity at low frequencies. At higher frequencies, the added mass was found to remain the same in magnitude. However, the value of the frequency that corresponds to the added mass peak was reduced as the current increases due to the reduction of the encounter frequency in following seas.

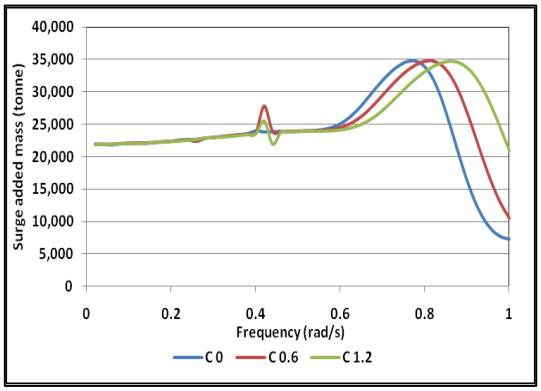

Figure 5-17 Surge added mass at different current velocities

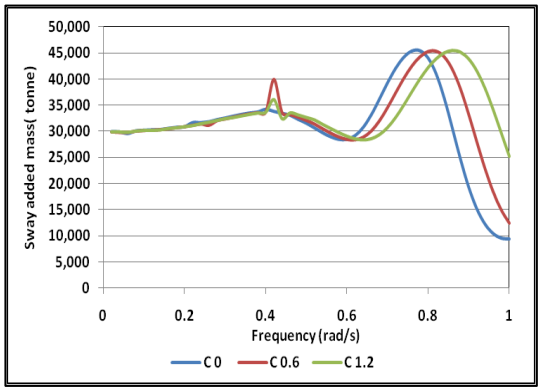

Figure 5-18 Sway added mass at different current velocities

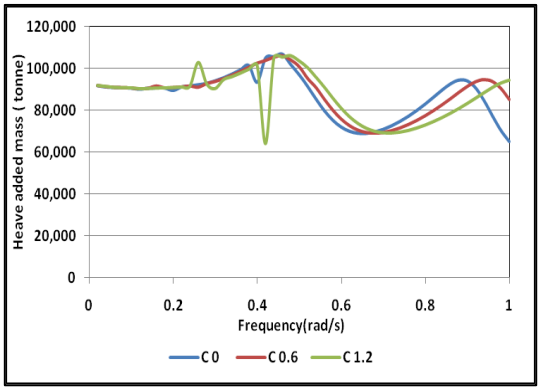

Figure 5-19 Heave added mass at different current velocities

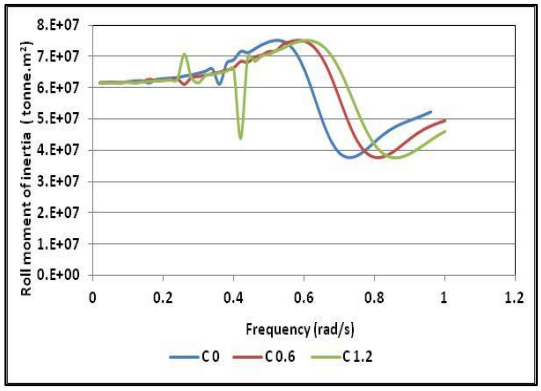

Figure 5-20 Roll moment of inertia at different current velocities

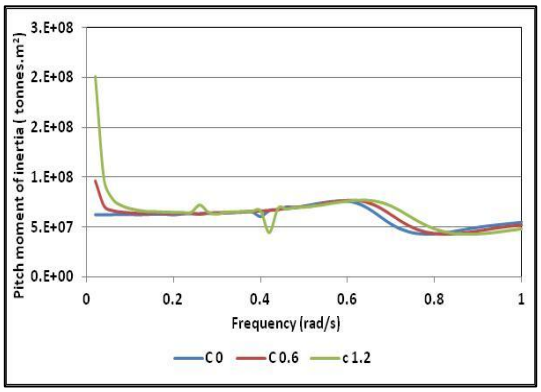

Figure 5-21 Pitch moment of inertia at different current velocities

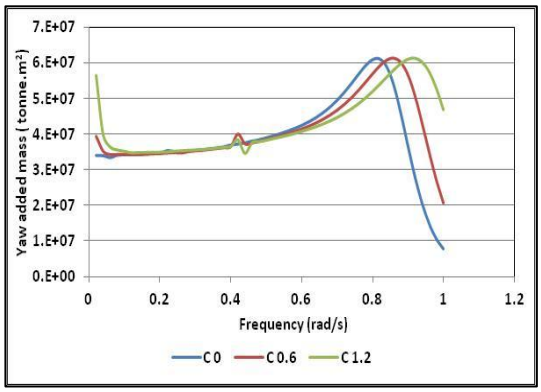

Figure 5-22 Yaw moment of inertia at different current velocities

5.4.6 Effect of current velocity on damping

As discussed earlier, the level of damping represents an important factor that controls the motion responses of the structure. The estimated potential damping was found to vanish at the low frequency region. On the other hand, the maximum value of the damping remained constant with the increase in current velocity; however, the frequency of the maximum damping was reduced in a similar manner that was described earlier for the added mass, due to the reduction in encounter frequency. The fact that the damping is very low in the low frequency region emphasizes the importance of the low-frequency wave forces, as it being low would allow large motion amplitudes to develop, and which would need to be taken into consideration in the process of the design of the mooring system.

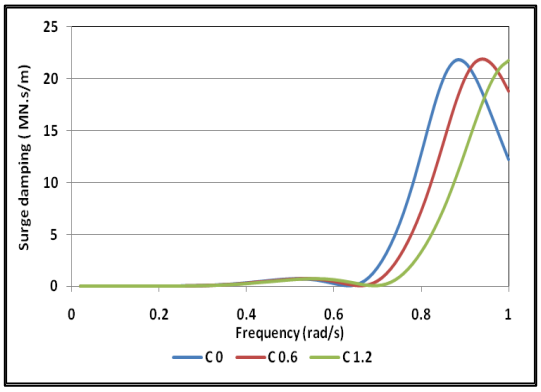

Figure 5-23 Potential surge damping at different current velocities

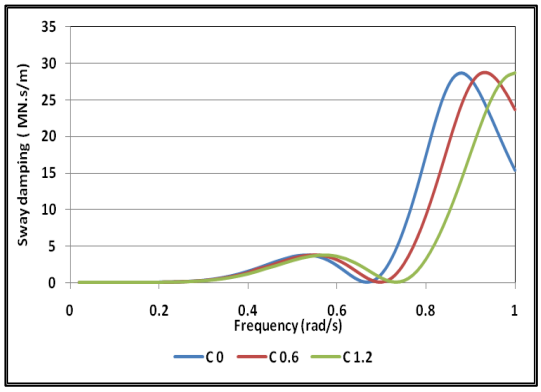

Figure 5-24 Potential sway damping at different current velocities

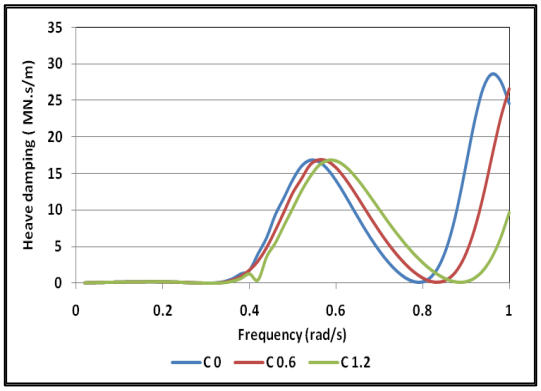

Figure 5-25 Heave potential damping at different current velocities

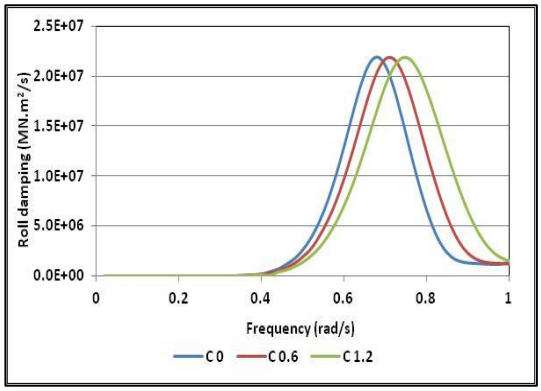

Figure 5-26 Potential roll damping at different current velocities

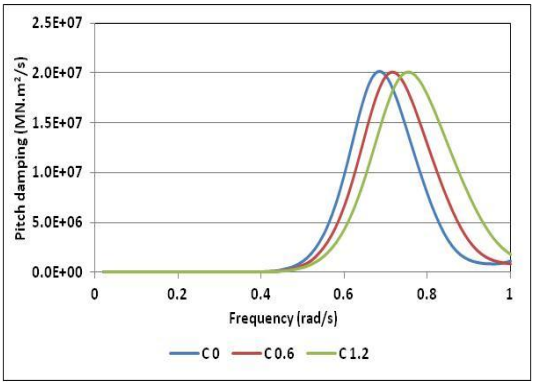

Figure 5-27 Potential pitch damping at different current velocities

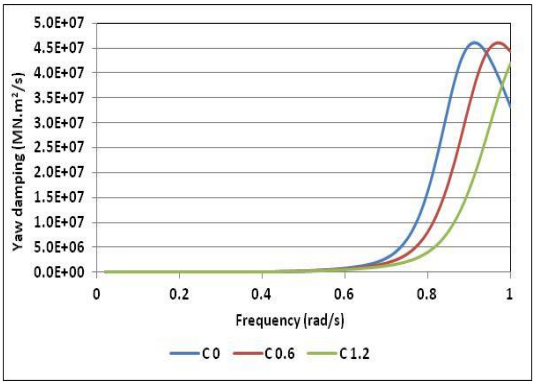

Figure 5-28 Potential yaw damping at different current velocities

5.4.7 Motion Response Amplitude (RAO)

In the earlier sections, the values of the first-order wave forces, potential damping and added mass per unit wave amplitude results were presented. These were not dependent on the mooring system. On the other hand, the mooring systems characteristics and forces on them affect the responses of the structure. Thus, in this section and in the following ones, a study of the effects of the mooring system was investigated specifically on the six degrees of freedom of the body of the first and second-order forces and the motion responses.

The presented results in this section are for the semisubmersible platform moored with alternatively the horizontal and the catenary mooring systems whose main characteristics are given earlier in Table 5-1 and Table 5-2 assuming following regular sea waves of unit wave amplitude.

As mentioned earlier, one of the main objectives of the study was the investigation of the motions, loading on and responses of the semisubmersible model in waves and currents. In the study, the wave direction remains fixed as a following sea, that is, where the waves are travelling in the direction of the main axis of the platform. In the cases of a combined wave- current field, both the current and the waves are in the same direction.

In Section 5.4.7.1, a study of the responses motion amplitudes (RAOs) at different water depth values for both the horizontal and catenary mooring systems is presented. Afterwards, in Section 5.4.7.2 , a study of the effect of the current velocity is presented and which shows the motions RAOs at current velocities of 0, 0.6 and 1.2 m/s.

For the two studies, the wave direction is following sea condition where the first-order forces of sway, roll and yaw vanish as shown previously in Section 5.4.1. Consequently,

the corresponding motion response amplitudes (RAO) of these motions of the semisubmersible platform also vanished. Thus, in the following two sections, only the responses associated with the surge, heave and pitch directions are presented.

5.4.7.1 Effect of water depth on RAO

The water depth effect was studied on the surge, heave and pitch motion in following sea at water depth values of 250,500,750 and 1000 m. Figure 5-29, Figure 5-31and Figure 5-33 show the surge, heave and pitch RAOs with the horizontal mooring system, respectively. In addition, Figure 5-30 , Figure 5-32 and Figure 5-34 show the RAOs of the same three motions with the catenary mooring system. For the catenary mooring system, the stiffness is linearized by the value of the stiffness at zero displacement.

Firstly, for the horizontal mooring system, it can be seen from Figure 5-31 that the heave motion RAO is not affected by the water depth.

As for the surge and pitch motions, the RAOs peaks, at the resonant frequencies, are reduced by the increase in the water depth value. This reduction is not significant for the pitch RAOs as all values are very small. Such a reduction is opposite to what is expected from solving the equation of motion as a single degree of freedom as theoretically, with horizontal mooring system, the water depth should not have an effect on the motion responses as the motions RAOs are generally controlled by the wave loading forces, mass, added mass, and damping. Thus, theoretically, one possible cause of such a reduction in motion responses may be due to the effect of the added mass. The comparison of the added mass shown earlier in Section 5.4.2 shows, however, that there is almost no change in added mass in the low frequency region thus making such an assumption invalid. Some minor changes were found at some frequencies but their values are very small with respect to the total mass of the platform and thus the added mass itself making such overall changes negligible. Thus, by investigating the exact values of both the first-order forces at the resonance frequency shown earlier in Figure 5-3 which indicated no change in the first-order force, small changes are which leads to larger difference due to the very low damping.

Secondly, for the catenary mooring system, the natural frequency is clearly dependent on the mass, added mass and stiffness of the overall system. Unlike the horizontal mooring system in which the mooring stiffness is constant at all water depth values; the stiffness of the catenary mooring system would change at each water depth in order to maintain the satisfaction of the catenary shape characteristics of the mooring lines.

Thus, the natural frequencies of the motions would consequently change. The change in the value of the motion natural frequency affects also the location of the corresponding peak of the motion RAO.

It is observed that the results at the water depth values of 500, 750 and 1000 metres show a consistent behaviour, as the peaks of the surge, heave and pitch RAOs are reduced as the water depth increases. On the other hand, however, at a water depth of 250 metres, the RAOs have peaks at different natural frequencies. This may be due to the observation that at this water depth and at very low frequencies, the wave length is relatively very large such that the water depth tends to behave as effectively shallow water. In addition, it is observed that the RAOs of the semisubmersible model with a catenary mooring system experienced smaller motion RAOs than those experienced when moored with the horizontal mooring system, and which is considered to be due to the increased damping due to the mooring lines.

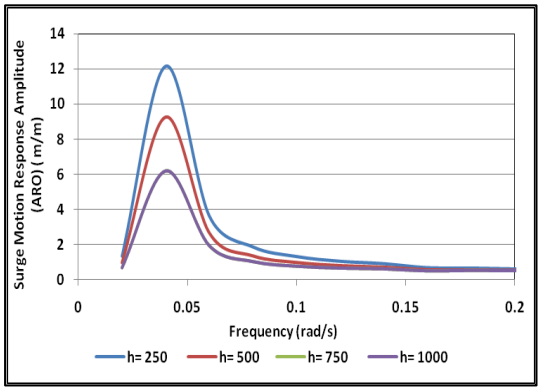

Figure 5-29 Surge RAO with horizontal mooring system at different water depths

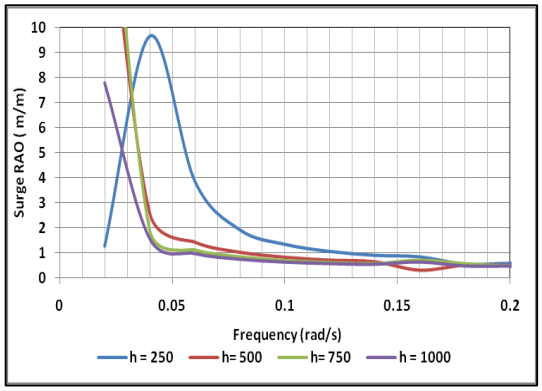

Figure 5-30 Surge RAO with catenary mooring system at different water depths

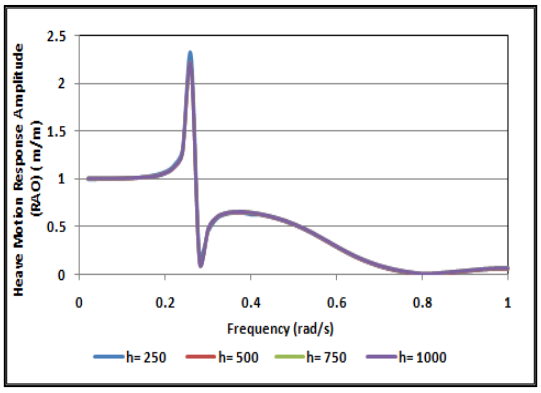

Figure 5-31 Heave RAO with horizontal mooring system at different water depths

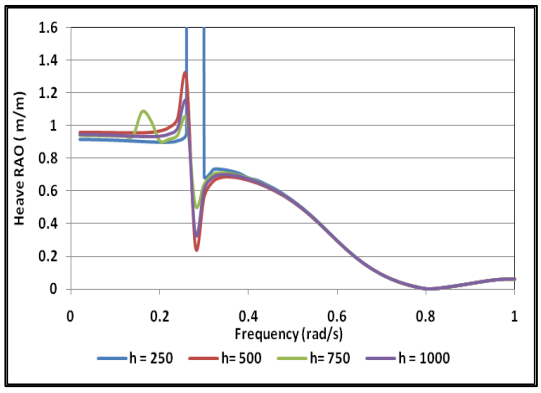

Figure 5-32 Heave RAO with catenary mooring system at different water depths

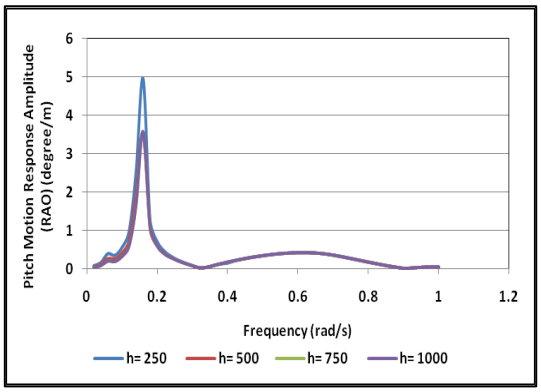

Figure 5-33 Pitch RAO with horizontal mooring system at different water depths

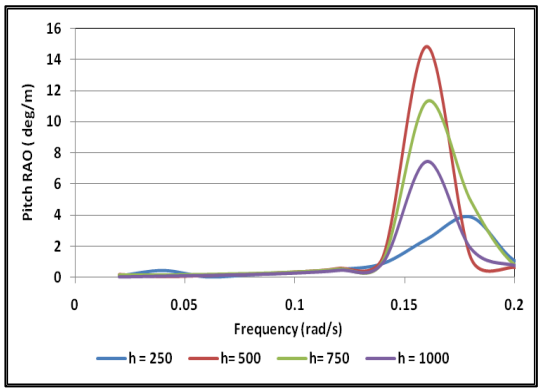

Figure 5-34 Pitch RAO with catenary mooring system at different water depths

5.4.7.2 Effect of current velocity on RAO

In this section, the results of a study on the effects of the current velocity on the body motion responses with both horizontal and catenary mooring systems is presented.

From the decay tests for the model that was moored with the horizontal mooring system mentioned earlier in Chapter Three, it is estimated that the natural frequencies of the motions of surge, heave, pitch, and yaw are 0.04, 0.27, 0.17 and 0.09 rad /s, respectively. A knowledge of the natural frequencies of different motions helps with identifying any coupled effect between the different motions during their study.

It is observed from the results shown in Figure 5-35 and Figure 5-36 that for both mooring systems the surge RAO is reduced as the current velocity increases. This coincides with the results from the decay tests that were made in different current velocities. Those decay tests, as described in Chapter Three, showed an increase in damping as the current velocity increases. In addition, no effect was observed due to any other motion interacting on the surge responses.

On the other hand, the increase in current velocities was found to result in an increase in the pitch motion RAO, at the critical frequencies in each case, for both mooring systems.

As for the heave motion, this mode of motion was found to be coupled with the pitch motion and small peaks of the heave RAO were found at around the natural frequency of the pitch motion. Comparing the heave RAOs at the two current velocities, shows that the higher peaks of heave occur at the higher current velocity of 1.2 m/s, than those obtained at 0.6 m/s. The coupled effect of pitch motion on heave is only observed in the existence of a current for the two mooring systems. In addition, a shift of the natural

frequency is observed as well at the current velocity of 1.2 m/s and this shift leads to the change of the peak frequency and hence the level of accuracy of the predicting the value of the peak of the motion RAOs.

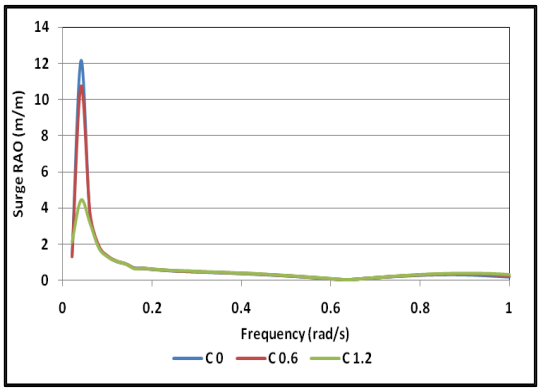

Figure 5-35 Surge RAO with horizontal mooring system at different current velocities

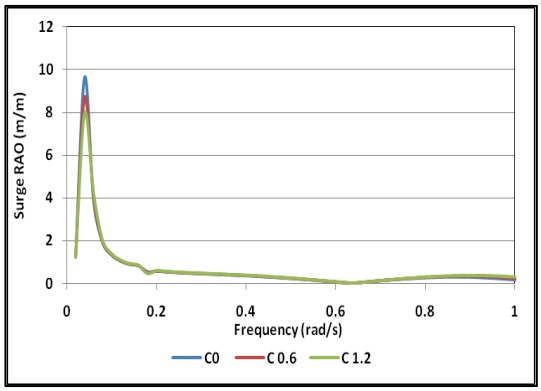

Figure 5-36 Surge RAO with catenary mooring system at different current velocities

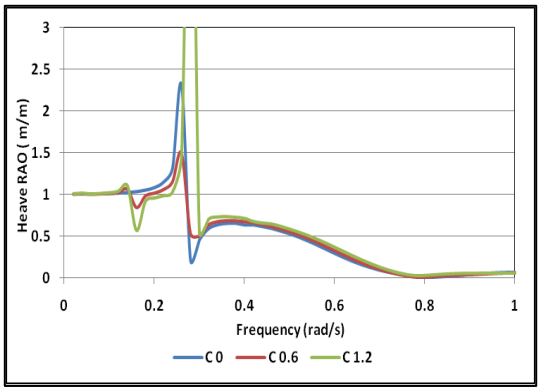

Figure 5-37 Heave RAO with horizontal mooring system at different current velocities

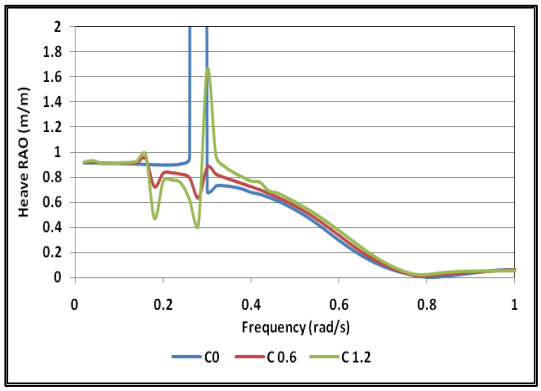

Figure 5-38 Heave RAO with catenary mooring system at different current velocities

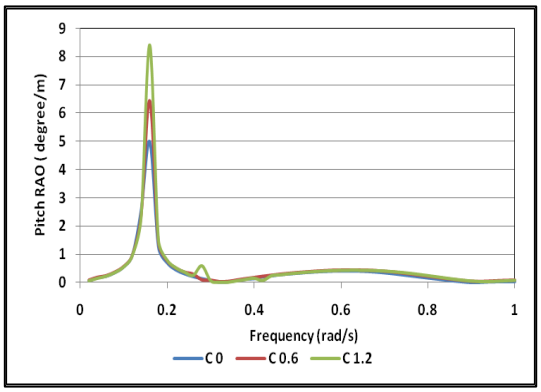

Figure 5-39 Pitch RAO with horizontal mooring system at different current velocities

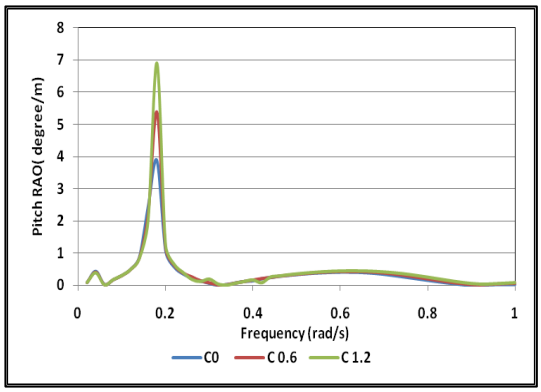

Figure 5-40 Pitch RAO with catenary mooring system at different current velocities

5.4.7.3 Effect of viscous damping on surge motion response

In all of the results produced and presented in Sections 5.4.7 and 5.4.8 of this chapter, the fluid was assumed to be inviscid and the viscous damping effect was not included.

In addition, Section 5.4.3 showed effect of that the potential damping was found to be negligible in the low frequency region around the resonance frequency.

Thus, in order to investigate the viscous effect on the motion responses, the approach described in Chapter Two which combines a three-dimensional technique together with a cross-flow approach, was applied. In the current section, an investigation of the effect of the viscous damping on the surge motion RAO is presented. Multiple values of the damping were chosen in order to cover damping ratios in the range between 0.01 to 0.88. The corresponding surge motion RAOs were estimated and are plotted in Figure 5-41 . This figure focuses on the responses at the natural frequency, which resembles the resonance situation of the surge motion. It was found that an increase in damping value results in a reduction in the peak of the surge response amplitude at the resonance frequency.

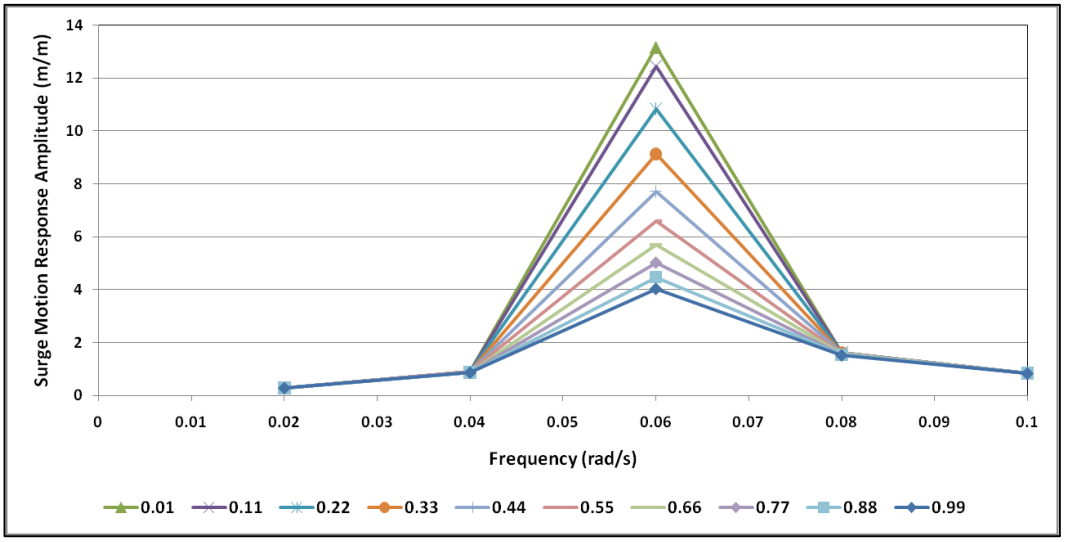

Figure 5-41 Viscous damping ratio effect on the surge response amplitude operator

5.4.8 Second-order drift forces

In spite of the facts that the second-order drift forces are smaller in magnitude than are the first-order forces however they occur in very low frequency region and where potential damping is negligible, as shown earlier in Section 5.4.3. The very small or negligible damping results in high motion responses when near to resonance frequencies. For moored structures, the drift forces in the horizontal plane play important role when investigating the loading on the mooring system that develop due to the low restoring forces.

In this section and the following one, the results of a study of the mean second-order drift forces and their components in a following sea and for different values of water depth and current velocities are presented.

5.4.8.1 Effect of water depth on mean second-order forces

In Figure 5-42 to Figure 5-47 inclusive, the second-order forces for surge, heave, and pitch motions are presented. As for the sway and yaw motions, they were found to vanish at all frequencies. In addition, roll mean second-order forces were found to be small enough to be neglected.

For the horizontal mooring system, Figure 5-42 and Figure 5-44 show that there is no change in the values of the mean second-order forces of the surge and pitch motions, respectively at the different water depth values ranging between 250 and 1000 m. In addition, the surge mean second-order force with horizontal mooring was not affected by any other motions. On the other hand, the pitch mean second-order force has small peaks at frequencies that correspond to the natural frequencies of the surge and heave motions.

As for the heave motion, Figure 5-43 shows that there is reduction in the drift forces at the low resonant frequencies as the water depth increases. In addition, the values of the heave second-order forces with respect to heave stiffness is found to be very small for the both horizontal and catenary mooring systems except at the heave resonant frequency with catenary mooring system at a water depth of 250 metres. At other values of water depth, the heave second-order forces are insignificant.

For the catenary mooring system, in the high frequencies region, similar results to those that were obtained when model was restrained with horizontal mooring were found. On the other hand, in the low frequency region, the surge second-order forces showed quite significant peaks corresponding to the natural frequencies of both the heave and pitch motions. These peaks vary with the water depth and vanished at water depth values of 500 and 1000 metres.

As for the heave second-order force, it was found that it is more affected by the water depth at the natural frequencies corresponding to the heave and pitch motions than being affected at the surge natural frequencies.

The effect of the catenary mooring lines on the second-order forces can be summarized as causing quite high peaks at frequencies corresponding to the heave and pitch resonant

frequencies for the three motions; surge, heave and pitch. The numeric values of these peaks are water depth dependant. In addition, the heave and pitch motions may have peaks as well at the surge resonant frequency.

For the horizontal mooring system, the mooring lines were assumed to have essentially they automatically zero vertical stiffness. On the other hand, for the catenary mooring lines, they automatically maintain the catenary shape properties, and thus the values of both the horizontal and vertical stiffness change from one water depth to another. This change in mooring line vertical stiffness may explain the changes in both the heave and pitch second-order forces.

The second-order forces of the different modes of motions were found to have negative values at some frequencies. This is investigated via the study of the different components of the surge second-order forces and presented later in Section 5.4.8.3.

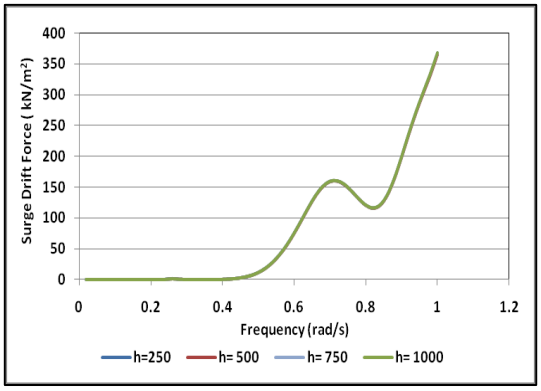

Figure 5-42 Mean second-order surge drift force with horizontal mooring system

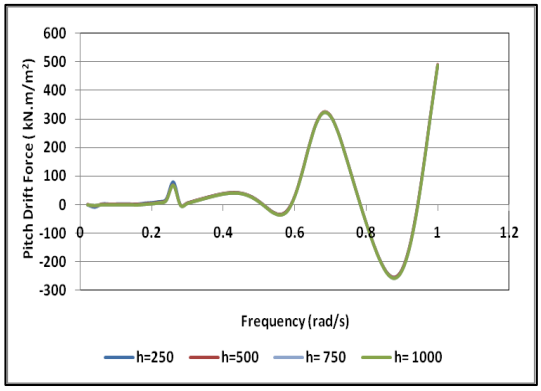

Figure 5-43 Mean second-order heave force with horizontal mooring system

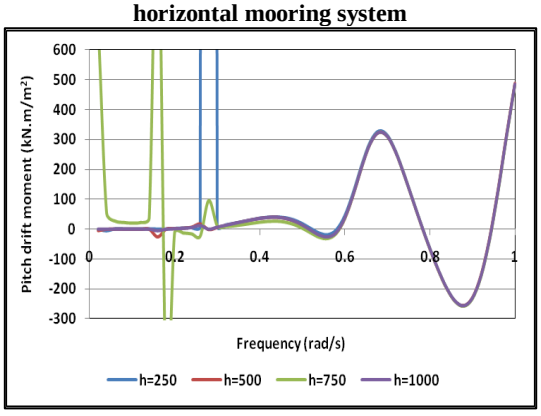

Figure 5-44 Mean second-order pitch drift moment with horizontal mooring system

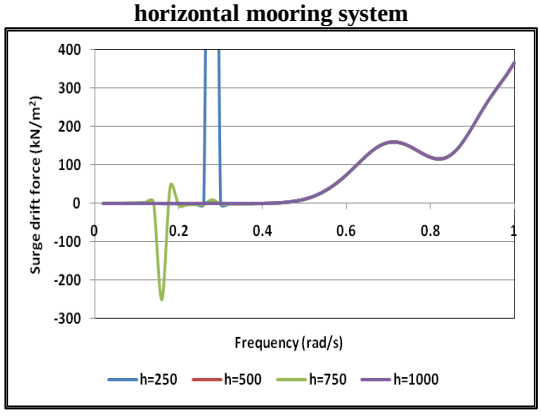

Figure 5-45 Mean second-order surge drift force with catenary mooring system

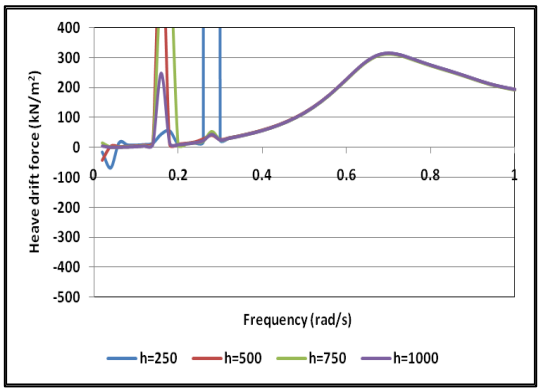

Figure 5-46 Mean second-order heave force with catenary mooring system

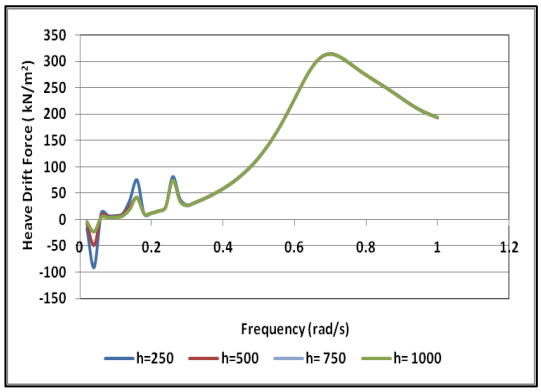

Figure 5-47 Mean second-order pitch drift moment with catenary mooring system

5.4.8.2 Effect of current velocity on mean second-order forces

In this section, the second-order forces acting on the semisubmersible model at a water depth of 250 metres and with current velocities of 0.6 and 1.2 m/s are plotted together with those with no current and given in Figure 5-48 to Figure 5-53 inclusive.

For the surge motion of the semisubmersible model with the horizontal mooring system, Figure 5-48 shows that the existence of a current results in peaks of the second-order forces at frequencies that correspond to the natural frequencies of each of the individual surge, heave and pitch motions. In addition, it was seen that the values of those peaks are larger at a current velocity of 1.2 m/s than those at a velocity of 0.6 m/s.

On the other hand, for the catenary mooring system and with no current, Figure 5-49 shows that the catenary mooring lines cause a peak in the surge mean second-order forces at the heave natural frequency. At current velocities of 0.6 and 1.2 m/s, these peaks still exist but with smaller values and other peaks show at the pitch natural frequency. In addition, the surge mean second-order forces at the current velocity of 1.2 m/s and at the pitch resonant frequency are found to be larger than those at a current velocity of 0.6 m/s. A similar behaviour is observed for the heave and pitch motions shown in the figures (Figure 5-50 to Figure 5-53 inclusive). As for the heave and pitch motions of the model with the horizontal mooring system, it is seen that the second-order forces have peaks at the surge, heave and pitch resonant frequencies and that the values of these peaks increase as the current increases from 0.6 to 1.2 m/s.

The study of the second-order forces given in Figure 5-49 , Figure 5-51 and Figure 5-53 show that the catenary mooring lines with no current caused a high peak at the heave resonant frequency level in the surge, heave and pitch second-order forces. That peak appeared but with much smaller value when using the horizontal mooring system as shown in Figure 5-48, Figure 5-50 and Figure 5-52. This peak continues to exist at

current velocities of 0.6 and 1.2 m/s but at a slightly different frequency in each case due to the change in the wave encounter frequency as a result of the simultaneous current velocity. In addition, an increase in current from 0.6 to 1.2 m/s increases the magnitude of the peaks that occur at the surge and pitch resonant frequencies. In addition, it is observed that this high peak at the heave resonant frequency appeared only at water depth of 250 meters and vanished at water depth values of 500and 1000 meters.

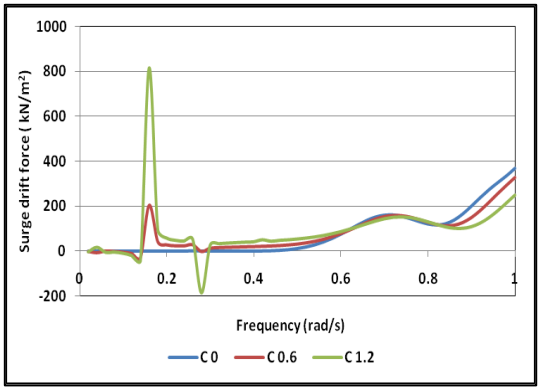

Figure 5-48 Mean second-order surge drift force at different current velocities with horizontal mooring system

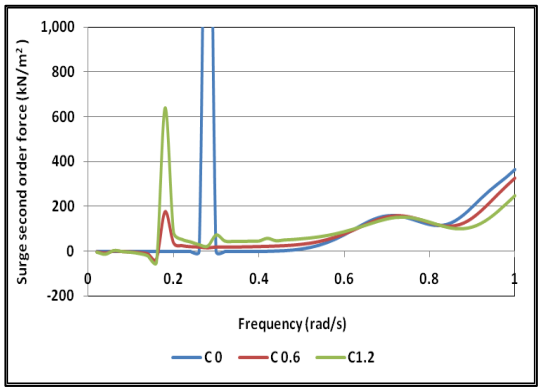

Figure 5-49 Mean second-order surge drift force at different current velocities with catenary mooring system

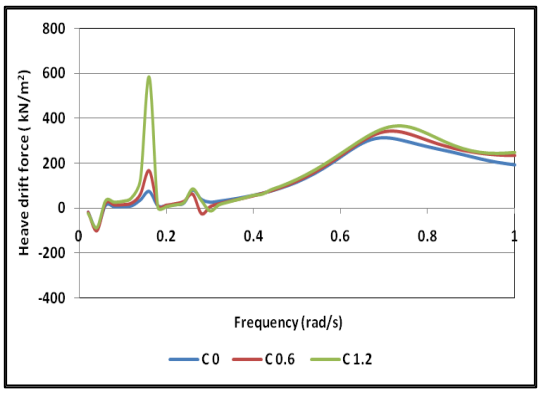

Figure 5-50 Mean second-order heave drift force at different current velocities with horizontal mooring system

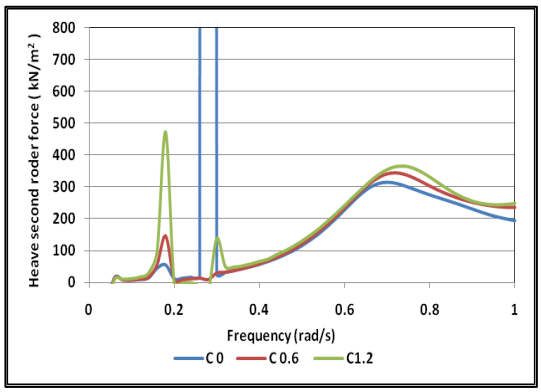

Figure 5-51 Mean second-order heave drift force at different current velocities with catenary mooring system

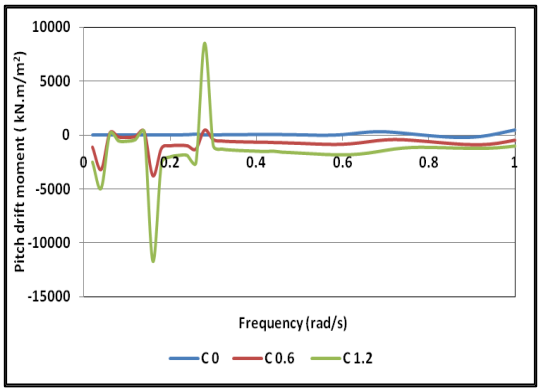

Figure 5-52 Mean second-order pitch drift moment at different current velocities with horizontal mooring system

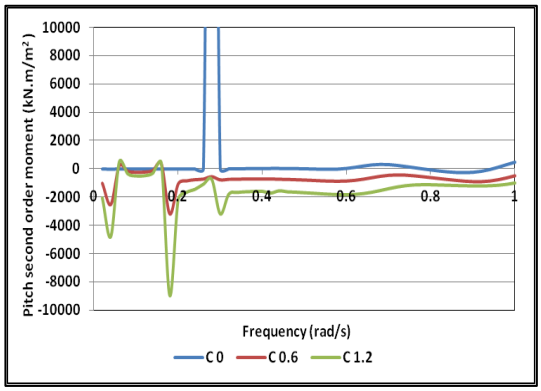

Figure 5-53 Mean second-order pitch drift moment at different current velocities with catenary mooring system

To have better understanding of this phenomenon, in the following section the results from a study of the six different components of the surge mean second-order force components, with the catenary mooring system, are presented.

5.4.8.3 Effect of current velocity on the components of the surge mean Second-order drift forces with a catenary mooring system

In Section 2.2.3 the six components of the mean second-order forces were presented. In this section, the effect of a current velocity on these components is studied. Figure 5-54 to Figure 5-58 inclusive show the first five components only as it was found that the sixth vanishes at all frequencies.

It is found that in the low-frequency region the second component is the main cause of the negative values of the second-order forces. This component is due to the pressure drop due to the first-order velocity field which is a quadratic term in Bernoulli's equation and is evaluated over the mean wetted surface.

In addition, it is found, from Figure 5-54 to Figure 5-57 inclusive that the first four components increase in magnitude in the high frequency region as the current velocity increases. On the other hand, there is no or only slight change in the low frequency region as the current velocity changes. Additionally, the peak- and zero–value frequencies are seen to increase as the current velocity increases. As for the fifth components as shown in Figure 5-58 and which represents the contribution due to current velocity and corrects the convective effect of the unsteady velocity field due to the current velocity on the mean surface to that on the instantaneous surface, it is found to be the only component that increases significantly in the low frequency region as the current velocity increases.

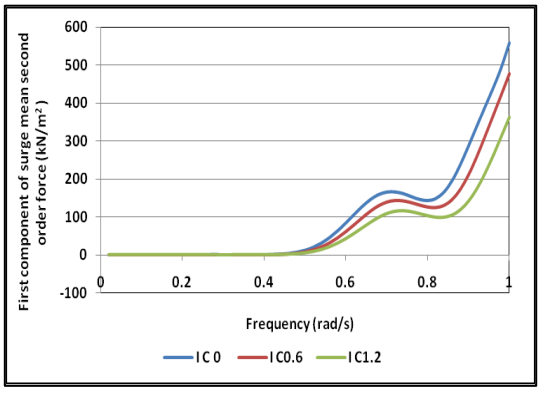

Figure 5-54 The first component (I) of the mean second-order surge force

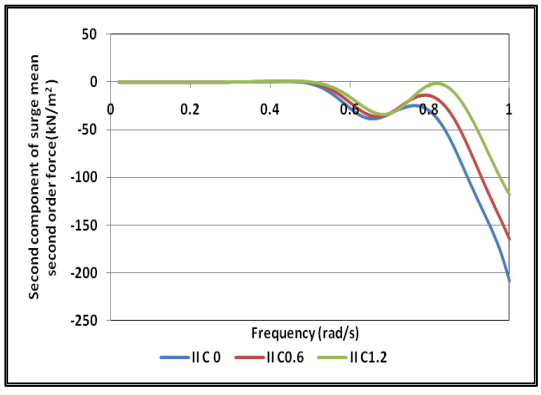

Figure 5-55 The second component (II) of the mean second-order surge force

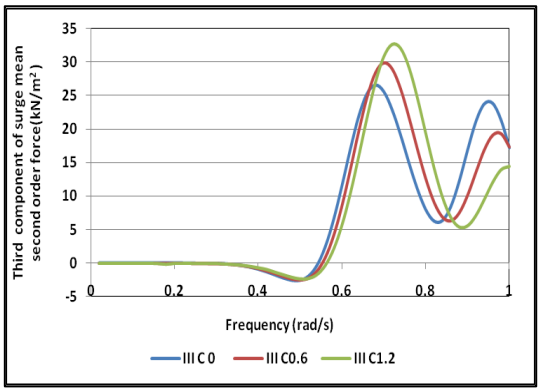

Figure 5-56 The third component (III) of the mean second-order surge force

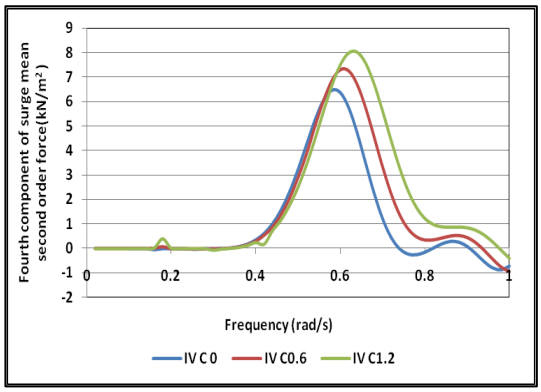

Figure 5-57 The fourth component (IV) of the mean second-order surge force

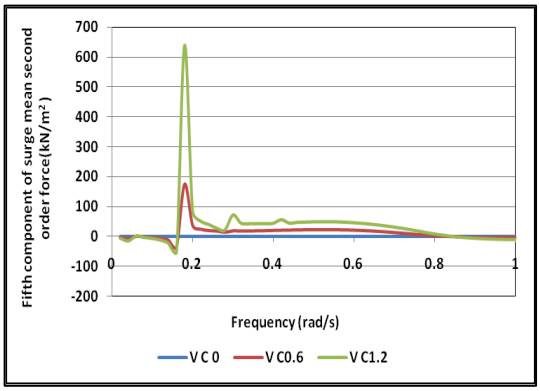

Figure 5-58 The fifth component (V) of the mean second-order surge force

5.5 *Morison's approach based method numerical computations*

In this part of the thesis, numerical results obtained from the approach that is based on Morison's equation are presented. The results include the estimation of the first-order surge wave forces and the corresponding body responses for the semisubmersible moored with a horizontal mooring system. In addition, the slowly varying drift force spectrum based on Pinkster's procedure (Pinkster, 1979) is presented.

5.5.1 Model specifications

Morison's approach was applied on two similar semisubmersible models (in terms of the general arrangement of columns and pontoons). In this section, the geometrical characteristics of these two models are given. The first model consists of square columns and rectangular pontoons and the second model consists of circular columns and circular pontoons. The dimensions of the first model were selected in order to match those of the structure model that was used in the experimental tests conducted and described in Chapter Three. As for the second model, its dimensions were chosen so that it would have the same waterplane area as the first model.

Firstly, the forces and responses of the second model (model with circular members) were calculated as a first approximation. Afterwards, the forces acting on the second model, which represents a semisubmersible platform with rectangular pontoons and square columns, were estimated by replacing the inertia forces term with dynamic pressure and acceleration forces. This is done by replacing the inertia coefficient (Cm) with (1+added mass coefficient) in all dynamic pressure and acceleration forces components. In addition, in the drag force calculation terms, the characteristic dimensions of the circular columns and pontoons which are the diameters (Dc and D_H) are replaced by column width and pontoon height dimensions, respectively. Table 5-3 shows the values of the general parameters that are used for both of the two models. The specifications of other variables for the two semisubmersible models are shown in Table 5-4 and Table 5-5.

Table 5-3 Specifications of the general parameters

Parameter	Definition	Value
Dr	Draft	21 m
g	Gravity constant	9.81 m/S^2
H	Water depth	250 m
H_C	Height of Column above base plane	12.5 m
H_W	Regular wave height/ significant wave height for irregular seas	2 m
KG	Centre of gravity height above base plane	4 m
K_x	Horizontal surge stiffness	144.81 kN/m
L	Hull length	53 m
S	Pontoon Spacing	67.84 m
U	Current speed	Zero and 1.2 m/s
α	Wave propagation angle	Zero
γ	Current propagation angle	Zero
ρ	Water density	1.025 tonne/m^3

Table 5-4 Model with circular members' specifications

Parameter	Definition	Value
∇	Displaced volume of the structure	50590 m^3
C_m	Wave inertia coefficient	2
D_C	Diameter of Column	18.7762 m
D_H	Diameter of Hull	13.3405 m
M	Mass	55867 tonnes
M_X	Surge added-mass	36731 tonnes

Table 5-5 Model with square columns and rectangular pontoons specifications

Symbol	Definition	Value
∇	Displaced volume of the structure	51885 m3
D_C	width of column	16.64 m
D_H	width of hull pontoon	8.4 m
M	Mass	55867 tonnes
M_X	Surge added mass	36731 tonnes
$\omega_{n\ surge}$	Surge natural frequency	0.04 rad/s

5.6 Results

The calculated wave loading forces and model responses based on application of the Morison's approach were obtained for the two structural models described in the previous section. The two semisubmersible models have different geometries but have same waterplane area and the same spacing between columns. This resulted in slightly different underwater volumes and thus displacements. Consequently, slightly different natural frequencies of the surge motion were estimated. Additionally, each of the two models cross section shapes has different added mass coefficients and which affect the value of the natural frequency.

Firstly, the results for the first-order surge forces and body responses are presented. Figure 5-59 shows a comparison of the wave first-order forces acting on the two semisubmersible structural models. The semisubmersible model with circular members is found to have slightly larger first-order forces which are explained by the fact that the columns have a larger diameter and which leads to higher forces.

The corresponding surge responses depend on both of the damping and the stiffness of the mooring system. Several study cases of the RAOs of the semisubmersible model with rectangular columns and horizontal mooring are presented in Figure 5-60. For the first case, the response was calculated with the assumption of no damping or stiffness. Then three more cases were estimated at damping ratios of 0, 0.2 and 0.4 and with a stiffness of the horizontal mooring system of k = 144.81 kN/m. Figure 5-60 shows the reductions in the surge RAO, at the resonant frequency, due to the increases in the damping ratio.

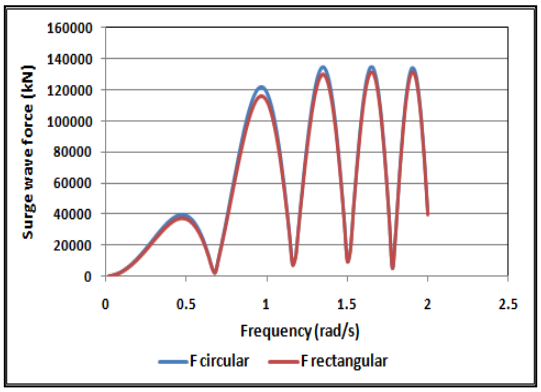

Figure 5-59 First-order surge wave force with horizontal mooring

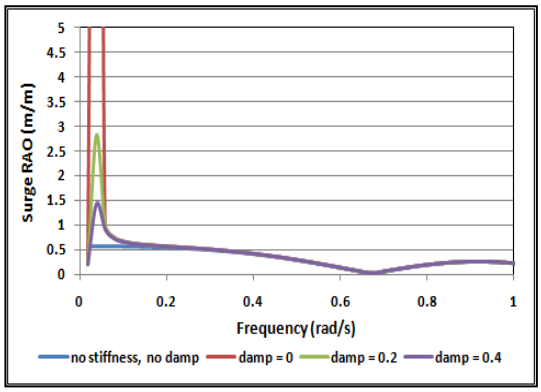

Figure 5-60 Surge RAO with horizontal mooring

Secondly, for the second-order forces, the mean surge drift force acting on the semisubmersible model with circular columns and pontoons is calculated from Equation 2-63 as a function of the drift force coefficient (R^2), the significant wave height and the cylinder diameter. In addition, the drift coefficient (R^2) is dependent on the natural frequency (μ). Figure 5-61 shows the change in (R^2) due to the change in the natural frequency (μ). The drift coefficient is known from other studies in literature to have value of 0.666 at high frequencies in deep water. The steady component of the drift force, or the mean drift force was estimated using Equation 2-63 via the drift force coefficient R^2, which is plotted in Figure 5-61 at various values of the natural frequency (μ).

In addition, the slowly varying drift force spectrum was calculated via Equation 2-69 by combining the surge drift force per unit wave amplitude in regular waves and the appropriate irregular wave spectrum. The drift force spectrum was estimated at four different irregular wave conditions; (H6, T12), (H12, T12), (H7.5, T15) and (H15, T15), and plotted in Figure 5-62 and Figure 5-63. It is seen from these two figures that the irregular waves of (H12, T12) and (H15, T15) produce very high drift forces spectra in comparison with those produced in waves (H6, T12) and (H7.5, T15). In addition, the corresponding surge response spectra in the four irregular wave conditions are calculated via Equation 2-70 in Section 2.4.9 and are plotted in Figure 5-64.

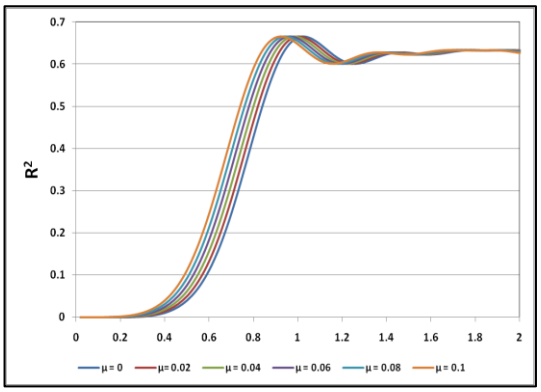

Figure 5-61 Drift force coefficient for circular columns

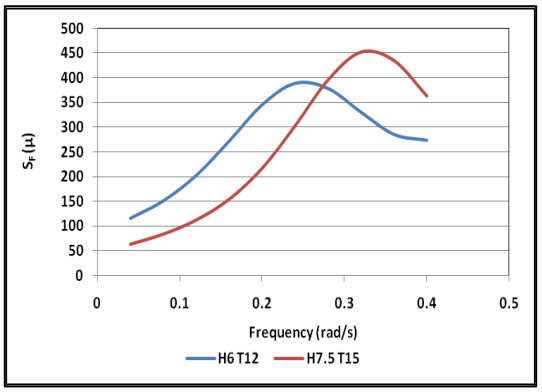

Figure 5-63 Surge slowly varying drift force spectrum at waves H 6 T12 and H12 T12

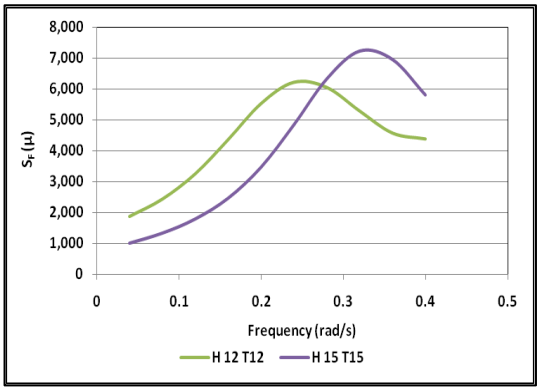

Figure 5-62 Surge slowly varying drift force spectrum at waves H12 T12 and H 15 T15

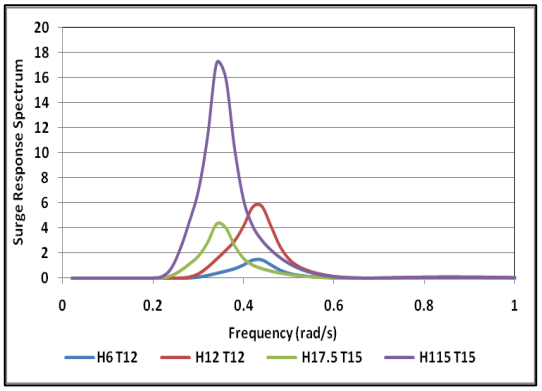

Figure 5-64 Surge response spectrum

5.7 Comparisons and discussion

This section presents selected comparisons that are made between the results obtained from both the numerical simulations and the model experiments. The comparisons include surge first and second-order forces and the surge response amplitude operator (RAO). In addition, a discussion is given of the mooring lines damping estimated via the energy dissipation method and via the model decay tests.

5.7.1 First-order wave surge forces

A comparison was made between the surge first-order forces estimated from the three-dimensional technique and those estimated using Morison's approach and illustrated in Figure 5-65. This comparison shows a very good agreement between the two methods with a slight shift in both the peaks and zero frequencies. This is to be expected due to the condition that each of the two methods involved estimating the mass, the added mass and the volume of the structure via different approaches and making different approximations.

5.7.2 Surge motion response amplitude operator (RAO)

The surge response amplitude operators (RAO) corresponding to the first-order forces, as obtained using the two methods presented in the previous section, are illustrated in Figure 5-66. A good agreement is found between the two RAOs. The peak value of the RAO that was estimated using the three-dimensional technique is found to be less than that obtained by the Morison's approach.

5.7.3 Second-order wave surge forces

The wave forces acting on a floating structure are classified as being first and second-order forces. The first-order forces are the oscillatory forces and moments which are proportional to the wave amplitude and cause the first-order motions of the structure. The mean value of the first-order forces over a regular wave period is zero. On the other hand, the second-order forces and moments are of a second-order level with respect to the wave amplitude and they produce a non-zero mean value that is constant for exposure to regular harmonic waves and is slowly-varying for exposure to random irregular waves (Chan, 1990). For the semisubmersible restrained with the horizontal mooring system, the surge mean second-order force was calculated via different approaches. It was calculated by the theoretical methods presented earlier in Sections 2.3.6 and 2.4.8. In addition, it was estimated from the experimental measurements of the steady surge motion responses of the model tests conducted in simulated regular waves. These tests were conducted at two wave periods (T = 10 and 15 seconds) and with different values of the wave height employed for each wave period.

Figure 5-67 shows a comparison of the surge mean second-order forces coefficient in regular waves (force per unit amplitude squared) obtained by using numerical calculations and by the experimental measurements. The comparison shows a very good agreement between the two methods for the measurements in the low frequency region. On the other hand, however, at frequencies higher than 0.1 Hz, it is observed that the Chakrabarti formula gives higher mean second-order forces than those obtained from the three dimensional technique. In addition, two more comparisons are made for the surge drift force coefficients at current velocities of 0.6 and 1.2 m/s and the results are shown in Figure 5-68 and Figure 5-69. These figures show a good agreement between the estimated and measured surge mean drift force coefficients for regular waves whose period is 15 seconds. For waves of 10 seconds period, a less agreement is observed for both current velocities.

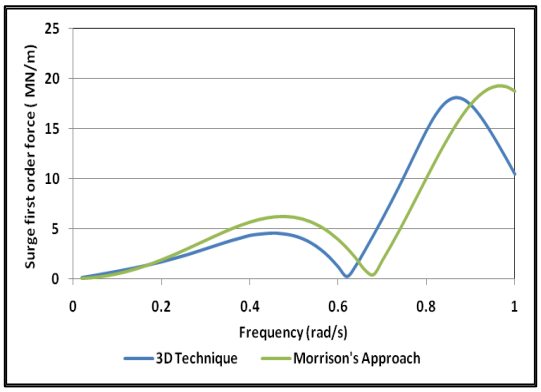

Figure 5-65 Comparison of the first-order surge forces

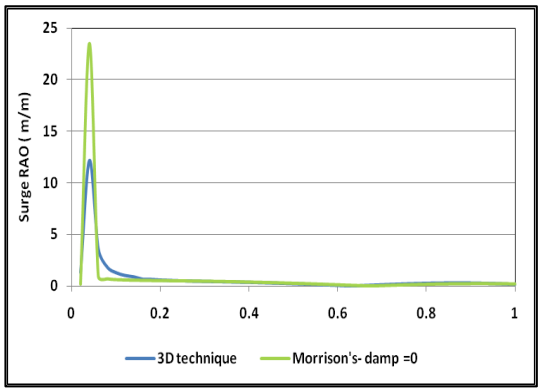

Figure 5-66 Comparison of the surge RAO with horizontal mooring system

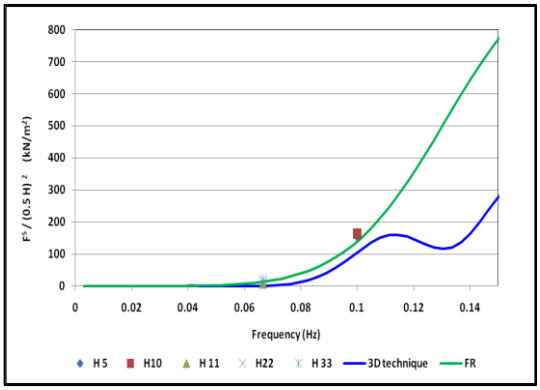

Figure 5-67 Comparison of mean second-order surge force at regular waves and no current with horizontal mooring system

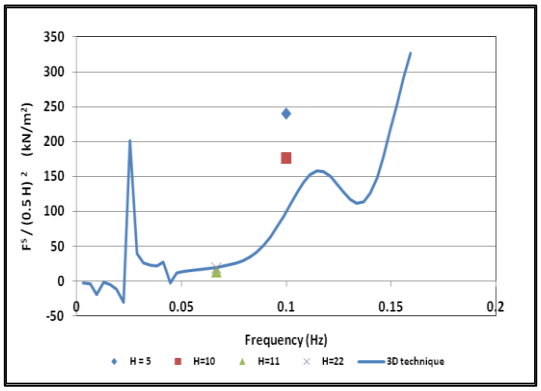

Figure 5-68 Comparison of mean second-order surge force at regular waves and current velocity U = 0.6 m/s with horizontal mooring system

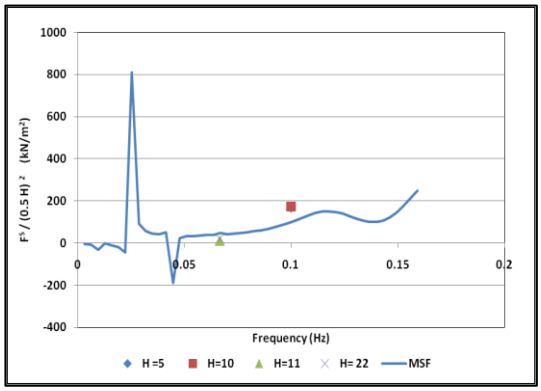

Figure 5-69 Comparison of mean second-order surge force at regular waves and current velocity U =1.2 m/s with horizontal mooring system

For the semisubmersible model with the catenary mooring system, the comparison in Figure 5-70 shows that for regular waves with no current, the three-dimensional technique overestimated the surge drift coefficients at the two wave periods included in the study (T= 10 and 15 seconds) and at all wave heights that were included. Additionally, Figure 5-71 shows same results with the exception of good agreement at the wave (H5, T10).

The three-dimensional technique gives one value of the drift force coefficient per unit wave amplitude at each wave frequency. On the other hand, the experimental tests in regular waves of the same wave period but with different wave heights gave different drift force coefficients after division by the wave amplitude squared. Figure 5-72 and Figure 5-73 show comparisons of the experimentally measured surge drift force coefficients for both horizontal and catenary mooring systems at wave periods of 10 and 15 seconds, respectively.

At a wave period T= 10 seconds, the available data related only to two wave heights (H =5 and 10 metres) and which is plotted in Figure 5-72 and Figure 5-74. These figures show that for both the horizontal and the catenary mooring systems, that the surge drift force coefficients at a wave height of 10 m are higher than those at a wave height of 5 m.

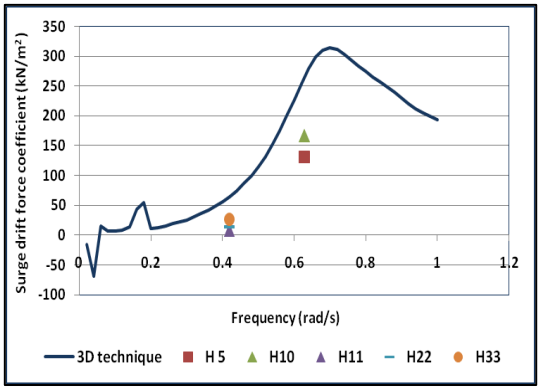

Figure 5-70 Surge drift force coefficients versus experiments measurements with catenary mooring system at no current

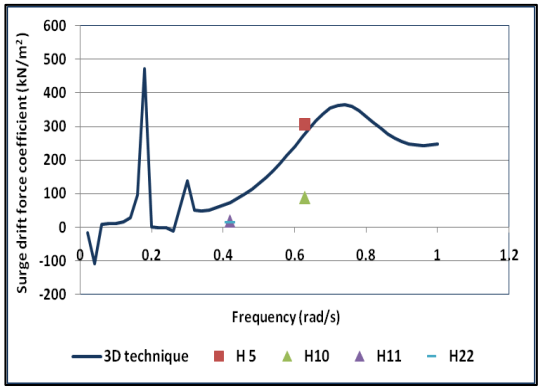

Figure 5-71 Surge drift force coefficients versus experiments measurements with catenary mooring system at current U = 1.2 m/s

At a wave period T = 15 seconds, three different wave heights of 11, 22 and 33 metres were used in the experiments. The corresponding surge drift force coefficients are plotted in Figure 5-73 and Figure 5-75. At this wave period, it can be seen that the drift coefficient increase is of a second-order with respect to the wave height. The rate of increase for the model with the horizontal mooring system is higher than that with the catenary mooring system.

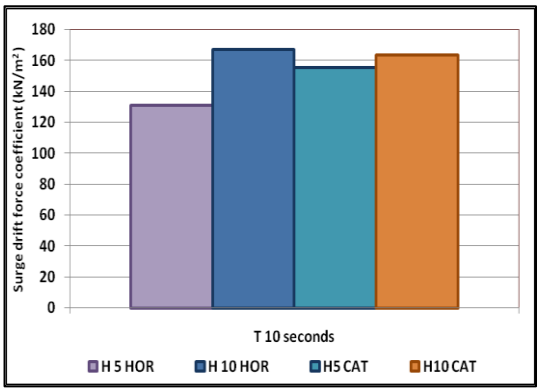

Figure 5-72 measured surge drift coefficients at T = 10 seconds

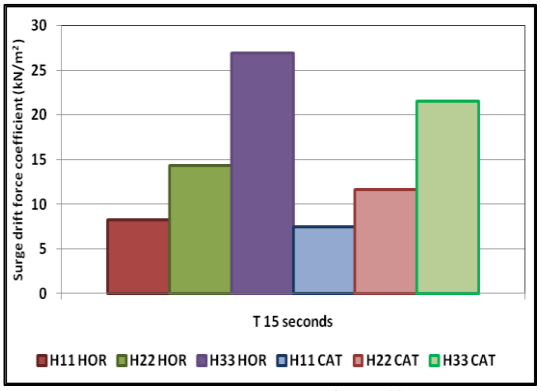

Figure 5-73 measured surge drift coefficients at T = 15 seconds

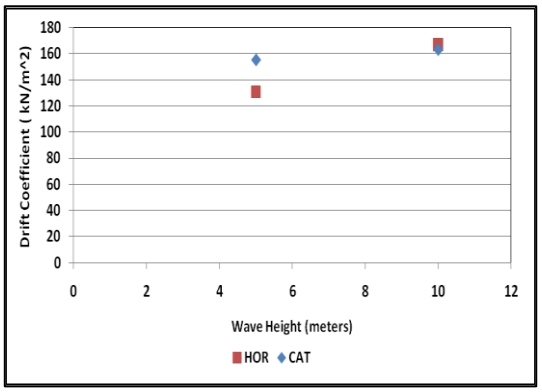

Figure 5-74 Surge drift force coefficients at T =10 seconds

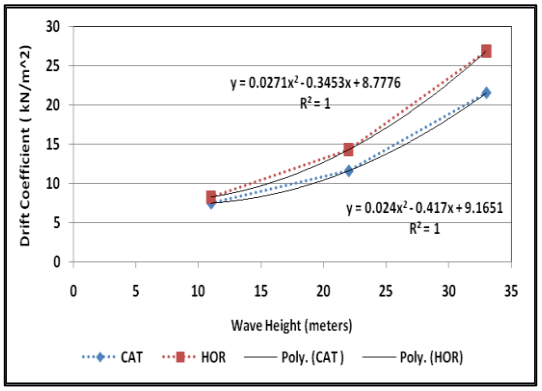

Figure 5-75 Surge drift force coefficients at T =15 seconds

5.7.4 Relative damping

As discussed in Chapter Three, a set of decay tests with the experimental model were conducted in both still water and in current speeds of 0.6 and 1.2 m/s. These tests were conducted using both the horizontal and the catenary mooring systems. The analysis of these tests helps with the investigation of the effect of the mooring lines on the total system damping. For the horizontal moorings system, the mooring lines are assumed to be not in contact with the water and that the interaction between horizontal lines and waves and/or current was negligible.

The results from still water decay tests are illustrated in Figures 3-20 to 3-23 and 3-28 to 3-31 inclusive, and the comparisons between decay responses with both horizontal and catenary mooring systems show that the catenary mooring lines caused an obvious reduction in the number of body motion cycles before the motion stopped. This is explained by the increase of the systems damping due to the underwater catenary mooring lines. In order to estimate the values of damping from the decay tests in the

form of a relative damping ratio, two methods were used; the logarithmic decrement method and the exponential approximation method.

The exponential approximation method provides a single value of damping that indicates the speed of decaying of the cyclic body motion with respect to time. On the other hand, the logarithmic decrement method provides changing relative damping values with respect to the mean value of cyclic motion amplitude. The body motion decay tests were conducted for both the horizontal and catenary mooring systems. Another method that can be used to estimate the mooring lines damping without decay tests is presented in Chapter Four and which is the energy dissipation method presented by (Huse and Matsumoto, 1988; Huse, 1986). In Chapter Four, this method was applied on vessels moored with a single catenary mooring line and then with four catenary mooring lines.

The exponential approximation method gave relative damping ratios of surge motion of 0.02 and 0.07 for the horizontal and catenary mooring systems, respectively. This shows that the mooring lines resulted in an increase of the overall systems damping that is almost double the damping due to that of the hull alone.

On the other hand, results from the logarithmic decrement method showed an increase of relative damping that depends on the mean amplitude of the surge motion. The increased relative damping value ranges between 0.02 and 0.04 at a surge mean amplitude ranging between 5 and 15 metres.

The results of the three-dimensional technique discussed, in Chapter Two, showed that the potential damping vanishes in the low-frequency region. This emphasizes the importance of the viscous damping as being a major contributor to the overall system damping and hence the structure motions and responses.

The energy dissipation method estimates the energy of the cable oscillations at a certain position that is shifted from the body static position. This method requires knowing the mean surge motion of the structure, the amplitude and the period of the oscillations. Afterwards, the method calculates the damping using the energy and the encountered wave frequency, and the motion mean amplitude. Thus, this method can be used to estimate the energy dissipated, however the relative damping ratios cannot be compared with those obtained from the decay tests in still water as in the decay test the structure

starts the induced oscillations from the static position with no mean surge motion being experienced.

In addition, with the existence of a current, theoretically the relative damping ratio from the energy dissipation method can be compared with that obtained from the decay test. But in the current experimental study undertaken at a current velocity of 1.2 m/s, the motion decayed after a very low number of cycles and which resulted in that there is no enough data for the comparison.

An approximate case study was made by assuming surge motion amplitude of 1 metre and at an oscillation period that equalled the surge natural frequency. Afterwards, the energy dissipation method was applied at motion amplitudes of 5, 10 and 15 metres.

One of the main assumptions that was made by Huse in the energy dissipation method is that the motion is that of sinusoidal oscillations of constant amplitude. In the decay tests, the amplitudes of the decay motions were changing at each cycle. Thus, the damping ratios estimated from Huse's approach are compared to those of the decay tests at a mean surge that is equal to the motion amplitude in Huse's method. In addition, the energy dissipation method takes into account the effect of the superposed high-frequency motion. Thus, the estimated energy still needs to be multiplied by the VAR coefficient.

Hence, by comparing the relative damping ratios estimated from the energy dissipation method to those obtained from analyzing the results from the surge decay test using the logarithmic decrement method, then the value of the corresponding VAR is estimated as shown in Table 5-6.

Table 5-6 Energy dissipated at different surge motion amplitudes

δ (m)	Energy (kN.m)	B (tonnes/s)	B_{rel}	$B_{rel\ exp}$	VAR
5	24	181.08	0.037	0.02	1.88
10	301	2225.95	0.462	0.03	15.43
15	706	5219.97	1.085	0.04	27.14

Where $B_{rel\ exp}$ is the relative damping ratio obtained from the decay test and which equals the difference between damping ratio of the catenary mooring system and the horizontal mooring system.

5.8 Summary

In this chapter, the numerical results obtained using the mathematical methods given previously in Chapter Two are presented. Comparisons were made between the first-order and second-order forces estimated from the numerical simulations. In addition, the damping ratios estimated from the experimental decay tests were compared with those estimated from the energy dissipation method in order to estimate the values of the velocity amplitude ratio (VAR).

In the next chapter a summary of the conclusions that have been drawn from this research is given.

Chapter 6. Conclusions

6.1 Introduction

The environmental loading forces on an offshore structure include wind, wave and current forces. The wave loads are by convention classified as first- and second-order forces with respect to wave amplitude.

The first objective of this thesis was to investigate and apply different analytical methods to estimate the first-and second-order forces and corresponding motions of a semisubmersible model. This was achieved by applying two mathematical approaches in order to study the first-order wave loading forces on and responses in regular sea states. In addition, the second-order drift forces were examined via two analytical methods. One of those methods incorporates the effect of the viscous damping.

The second objective was to carry out experimental tests in order to measure wave and low frequency motions of the semisubmersible model that was moored in both regular and irregular waves. The test programme was conducted at MARINTEK ocean basin, Trondheim, Norway and included both regular and irregular sea states both with and without a current. The model used was held in position using both horizontal and catenary mooring systems. The measured data included the six degrees of freedom motions and mooring line tension forces.

The results of the second-order forces obtained from the analytical approaches were compared to those obtained from of the experimental measurements as planned in the third objective.

The fourth objective was to investigate the role of the mooring lines on the slowly varying motions with special attention being given to the mooring stiffness and mooring line damping. Hence, the mooring lines viscous damping was investigated via the application of an analytical method that estimates the dissipated energy due to the movements of the mooring lines in regular waves. This dissipated energy is used to estimate the corresponding viscous damping due to the mooring lines.

In addition, the effect of the mooring lines on the slowly varying motions was investigated through the analysis of the experimental measurements of the semisubmersible model that was moored with horizontal mooring system followed by being moored with catenary mooring system.

The conclusions of this study are presented in the following sections and are grouped in the following sections.

6.2 Mathematical models

The first method that was employed for estimating the first-order loading forces was a three-dimensional technique that solves the radiation and diffraction problems simultaneously using a translating pulsating source modelling method. The second method was conducted through applying Morison's equation to estimate the first-order wave surge force and corresponding surge response of the semisubmersible model. A comparison was then made of the surge motion responses using the results of the two methods for the semisubmersible model in following seas and a good agreement was found.

As for the mean steady component of the second-order force, the selected three-dimensional technique was employed and combined with a cross flow approach in order to estimate the second-order forces. The technique estimated the fluid pressure from Bernoulli's equation. Then, the fluid pressure components were integrated over the mean wetted body surface of the semisubmersible in order to evaluate the components of the mean steady forces.

The second method estimated the steady component of the second-order drift force of the surge motion mode via an approach that was proposed in (Chakrabarti, 1984).

The results from the two methods that were focused on the second-order forces were compared for the surge mean second-order forces in waves only with the horizontal mooring system. It was found that the two methods give similar numerical values for the range of wave frequencies up to 0.1 Hz (0.628 rad/s) in spite of that the Chakrabarti method is for fixed cylinders and the relative response of the structure is ignored. At higher frequencies, it was found that the three-dimensional technique gave higher results than those obtained via the Chakrabarti method. The results from the two numerical methods were then compared with the experimental measurements at wave periods of 10 and 15 seconds (which correspond to frequencies of 0.1 and 0.067 Hz) and at several wave heights and good agreement were found.

Another two comparisons were conducted with combined regular waves and a steady current field at two current velocities of 0.6 and 1.2 m/s which were between the results obtained from the three-dimensional technique and the experimental tests at the same wave frequencies mentioned earlier. Good agreement was found at a wave frequency of 0.067 Hz. In addition, a good agreement was found at a current velocity of 1.2 m/s

where the three-dimensional technique underestimated the actual values obtained experimentally of the mean surge second-order forces.

On the other hand, at a current velocity of 0.6 m/s, it was seen that the experimental results showed that the value of the surge drift force coefficients $\frac{F^S}{(0.5\ H_w)^2}$ changed with the wave height.

For the semisubmersible model that was restrained using the catenary mooring system, the three dimensional technique was found to overestimate the surge drift force coefficients in most cases when compared with the experimental results for the studied cases. The studied cases included sea states of regular waves only and regular waves combined with a current of mean velocity of 1.2 m/s.

Additionally, the variation of the surge drift force coefficient with the wave height was observed and it was found to be of the second-order level for both the horizontal and the catenary mooring systems

6.3 Catenary mooring system damping

In order to properly investigate the slowly varying motions of the selected semisubmersible structure, several series of physical model experiments in an ocean basin were conducted on a scale of 1/50 with the effects of both horizontal and catenary mooring systems being examined.

Two methods were used to estimate the relative damping of the system with respect to the critical damping based on the results obtained from the decay tests that were conducted in both still water and in currents; the exponential approximation method and the logarithmic decrement method.

The comparison of the relative damping of horizontal and catenary mooring system via the two methods showed an increase of the total damping of the system due to the existence of the catenary mooring lines. On the other hand, the first method would provide a single value of relative damping for each studied case unlike the later which gives the relative damping as a function of the amplitude of the decay motion. In addition, the current velocity was found to increase the relative damping for both the horizontal and catenary mooring systems.

A more investigation of the obtained results gave the following conclusions:

- The comparison of the decay tests time series results of the semisubmersible moored with the horizontal mooring system and then followed by tests with the catenary mooring system showed a profound change in the number of cycles that occurred until the motion decayed and the corresponding slope at which the motion peaks decayed. The decay motion when moored with catenary mooring system was found to have less number of cycles than that of the decay motion with horizontal mooring system. Similar observations were made from the decay tests in currents and as the current velocity increased. The analysis of this data was conducted using two methods; the logarithmic decrement and the exponential approximation methods.
- The exponential method gave a single value approximation for each decay test for the value of the relative damping of the overall system including the associated mooring lines.
- The estimated relative damping values that were obtained via the exponential method for the semisubmersible moored with horizontal lines revealed that a large increase occurred due to the increases of current velocity from zero to 0.6 and 1.2 m/s. The amount of increase differs according to the motion mode. For the surge motion, the relative damping at a current of 1.2 m/s was more than 10 times its value at no current situation. On the other hand, for the yaw and pitch motions, the damping increase to a value that was more than two and half times its value in the no current situation.
- For the semisubmersible moored with the catenary mooring system, only decay tests for surge and pitch motions in still water and with a current of 1.2 m/s were carried out. The relative damping for the pitch motion was found to increase to a level of two and half times of that the no current situation, similar to the increase that was found when using the horizontal mooring system. However, for the surge motion, the existence of a current with the catenary mooring system resulted in a large increase in the values of the relative damping of the system which made the motion decay rapidly without giving enough number of decaying cycles to be able to estimate the corresponding relative damping value.

All of the previous conclusions were reached based on the results obtained from the decay tests in both still water and in a current. More experiments were employed in order to investigate the slowly varying motions of the semisubmersible model in irregular sea states. Then, the results were analysed statistically via a study of the mean and standard deviation values of the surge motion responses of the semisubmersible model. This statistical analysis leads to the following conclusions:

- The superposition method was found to give good accuracy of the mean values of the low-frequency surge motion responses in sea states of combined moderate sea states and current with horizontal mooring system. The superposition method underestimated responses in high sea states. This conclusion is for both the two studied current velocities of 0.6 and 1.2 m/s.
- When the horizontal mooring system was replaced with the catenary mooring lines, the superposition method was found to overestimates the mean value of the low-frequency surge responses at the studied high sea states of combined regular waves and a current velocity of 1.2 m/s and to correlate well the measured mean values of responses in moderate sea states.
- As for the standard deviations of the measured responses, it was found that for the horizontal mooring system for both used current velocities, a good agreement between the measured and the superposition values was found at moderate sea states. In addition, in the high sea states, the superposition method was found to underestimate the standard deviation values. On the other hand, for the catenary mooring system, the superposition was found to overestimate the standard deviation values in all sea states but with more pronounced effect in the moderate sea states.

6.4 Effect of mooring system and wave-current interaction on the low-frequency motions

Due to the non-linear nature of the stiffness of the catenary mooring system unlike the linear stiffness, a direct comparison between the responses of the two mooring systems required eliminating the effect of the different stiffness behaviour.

A simple procedure to conduct this comparison between the surge motion responses with the two mooring systems was introduced and applied on four study cases. In all the four cases, different effects were investigated on the mean and standard deviation

values of the surge responses of the semisubmersible model in irregular sea states with and with a current.

The first case study was for the investigation of the effect of the catenary mooring lines on the surge mean and standard deviation values in the existence of irregular waves. It was found that in three out of the four studied sea states, the measured motion responses with catenary mooring lines are found to be less than those expected when the same force acts on the model with horizontal mooring lines. This shows that the mooring line system has an effect other than the stiffness on the semisubmersible responses which is damping. This can be seen from decay tests.

The second case study examined the effect of the catenary mooring line on the surge mean and standard deviation values in the existence of current of 1.2 m/s. It is found that the measured body mean surge response is larger than that anticipated as a result of the different value of the stiffness. The decay test analysis showed that the damping ratios in current are higher than those in still water. Thus , the increase in the responses indicate that there is an increase in the total forces acting on the overall system and the mooring lines that were higher. The effect of increased forces was higher than the effect of the increased damping.

The third and fourth cases of the procedure mentioned in the previous section investigated the wave-current interaction effects on the surge mean and standard deviation values with horizontal and catenary mooring systems, respectively.

In the third case it is assumed that there is no interaction between waves or current with the horizontal mooring lines and the measured surge responses in the wave-current field is compared to that estimated via the superposition method of the responses due to wave and current separately. It was found that the superposition method gave a good agreement with the measured values in moderate sea states while in high sea states, there is a large increase in the measured values compared with the superposition obtained values and which is considered to be due to the wave - current interaction.

The last studied case showed that in all studied sea states, the measured mean surge responses with catenary mooring lines in a wave-current field are larger than those when calculations were carried out using the superposition method. This increase is the net combined effect of the wave-current interaction (increasing the responses as stated

in third case study) and their interaction with the mooring lines (reduction due to waves and increase due to current).

6.5 Mooring line damping via energy dissipation method

The energy dissipation method was applied on two main semisubmersible models. The first was moored using a single line and the second was moored using four lines that are symmetrically arranged. The energy depends mainly on the mean value of the displacement of the vessel and the amplitude of its sinusoidal oscillations. The energy dissipation method was used to investigate the effect of the water line depth on the dissipated energy by the mooring lines and hence, the corresponding damping at different values of vessel displacement distance and amplitude of the oscillations. It was found that for single line moored semisubmersible, an increase in the cyclic motion amplitude would result in an increase in the dissipated energy at all the studied values of water depth. On the other hand, an increase in the vessel displacement from the static position results in a reduction in the dissipated energy. Additionally, it was observed that at each value of the motion amplitudes there is a corresponding value of water depth at which the lowest energy and hence the lowest damping of the mooring line.

The energy dissipation method was applied to a semisubmersible that is moored with four mooring lines in regular waves of mean surge displacement and motion amplitudes that are similar to those measured from experiments. It was found that not necessary that the sea state that produces the highest surge motion response or the highest wave height would produce the highest dissipated energy. The amount of energy dissipated depends on both the vessel displacement distance and amplitude of the oscillations which determine the shape of the vertical profile of the mooring lines in the extreme positions of the oscillations. The energy dissipated was found to increase with the increase in the difference of the vertical positions of the mooring line points between the two extreme positions.

6.6 Recommendation for Future Work

This study was concerned with the wave and current forces acting on a semisubmersible structure. The effects of wind forces should be taken into account in order to simulate real environmental conditions.

This thesis studied the motion responses of a semisubmersible in different following sea states. Special attention was given to the surge motion, which was in the same direction

of the propagation of the waves and/or current if any. The effect of the wave and current heading angles on the low-frequency motion responses is an area that would benefit from further research.

Another area of extending this research is to investigate the reduction in air gap which is one of the important areas of study of the motion responses of a semisubmersible in high sea states. The available experimental measurements of the relative wave heights at different locations in addition to the six degrees of freedom motion responses are to be used for further analysis of the vertical motion of the structure and consequently the effect of high sea states on the air gap.

The mathematical model that is based on Morison's approach is to be extended to take into account the catenary mooring stiffness and compare results with experimental measurements.

The experimental programme needs to be extended to cover both regular and irregular waves over a wider range of frequencies to improve the quality of the comparison with the numerical simulations results.

In addition, in the future experimental tests, the measurements are to be extended to include the high frequency motions of the mooring lines in order to be employed in conjunction with the energy dissipation method and investigate the level of importance of the superposed high frequency motions in wave, a current and combined wave and current sea states.

The characteristics of the employed mooring system configuration are to be modified in order to increase the system stiffness and damping and investigate the corresponding effect of the added stiffness and damping on the low-frequency motion responses.

References

Baarholm, R., Fylling, I., Stansberg, C. T. and Oritsland, O. (2006) 'Model testing of ultra-deepwater floater systems: Truncation and software verification methodology', *25th International Conference on Offshore Mechanics and Arctic Engineering (OMAE 2006)*. Hamburg , Germany, pp. 1-11.

Bearman, P. W., Downie, M. J., Graham, J. M. R. and Obasaju, E. D. (1985) 'Forces on cylinders in viscous oscillatory flow at low Keulegan-Carpenter numbers', *Journal of Fluid Mechanics*, 154, (1), pp. 337-356.

Berthelsen, P. A., Baarholm, R., Pakozdi, C., Stansberg, C. T., Hassan, A., Downie, M. and Incecik, A. (2009) 'Viscous drift forces and responses on a semisubmersible platform in high waves', Honolulu, HI, United states, American Society of Mechanical Engineers, pp. 469-478.

Chakrabarti, S. K. (1984) 'Steady drift force on vertical cylinder - viscous vs. potential', *Applied Ocean Research*, 6, (2), pp. 73-82.

Chakrabarti, S. K. (1985) 'Recent advances in high-frequency wave forces on fixed structures', *Journal of Energy Resources Technology, Transactions of the ASME*, 107, (3), pp. 315-328.

Chakrabarti, S. K. (2001) 'Empirical calculation of roll damping for ships and barges', *Ocean Engineering*, 28, (7), pp. 915-932.

Chan, H. S. (1990) *A three-dimensional technique for predicting first-and second-order hydrodynamic forces on a marine vehicle advancing in waves.* thesis. University of Glasgow.

Chan, H. S. (1992) 'Dynamic structural responses of a mono-hull vessel to regular waves', *International Shipbuilding Progress*, 39, (419), pp. 287-315.

Chan, H. S., Atlar, M. and Incecik, A. (2002) 'Large-amplitude motion responses of a Ro–Ro ship to regular oblique waves in intact and damaged conditions', *Journal of Marine Science and Technology*, 7, (2), pp. 91-99.

Chen, X. B. and Molin, B. (1990) 'Numerical Prediction of Semi- Submersible Non-Linear Motions in Irregular Waves', *Fifth International Conference on Numerical Ship Hydrodynamics.* pp. 391-402.

Clough, R. W. and Penzien, J. (1993) *Dynamics of structures.* McGraw-Hill, New York.

Dev, A. K. and Pinkster, J. A. (1994) 'Experimental Evaluation of the Viscous Contribution to Mean Drift Forces on Vertical Cylinders', *BOSS'94 7th International Conference on the Behaviour of Offshore Structures.* Massachusetts Institute of Technology pp. 855-875.

Dev, A. K. and Pinkster, J. A. (1997) 'Viscous Mean and Low Frequency Drift Forces on Semi-Submersibles', *BOSS'97 8th International Conference on the Behaviour of Offshore Structures.* Delft, The Netherlands pp. 351–365.

Drake, K. R. (2011) 'An analytical approximation for the horizontal drift force acting on a deep draught spar in regular waves', *Ocean Engineering*, 38, (5-6), pp. 810-814.

Drake, K. R., Eatock Taylor, R. and Matsui, T. (1984) 'Drift of an articulated cylinder in regular waves', *Proceedings of The Royal Society of London, Series A: Mathematical and Physical Sciences*, 394, (1807), pp. 363-385.

Faltinsen, O. M. (1993) *Sea loads on ships and offshore structures.* Cambridge University Press.

Fang, C. C. and Chan, H. S. (2007) 'An investigation on the vertical motion sickness characteristics of a high-speed catamaran ferry', *Ocean Engineering*, 34, (14-15), pp. 1909-1917.

Graham , J. M. R. and Neish, A. (1997) 'Numerical predictions of the viscous contribution to slow drift damping', *BOSS'97 8th International Conference on the Behaviour of Offshore Structures.* Delft, The Netherlands, Elsevier Science Ltd, pp. 383-394.

Hassan, A., Downie, M., Incecik, A., Baarholm, R. J., Berthelsen, P. A., Pákozdi, C. and Stansberg, C. T. (2009) *Proceedings of the ASME 2009 28th International Conference on Ocean, Offshore and Arctic Engineering OMAE2009.* Honolulu, USA:ASME.

Haug, N. and Greiner, W. (1999) 'Polyester and steel mooring designs in the Atlantic Margin', *Institute of Marine Engineers,* 111, pp. 119-126.

Hearn, G. E. and Tong, K. C. (1989) 'A comparative study of experimentally measured and theoretically predicted wave drift damping coefficients', *Offshore Technology Conference.* pp. 699-714.

Helvacioglu, I. H. (1990) *Dynamic Analysis of coupled Articulated Tower and Floating Production Systems.* thesis. Glasgow.

Hermans, A. J. (1999) 'Low-frequency second-order wave-drift forces and damping', *Journal of Engineering Mathematics,* 35, (1-2), pp. 181-198.

Hogben, N. (1976) 'Wave Loads on Structures', *Behaviour of off-shore structures: proceedings of the first international conference: BOSS'76.* pp. 187-219.

Huse, E. (1986) 'Influence of mooring line damping upon rig motions', *Offshore Technology Conference.* Houston, Texas , USA, pp. 433-438.

Huse, E. and Matsumoto, K. (1988) 'Practical estimation of mooring line damping', *Offshore Technology Conference.* Houston, Texas, USA, pp. 543-552.

Incecik, A. (1993) 'Effect of non-colinear wave, wind, and current loading on dynamic response of a tension leg platform', *Proceedings of the International Conference*

on Offshore Mechanics and Arctic Engineering - OMAE. Glasgow, UK, ASME, pp. 17-22.

Jang, T. S., Choi, H. S. and Han, S. L. (2009) 'A new method for detecting non-linear damping and restoring forces in non-linear oscillation systems from transient data', *International Journal of Non-Linear Mechanics,* 44, (7), pp. 801-808.

Jang, T. S., Kwon, S. H. and Lee, J. H. (2010) 'Recovering the functional form of the nonlinear roll damping of ships from a free-roll decay experiment: An inverse formulism', *Ocean Engineering*, pp. 1337-1344.

Kinoshita, T. and Takaiwa, K. (1990) 'Added mass increase due to waves for slow drift oscillation of a moored semi-submersible', Houston, TX, USA, Publ by ASME, New York, NY, USA, pp. 225-230.

MARINTEK, T., Norway (2011) *The Ocean Basin Laboratory* Available at: http://www.sintef.no/home/MARINTEK/Laboratories-at-MARINTEK/The-Ocean-Basin-Laboratory/ (Accessed: 5th August 2011).

Maruo, H. (1960) 'The drift of a body floating on waves', *Journal of Ship Research,* 4, (3), pp. 1-10.

McClure, A. C. (1965) 'Development of the Project Mohole Drilling Platform ', *Society of Naval Architects and Marine Engineers*, pp. 50-99.

Morison, J. R., O'Brien, M. P., Johnson, J. W. and Schaaf, S. A. (1950) 'The force exerted by surface waves on piles *', Petroleum Transactions, AIEM.* pp. 149-154.

Newman, J. N. (1967) 'The drift force and moment on ships in waves', *Journal of Ship Research,* 11, (1), pp. 51-60.

Pinkster, J. A. (1975) 'Low-Frequency Phenomena Associated with Vessels Moored at Sea ', *Society of Petroleum Engineers of AIME Journal,* 15, (6), pp. 487-494.

Pinkster, J. A. (1979) 'Mean and Low Frequency Wave Drifting Forces on Floating Structures', *Ocean Engineering,* 6, pp. 593-615.

Pinkster, J. A. (1980) *Low frequency second order wave exciting forces on floating structures.* thesis.

Pinkster, J. A. and Van Oortmerssen, G. (1977) 'Computation of the first and second order wave forces on bodies oscillating in regular waves', *Proceedings of the Second International Conference on Numerical Ship Hydrodynamics.* pp. 136-156.

Remery, G. F. M. and Hermans, A. J. (1971) 'The slow drift oscillations of a moored object in random seas', *Offshore Technology Conference*.

Saito, K. and Takagi, M. (1988) 'On the increased damping for a moored semi-submersible platform during low-frequency motion in waves', Houston, TX, USA, ASME, New York, NY, USA, pp. 147-151.

Sarkar, A. and Taylor, E. (2001) 'Low-frequency responses of nonlinearly moored vessels in random waves: coupled surge, pitch and heave motions', *Journal of fluids and structures,* 15, (1), pp. 133-150.

Sarkar, A. and Taylor, R. E. (2002) 'Dynamics of mooring cables in random seas', *Journal of fluids and structures,* 16, (2), pp. 193-212.

Sarpkaya, T. and Isaacson, M. (1981) *Mechanics of wave forces on offshore structures.* Van Nostrand Reinhold New York.

Söylemez, M. and Incecik, A. (1997) 'Identification of Non-linear Effects in Predicting the Motion Response of an Offshore Platform', *Ocean Engineering* 24, (8), pp. 695-720.

Standing, R., Brendling, W. and Wilson, D. (1987) 'Recent developments in the analysis of wave drift forces, low-frequency damping and response', *Offshore Technology Conference* pp. 307-315.

Standing, R. G. (1988) 'Second-order wave spectral methods, mooring forces and low-frequency response of floating structures', *Journal of the Society for Underwater Technology*, 14, (4), pp. 2-12.

Standing, R. G. and Dacunha, N. M. C. (1982) 'Slowly-varying and mean second order wave forces on ships and offshore structures'.

Stansberg, C. T. (1994) 'Low-frequency excitation and damping characteristics of a moored semisubmersible in irregular waves estimation from model test data', *BOSS'94 7th International Conference on the Behaviour of Offshore Structures.* Massachusetts Institute of Technology, pp. 43-54.

Stansberg, C. T., Yttervik, R. and Nielsen, F. G. (1998) 'Wave Drift Forces and Responses in Storm Waves', pp. 1005-1012.

Sunahara, S. (2004) 'Viscous drift forces on a semi-submersible type mega-float comprised of circular cylinders', Vancouver, BC, Canada, American Society of Mechanical Engineers, pp. 757-764.

Wichers, J. and Huijsmans, R. (1984) 'On the low-frequency hydrodynamic damping forces acting on offshore moored vessels', *Offshore Technology Conference* pp. 315-324.

Wichers, J. E. W. (1988) 'Wave-Current Interaction Effects on Moored Tankers in High Seas ', *Offshore Technology Conference (OTC), Houston* pp. 141-154.

Xiao, L., Yang, J., Yang, L. and Lu, H. (2009) 'Analysis on low frequency heave, roll and pitch motions of a deepwater semisubmersible', Honolulu, HI, United states, American Society of Mechanical Engineers, pp. 185-190.

Yilmaz, O. and Incecik, A. (1996) 'Extreme Motion response Analysis of Moored Semi-Submersible ', *Ocean Engineering* 23, (6), pp. 497-517.

Appendix A

This appendix contains a paper describing some of the preliminary findings of this research, presented by the author at the 28th international conference on Ocean, Offshore and Arctic Engineering (OMAE) 2009 in Honolulu, Hawaii, USA.